Modelling, control and performance optimisation of renewable energy systems

A thesis submitted by

Yingxue Chen

in partial fulfilment of
the requirements of the degree of

Doctor of Philosophy

in the

School of Engineering and Materials Science
Queen Mary, University of London
Mile End Road
London, E1 4NS
UK

2018

School of Engineering and Materials Science
Queen Mary, University of London

PhD THESIS

DECLARATION

This thesis entitled

Modelling, control and performance optimisation of renewable energy systems

was composed by me and is based on my own work. Where the work of the others has been used, it is fully acknowledged in the text, captions, tables and illustrations. This thesis has not been submitted for any other qualification.

Name Yingxue Chen

Signed

Date

Abstract

This thesis presents an investigation into the modelling, control and performance optimisation of renewable energy systems including: Pressure Retarded Osmosis (PRO), Photovoltaic (PV), and Wind Turbine (WT). In doing so, various traditional and machine learning based approaches have been reviewed and their performance compared.

The PRO process is modelled and optimised in terms of key operating parameters to extract maximum power from the system. The optimisation process is carried out based on different salinity gradients between the feed and draw solutions in a PRO process consisting of one to four modules packed in series. This study has revealed that the recommended operating pressure and the ratio of feed or draw solution to the total mixture solution, 0.5, in a laboratory scale PRO unit or in an ideal PRO process are not valid in a non-ideal full-scale PRO module. The optimisation of hydraulic pressure resulted in a 4.4% increase of the energy output in the PRO process. Conversely, optimisation of feed fraction in the mixture has resulted in 28% to 70% higher energy yield in a single-module PRO process and 9% to 54% higher energy yield in a four-modules PRO process. The net energy generated in the optimised PRO process is higher than that in an unoptimised (normal) PRO process. The findings of this study also reveal the significance of incorporating nature inspired machine-learning algorithms in the optimisation of a PRO process and in identifying the preferable operating conditions in a non-ideal system.

In the PV system, a new performance index is proposed to develop a variable step-size based adaptive model predictive control (MPC) algorithm for maximum power

point tracking (MPPT). The algorithm is validated with relatively large additions of process and environmental noise to emulate real operating operational conditions.

Finally, a strategy in controlling a permanent magnet synchronous generator (PMSG) driven by a wind turbine (WT) is also proposed in this investigation to deliver a desired reduced amount of power as required is also proposed in this study. The WT is regulated in a way that the generator delivers the demanded power output to the load.

Table of Contents

List of Figures

List of Tables

Acronyms

AC	Alternating Current
DC	Direct Current
ECP	External Concentration Polarization
GMPP	Global Max Power Point
GWO	Grey Wolf Optimisation
IMR	Incremental Mass Resistance
IC	Incremental Conductance
ICP	Internal Concentration Polarization
MPPT	Maximum Power Point Tracking
MFC	Mass Feedback Controller
MPC	Model Predictive Control
NN	Neural Network
P&O	Perturb & Observe
PMSG	Permanent Magnet Synchronous Generator
PRO	Pressure Retarded Osmosis
PV	Photovoltaic
RSP	Reverse Salt Permeation
STC	Standard Test Conditions
WOA	Whale Optimisation Algorithm
WODE	Whale Optimisation with Differential Evolution

WT	Wind Turbine

Greek Symbols

a	ideal diode constant
β	pitch angle
k	Boltzmann constant
$\emptyset$	number of ions in the solution
θ_D	fractions of draw volume
θ_F	fractions of feed volume
π_d	osmotic pressure of the draw solution
π_f	osmotic pressure of the feed solution
δ	boundary layer thickness
ρ_P	density of permeating water
ρ_D	density of the draw solution
λ	tip speed ratio

λ_{si} solar irradiance ratio

τ_b blade actuator time constant

ω_m mechanical shaft speed of the wind turbine

ω_{ms} steady state rotor mechanical speed of the wind turbine

Γ Gamma function

Nomenclature

Δm_p	mass flow rate of the permeated water
Δm_s	mass flow rate of the reverse water
ΔP	hydraulic pressure of the draw solutione (bar)
ΔV_P	flow rate of the permeated water per volume
$\Delta\pi$	osmotic pressure difference between the membrane
A	membrane water permeability coefficient
A_m	membrane exposed area
B	salt permeability coefficient
C_p	output power coefficient of the wind turbine
D	the bulk diffusion coefficient
E	specific energy extraction
G	irradiance in watts per square meter
G_n	nominal irradiance in watts per square meter

I_0	saturation current of the diode
i_d	d axis current
I_d	current from the diode
I_{pv}	photovoltaic current
i_q	q axis current
J_w	water permeation flux
K_I	short circuit current coefficient in Ampere
N_S	number of PV cells connected in series
P	output power
P_w	wind power output
p	number of generator pole pairs
q	electron charge in Coulombs
Q_D	draw solution flow rate
Q_F	feed solution flow rate

Q_p permeate flow rate

R gas constant

R_S equivalent series resistance

R_p equivalent parallel resistance

S substrate structural parameter coefficient

T temperature in Kelvin

T_{em} electro-magnetic torque

T_n nominal temperature

V measured cell voltage

V_{pv} photovoltaic voltage

V_D volumetric flow rate of draw solution

V_F^0 flow rate of the feed solution

V_F volumetric flow rate of feed solution

ΔV_P thermal voltage of PV arrays

V_w wind speed

$\bar{W}$ average power density

Acknowledgments

I would like to express my sincere thanks to various wonderful people I met in Queen Mary, University of London.

I wish to give my deepest gratitude to my supervisor Dr M Hasan Shaheed for his valuable help during my three years PhD studies. His scientific attitude and rigorous academic spirit left an unforgettable impression on me and have had a remarkable influence on my life. His endless encouragement, advice at the inception, widely knowledge and constructive comments enabled me to pursue my research successfully.

I would like to give my profound and warm thanks to Dr Ranjan Vepa and Dr Guang Li in School of Engineering and Material Science at Queen Mary. They gave me valuable suggestions and supports on my research project when I encountered problems. I would also like to owe my sincere thanks to my colleges, Ololade, Stephen, Chaoran and Vahid at 371A in SEMS. They gave me gorgeous help and support in my research and daily life. It will be the most unforgettable memory in my life to work with you. I would like to express my profound gratitude to Dr Ali Altaee and Dr Alireza.

This work was supported by [Chinese Scholarship Council (CSC)- Queen Mary, University of London] [grant NUMBER 201506460019]. I would like to thank Queen Mary, University of London and Chinese Scholarship Council (CSC) for the sponsorship to my PhD project.

Last but not least, I wish to express my special appreciation and thanks to my families and friends. It is a happy and lonely journey to finish PhD. It is the infinite tolerance, company, love and care of you that made the life of PhD studies become more colourful.

Yingxue Chen

28 November 2018

Chapter 1 Introduction

1.1 Background

Renewable energy is emphasized to be used all over the world in order to mitigate the increasing green-house gas emissions challenge. Research in renewable energy sources is being increased day by day to facilitate the sustainable development of the whole human race. Compared to conventional energy sources such as fossil fuels, renewable energy has viable long-term benefits. In order to diminish global carbon emissions, it is essential that environment-friendly sources of energy are required to be explored across the world. Several renewable and sustainable energy technologies such as solar power and wind power are already being exploited to resolve the global climate change and the energy shortage problems, which are growing at accelerating rates. However, there are other renewable energy sources, such as salinity power that can be extracted through pressure retarded osmosis (PRO), with a huge potential to contribute to solving world energy problem as well as environmental pollution by cutting greenhouse gas emissions.

In 1975, Pressure Retarded Osmosis (PRO) was firstly proposed by Sidney Loeb [1-2] as a production from the salinity gradients. The energy can be generated from the spontaneous mixture of two different salinity solutions, namely the draw solution and feed solution. The potential of PRO energy is significant. Research shows that the potential power can be obtained is in the units of -tera watts (TW) when sea water and the river water mixing [3]. As one of the osmotic power sources, this technology has become a promising renewable source.

Pressure retarded osmosis (PRO) has been broadly investigated for power generation from a salinity gradient resource [4-5]. For the purpose to obtaining the potential power using PRO and improving the power efficiency, extracting the maximum power from the salinity gradient energy is a significant work. Therefore, the control of renewable energy generation is becoming popular with the purpose of extracting more osmotic energy. In this field, the most widely investigated approach to obtain maximum power from a renewable energy sources are called Maximum Power Point

Tracking (MPPT) that aims to track the maximum power point under various operational conditions.

Examples of MPPT algorithms to extract maximum energy from scaled-up PRO systems have been investigated. The algorithms studied for a scaled-up PRO process include incremental mass resistance (IMR) method and perturb & observe (P&O) method [6-7]. The above techniques are all inspired by the well-known MPPT methods in the photovoltaic (PV) system. In the case of a MPPT approach, the power efficiency directly depends on two main components: convergence speed and the obtained maximum power. A faster tracking time and higher extracted maximum power results in less steady state oscillations and less power loss in the output, and vice versa. Both P&O and IMR algorithms must find a balance between the oscillations and the response speed, which causes more power loss. Therefore, a robust and efficient MPPT method is required for a scaled-up PRO system.

As described above, the PRO process converts chemical potential across a semipermeable membrane into a hydraulic energy using concentrated draw solution and diluted feed solution salinity gradient. The feed and draw solutions have a significant impact on the energy output of the PRO process, which can be increased by optimising the applied hydraulic pressure on the draw solution side [8]. Additionally, the energy output in the PRO process is sensitive to the volume of the feed or draw solution in the total mixture[4, 9]. Optimisation of the PRO process is, therefore, a critical process to maximize the energy output from a salinity gradient resource. The technology has been demonstrated in pilot and laboratory scales with the potential of being commercialized as a source of renewable energy [10-11]. However, former studies focused mostly on the optimisation and performance of the PRO in a laboratory scale experiments or assuming an ideal system that ignored the intrinsic properties of the process such as concentration polarization effects [8, 12]. This has resulted in a misunderstanding of the capability of the PRO process and widened the discrepancies between laboratory and field results. To date, studies carried out on the performance and optimisation of a full-scale PRO module are, unfortunately, scarce.

Among renewable energy sources, photovoltaic (PV) systems and wind turbines (WT) are taking the lead. These PV systems are expected to make a crucial effect in future electricity supply instead of the traditional energy structure, for it has plenty

of merits such as: sufficiency and abundance, environmentally friendly, inexhaustible due to sustainable solar radiant energy, etc.

PV resources are not only easy to get because of its ubiquity, but they are also free of cost. A PV cell can directly convert sunlight into electricity at an atomic level by the photovoltaic effect [13]. Several PV cells make a PV module, and a PV system consists of several PV modules. The basic device of a PV system is the PV cell, which is basically made up of semiconductor materials like mono-crystalline or poly-crystalline silicon [14]. In an actual sense a PV cell is a semi-conductor diode which has its p-n junction exposed to light. Sunlight consists of little parkers of solar energy called photons. When a PV cell is exposed to sunlight, electrons are knocked loose from the atoms in the semiconductor material and then the p-n junction of semiconductor forms a new hole called electron pairs. Under the action of a p-n junction, holes from the n region move to the p region while electrons flow from p region to the n region. As the material absorbs photons, energy is transferred into the solar cell. If electrical conductors are attached to the positive and negative sides, an electrical circuit will be formed, and the electrons can be captured in the form of an electric current, which is electricity. However, there are two main challenges posed by a PV system. One is that the conversion efficiency of most solar panels is less than 15% [7]. Although PV energy is free of cost, a PV system requires a high installation charge. Consequently, Maximum Power Point Tracking (MPPT) control method is significant to maximize the utilization efficiency of a PV system. Another hindrance is that the nonlinear Current-Voltage (I-V) and Power-Voltage (P-V) characteristics of a PV panel vary with external conditions such as inside temperature, solar irradiance and output voltage of PV modules. [8]. The DC micro grid was proposed several years ago with the purpose of integrating various renewable energy system. In a DC micro grid, droop control is a basic control method for load current sharing. In a PV based DC micro-grid system, the DC link voltage is kept constant and the power coming out of the converter (and the power coming out of the PV array) can be boosted by increasing the current going into it with this method.

The appearance of high-efficiency photovoltaic system makes the development of Direct Current (DC) power grid supplied by DC-DC converter. Its efficiency exceeds that of a typical traditional high voltage AC-AC (Alternating Current) 50 hertz (hz) transformer. Instead of the classical unidirectional power flow in the present AC power grids, DC power grids is not the traditional one-direction power flow, but bi-directional, which are suitable for power supply to medium and low voltage grids. A

main issue is to control the energy distribution throughout the whole power grid while also balancing the energy generation and energy demand. Therefore, DC power grids can not only integrate renewable energy, but also allow continuous control of the power flows in and out of the grid.

Research on Wind Turbine (WT) systems using advanced control methods has been increasing more recently. Hur [15] presents MPC for maximum power tracking of variable speed wind turbines, and it gives a better performance comparing with two loop separation frequency (2LPSF). Moreover, an offset predictive control was proposed for variable speed wind turbines [16]. Hosseini [17] also presents a variable speed wind system through MPC base on INC to improve the dynamic response of the wind turbine. Yaramasu [18] proposed a predictive control method for medium voltage wind energy conversion systems. Later, a finite-control-set MPC (FCS-MPC) technique for low-voltage, ride-through (LVRT) enhancement of wind turbine system was proposed [19]. Dizqah [20] proposed a coordinated optimal energy management strategy for a PV and wind turbine system of a DC micro-grid.

1.2 Recent Developments

The focus of this research project is mainly on modelling, control and performance optimisation of renewable energy systems. Within the field of renewable energy sources, this study is mostly limited to three renewable energy systems, which are the PRO, PV and WT systems.

PRO systems

Energy generation from saline water using pressure retarded osmosis (PRO) was first proposed by Loeb [2] in 1975 as a novel alternative clean energy. Since then PRO has been investigated increasingly as a promising energy source by several researchers [6, 21-24]. This osmotic pressure gradient-based energy extraction method is easy to scale-up and can harvest free energy using membrane-based technologies spontaneously without being affected by wind variations or solar irradiance. In a typical PRO process, fresh water, such as river water forms the feed solution on one side of a semi-permeable membrane. The draw solution, for example seawater is on the other side of the semi-permeable membrane and has higher saline concentration and provides a natural salinity gradient across the membrane. When two solutions with different salt concentrations are present, the less concentrated saline water diffuses across the membrane and the differential pressure energy can

be extracted [21]. For instance, with the seawater and the river water which are the draw and feed solutions, respectively. In theory, when seawater and river water mixed, the worldwide potential chemical salinity pressure from the two sides of the membrane is equivalent to a 270m waterfall – free energy of mixing up to 0.81kWh/m^3[22-24]The potential power on the earth that can be tapped during the mixing process by the PRO system is estimated to be equivalent to be 1.4-2.6TW [23], which is a significant amount of renewable power. The value is estimated when all global river water mixing seawater, though, the reported amount of produced power can be reduced in reality. The globally availability of produced gradient power is around 60% of potential power regarding energy conversion techniques[23, 25], which remains an enormous resource. Thus, tracking the maximum power that can practically be extracted from the PRO system is one of the most significant topics in renewable energy generation.

To make energy generation from a PRO process practically feasible, its production cost needs to be comparable with that of the other renewable energy sources such as wind, hydro and solar. This will require increasing the efficiency of a PRO process through several developments including inexpensive membrane design and fabrication tailored for a PRO process, novel PRO process design, such as multi-stage PRO, and the design of appropriate control methodologies to extract maximum power from a PRO process. However, while a significant number of state-of-the-art MPPT techniques exist for wind and solar energy, very limited work has been carried out on the design of novel control techniques to extract maximum power from a PRO process with comparatively faster speed. A few MPPT strategies have been proposed to improve the efficiency of a PRO module and yield the maximum energy; these include Perturb & Observe (P&O), Incremental Mass Resistance (IMR) and Mass Feedback Controller (MFC) [6]. Similar to the P&O methods for the PV system, the P&O for PRO system involves a perturbation in the pressure on the draw side of PRO system. However, it results in oscillations at the maximum power point (MPP) due to the variations in the perturbations around the MPP. IMR was subsequently proposed to reduce the oscillation as well as the power loss by calculating the slope of the PRO power curve. The idea was inspired by the Incremental Conductance (IC) technique for the PV system [25]. The performance of the PRO system using IMR depends on the incremental pressure. The merit of IMR is that it is more flexible and stable compared with P&O. Yet the accompanying oscillations persist. Furthermore, a feedback control-based technique, MFC was proposed to improve the efficiency. Inspired by the PID controller, the MFC is implemented to minimize the error of the

power slope. The weighted sum of both the slope and the change of the slope is utilised to determine the error, resulting in fast convergence and lower power loss. The challenge is to balance three designed PID controller gains under the effect of disturbances and uncertainties from the system. When the system encounters a variation in the operating environment such as salinity and temperature, IMR algorithm may be less robust in performance.

In a PRO osmotic power plant, under rapidly changing salinity and operational conditions, the need for a trade-off between oscillation and the tracking speed is an unavoidable complication that reduces the efficiency of the overall system significantly. Therefore, a better performing method is required to find the global maximum power point [25]. In order to track the global maximum power point, a novel evolutionary algorithm, Whale Optimisation with Differential evolution (WODE) is studied as an alternative approach. The Whale Optimisation Algorithm (WOA), proposed by Mirjalili et al. [26], is an evolutionary computing approach inspired by the hunting strategy of humpback whales in the ocean. The proposed novel algorithm can handle the non-linear objective functions and performs well as a new optimising tool for the design of closed loop control systems.

Furthermore, several applications based on this meta-heuristic technique have been evaluated in literature[27-28]. The novelty of the WODE-based MPPT is found to have the ability to track the global best-peak position in a few steps with oscillation-free convergence. Additionally, this algorithm requires fewer iterations, converges faster and has less computational burden owing to fewer search particles being needed to find the best solution. This results in lower steady state oscillation as well as less power loss in the output. However, after a thorough literature survey, it was noted that the advantages of WODE are yet to be exploited in optimising a PRO system for a better performance. Thus, WODE-based MPPT of a PRO system is proposed in this work, which aims to design a better-performing MPPT controller for a classic scaled-up PRO system. The design also aims to improve the performance of a the scaled-up PRO system with various physical constraints and salinity profiles

Performance of the PRO process in a full-scale module is different to that in a flat-sheet laboratory scale unit. Based on the laboratory size experiments, most studies have used equal feed and draw solutions flow rates, which ignored the effect of dilution and concentrations along the PRO module [8,29]. Masaru and Masayuki [10]

performed a pilot plant test for power generation using eight 10-in, hollow fiber membrane modules. The PRO achieved a power density equal to 4.4 W/m^2, which is closer to the minimum theoretical threshold value suggested for an economic PRO process [11]. The study did not perform an optimisation process to enhance the energy output in the PRO process. Achilli et al, [12] conducted a laboratory test on a flat sheet PRO unit and concluded that maximum power density occurs at a hydraulic pressure equal to $\Delta\pi / 2$. The study, however, did not investigate the effect of varying the feed or draw solution flow rate on the power generation in the PRO process. Elimelch et al, [8] investigated energy yield from various salinity gradient resources in the PRO process. The study presented the performance of the PRO module and suggested that the maximum specific energy was achieved at hydraulic pressure and feed or draw fraction in the mixture equal to $\Delta P = \Delta\pi / 2$ and 0.5 respectively. The study assumed an ideal system and ignored the effects of concentration polarization in the PRO process. Altaee et al, [29] performed a thermodynamic analysis study on a full scale PRO module and found that increasing the number of modules in the pressure vessel maximized the energy yield of the PRO system. The study was performed at hydraulic pressure and feed or draw fraction in the mixture equal to $\Delta P = \Delta\pi / 2$ and 0.5 respectively. In a different study, Altaee et al, performed PRO performance analysis considering the impact of feed and draw slow rates, hydraulic pressure, and membrane area on the energy output in the PRO process [30]. The study showed that increasing the flow rate of feed and draw solution reduced the effects of concentration polarization and improved the performance of PRO process. The stud, however, considered neither the impact of concentration polarization nor the impact of module length of the process performance. Yang and co-workers developed a numerical simulation procedure for a counter-current flow PRO process [31]. The numerical model predicted the flow rates and salt concentrations along the membrane channels for any feed fractions. However, the modelling results are only valid for an ideal PRO process and ignored the effects of concentration polarization along the PRO module.

Salinity gradient processes experiences dynamic changes in the full-scale PRO element due to the continuous dilution and concentration of the draw and feed solutions, respectively [9, 29]. Furthermore, the pressure vessel may contain several PRO elements packed in a series and operates under a constant hydraulic pressure while the concentrations of the feed and the draw solution undergo continuous changing along the PRO module and in each module in the pressure vessel. As such, the optimum value of hydraulic pressure for a laboratory scale PRO unit and equal

to $\Delta P = \Delta\pi / 2$ would not be valid for a full-scale PRO element or a pressure vessel of multi PRO elements. Although the optimum value of hydraulic pressure $\Delta P = \Delta\pi / 2$ has been validated on a laboratory scale unit, but it is still used in pilot plant tests. Module optimisation requires large system setup and testing, which is time and labour intensive.

PV systems

Over the years, several researchers have worked on the PV panel and studied PV characteristics including factors that affect them. It is essential to provide a robust model of PV cells. Sera [32] provides a PV panel model based on manufacturer's data sheets in Standard Test Conditions (STC). However, it depends on only one operating condition. Villalva [13] proposes an effective and straightforward solution to fit the mathematical equation of the nonlinear I-V characteristic with three crucial points of a practical PV array, but it is only suitable for single-diode models. Krismadinata [33] defines both mathematical model and simulation model employed in the MATLAB/ Simulink environment. Soto [34] proposes a five-parameter model for four different cell technologies. Though effective, this research lacks the study on the choice of tilt angle. Costa [35] and Armstrong [36] mainly propose the temperature control law and the methodology to choose the optimum tilt angle for a PV panel respectively. Patel [37] proposes a MATLAB-based modelling and simulation scheme under partial shaded conditions. Dolara [38] compares three physical models of PV cells using actual weather data.

PV arrays have their specific non-linear characteristics and the maximum power point (MPP) depends on conditions like temperature, insolation and so on. Also, the low conversion efficiency of PV systems is a considerable hindrance [39]. There are a few ways to improve the efficiency of solar power. These include: promoting the Review on Maximum Power Point Tracking (MPPT) algorithm, automatic tracking systems, increasing conversion efficiency of PV panels and better power storage technology [40]. The effective MPPT technique is developed and harnessed to locus the maximum power point and produce better efficiency [41]. In the literature, various MPPT methods have been studied by researchers, like Perturbation and Observation (P & O) [42], Incremental Conductance (InC) [43], Fuzzy Logic (FL) [44], Neural Network (NN) [45], etc. The relative achievements are discussed in [39].

There are two stages to connect photovoltaic power to DC power grid. Firstly, through the DC-DC converter is regulated by the controller from the PV modules to yield the maximum power. A DC-DC converter is utilised to provide an output voltage. A regulated power supply is implemented [46]. DC-DC converters are intrinsically non-linear in their dynamic behaviour. Considering not only all parasitic inputs but simulate their effects on the dynamic response of dynamic models, it is not easy to obtain the model accurately. Due to variations of power input, the DC voltage output of this system can be subject to a wide range of transient conditions. Amato et al [47] discussed the feedback control in the application to the stabilization of linear state bilinear systems. It was applied to a Ćuk DC-DC converter design, he effectiveness of this method was verified,

For the purposes of controlling the DC voltage, the power output driven voltage variations should be adequately compensated to guarantee a regulated, steady voltage output. The DC voltage control is realized by controlling the power exchange between the converter and the grid, using a converter interface. The converter interface delivers a current to the DC grid at a constant voltage. It is also controlled actively by continuously switching the output current and voltage whenever they exceed or fall below a reference value. Controller with switch mode based on MPC technique is utilised for MPPT and for regulating the grid voltage. MPPT controllers are verified to be efficient in photovoltaic systems under different conditions, to track the maximum energy [48]. Several researchers have presented various MPPT methods for a PV system [42-49]. These include: i) short circuit technique, ii) open circuit algorithm, iii) P&O method [42], iv) incremental conductance technique [43], v) ripple correlation control, vi) single cycle control using an inverter [49]. Most of these algorithms can be implemented adaptively, or with the state estimator coupled to compensate for the lack of some measurements. The output power can also be generated using suitable MPPT techniques in each case. Among these methods, the most popular technique is “P&O” as it does not require short-circuit current or open-circuit voltage [43]. The principle of P&O is simple. The distribution in voltage or current at the maximum power point reduces the output power. Otherwise the operating point moves in the direction of increasing power.

Kakosimos et al.[50] have designed a MPC based two-step MPPT algorithm. The control principle is a modification of the incremental conductance (INC) algorithm with two-step predict control method. A MPC controller is proposed by Gonzalez et al. [51] to adjust the converter powered by a photovoltaic power. Sajadian and

Ahmadi [52] present an optimal MPC method for PV system based on the use of single-stage grid-tied Z-source inverter. The possibility of developing a high voltage DC bus to facilitate the energy transport in the smart grids was studied [54-55], using high efficiency DC-DC converters. Shadmand et al. [55] have developed a P&O method which uses MPC with fixed step size, and the insolation varies rapidly. The utilise of MPPT based MPC technique predicts errors before applying switching signals to fly back DC/DC converter by introducing a control loop. Later, an MPC-based MPPT and droop regulator are evaluated to connect PV module to a DC distribution system [40]. Hu et al. [56] have also applied the MPC methodology to direct power control of a grid-connected inverter fed by a PV system. Geyer et al. [57] have developed a new method for the modelling and controller design problem associated with fixed-frequency converters. Adhikari and Li [58] have designed a coordinated and integrated controller for PV generators with MPPT. In a doctoral thesis, Jiang and Jaber [59] developed a new method of load current adaptive step size MPPT controller.

One of the most popular methods to regulate the output voltage of power grid is the droop control technique. Li et al. [60] and Fuente et al. [61] have developed methods of analysis for droop controlled DC micro-grids and used droop control to serve as a stable voltage source for power management or power management of DC micro-grid flow. For droop control, the DC link voltage is generally regulated while the power output of the converter (and the power output of the PV array) may vary due to variations of the current supply. However, beyond the optimum operating point the DC link voltage begins to droop as the voltage output of the source reduces with increasing current. Thus, the current input is maintained at a value just prior to when the DC link voltage begins to droop.

WT systems

The conventional method of power generation from a wind turbine has been based on the use of a doubly fed induction generator. However, there has been a growing interest in the development of small-scale wind turbine power generating units, which typically drive a permanent magnet synchronous generator (PMSG). There have been many recent studies related to the dynamic model and control of wind turbines driving a PMSG. Elbeji et al. [62] have investigated the dynamic model and control of a PMSG driven by a wind turbine. They have investigated several suitable control schemes. Hussein et al. [63] have considered the application of simple control schemes to control both the generator side and grid side of the PMSG system.

There have been several applications related to the maximum power point tracking (MPPT) control. Rolan et al. [64] reported the implementation of a MPPT system by simple speed adjustment of the wind turbine. Aliprantis et al. [65] discussed the modelling and active control of a stall-regulated variable-speed PMSG driven by a wind turbine. Camara et al. [66] developed a MPPT system for PMSG speed control as well as active and reactive power control, management of the DC-bus voltage and battery's power control. Tafticht et al. [67] have discussed the estimation of power quality, control strategies for MPPT and the connection of the wind turbine to a variety of storage or grid systems. Hamatwi et al. [68] have implemented rotor speed control for MPPT using phase lag compensation. Other important studies related to wind turbines driving a PMSG include the control of the inertial frequency response using a full-rated Voltage Source Converters (VSC), by Cheah-Manee et al. [69] and the development of a systematic approach to model reduction by Hackl et al. [70]. The important issue of the coupled stability and control of the permanent magnet synchronous generator (PMSG) when driven by a wind turbine was considered by Hamied et al. [71]. However, it appears that most of the focus of the current research's focus has been on the control of the electrical side of PMSG's driven by a wind turbine, and a few important issues haven't been explored yet.

1.3 Motivation

Research on control algorithms has been an area of my interest since my undergraduate studies. The future of energy consumption is an issue with regard to climate change and scarcer fossil fuels. Sustainable development in various types of energy is of importance to everyone in the world at large. However, the global environment faces the risk of a lack of access to clean and modern energy services due to today's rapidly increasing energy demand and the rapidly depletion in conventional energies. Carbon dioxide released by burning fossil fuels has led to a myriad of problems, such as global warming and environmental pollution. The Great Smog in London in 1952 mostly had its origins in the use of coal. More recently, China has begun to suffer from a smog problem for the same reason.

In recent times, PRO, PV and WT systems have become the three most promising renewable energy systems. As introduced above, there are several challenges with these sources. Thus, the motivation is to investigate and design high-efficiency renewable energy systems, PRO, PR and WT, using control and optimisation techniques.

1.4 Aims and objectives

The main aim of this study is to investigate energy efficiency improvement of three sustainable energy systems: PRO, PV and WT systems by system modelling, control and operating parameter optimisation. The aim and objective of the thesis is firstly to develop mathematical models for these three renewable energy systems and study their system characteristics, in which environmental and operational variables are taken into account to improve their simulation accuracy. For each individual renewable energy system, model-based control methods and performance optimisation techniques are proposed and evaluated through simulation under different case studies in order to validate the systems' behaviours and robustness.

The specific objectives of this research are depicted below:

- investigate efficient extraction techniques for a scaled-up PRO system subject to various salinity profiles.

- optimise operating parameters on a number of salinity gradients in a PRO process to enhance overall energy extraction.

- design and implement effective control mechanism for a PV system and develop a performance index and to investigate a bi-linear PV model under disturbances.

- develop de-coupled dynamic and equilibrium models of a permanent magnet synchronous generator (PMSG) driven by a variable speed wind turbine system and to develop an MPC method to achieve desired power generation.

1.5 Chapter outline and organization

A brief outline of the thesis is shown below.

- **Chapter 2** presents an analytical model of a scale-up PRO osmotic power plant. Based on the module-scale PRO process, the non-linear characteristic of the PRO system $\Delta V - \Delta P$ characteristics and $\overline{W} - \Delta P$ characteristics are studied and used to explore the osmotic energy efficiency. Further, a full-scale PRO model is developed. Four types of salinity gradient resources (Dead Sea-seawater, Dead Sea-Reverse Osmosis brine (ROb), seawater-

wastewater effluent, and RObwastewater effluent) were evaluated for power generation in the PRO process along the membrane.

- **Chapter 3** depicts four salinity gradient resources following the mathematical full-scale PRO model derived in Chapter 2. A computer model is applied to predict the performance of the PRO process and the system optimisation has been carried out. In this study, GWO is used to suggest the optimal values of key operating parameters for a maximum energy extraction. The net energy generated in the optimised PRO process is higher than that in the unoptimised (normal) PRO process.

- **Chapter 4** presents an evaluation on maximum power point tracking using various MPPT methods including P&O, IMR and PSO based the developed module-scale PRO characteristics, the performance curve and modelling framework of a scaled-up PRO system in Chapter 2. Furthermore, a novel evolutionary optimisation algorithm WOA based MPPT method was proposed and implemented, which is verified to be superior to previous methods.

- **Chapter 5** presents a mathematical model of PV cells. A model predictive control (MPC) algorithm is utilised for maximum power point tracking (MPPT) and for regulating the power output from a PV panel. A novel feature of the proposed methodology is that the parameters of the converter are chosen to always guarantee stability to ensure the robustness of the system. Another novel feature of the proposed variable step size algorithm is that it is adaptive. It has been validated with relatively large additions of process and environmental noise to emulate real operational conditions. This chapter also emphasises the main features of the controllers that can adjust the output power of a PV system. In addition, PV thermal analysis is studied and evaluated based on the weather condition in Egypt to examine the effectiveness of a seawater cooled PVT cell.

- **Chapter 6** analysed and developed a common strategy in controlling a permanent magnet synchronous generator (PMSG) driven by a wind turbine for the maximization of output power of the wind turbine. The stability of the wind turbine system is analysed, and a blade pitch controller is designed,

based on the linearised, parameter-varying, model-predictive control and is validated. Moreover, the blade pitch control system also performs the key function of augmenting the stability of the wind turbine, for the right choice of the gains.

- **Chapter 7** presents the conclusions of this research investigation, discussion and an outline of future work.

Chapter 2 Modelling of Pressure Retarded Osmosis plant

2.1 Introduction

Pressure retarded osmosis (PRO) has been broadly investigated for power generation from a salinity gradient resource [4, 29]. The technology has been demonstrated in pilot and laboratory scales with the potential of being commercialized as a source of renewable energy [10, 11]. The PRO process converts chemical potential across a semi-permeable membrane into a hydraulic energy using concentrated draw solution and diluted feed solution salinity gradient. As mentioned before, today the experiment for PRO system in a development stage. Therefore, when analysing, an accurate mechanical model of PRO process is of important.

In this Chapter, two PRO models are developed and considered. Firstly, basic principles of a module-scale PRO model are introduced and investigated with regards of the detrimental effects. The three essential operational elements, namely draw and feed flow rates and applied pressure are thus developed to evaluate the generated energy. The characteristic of a module-scale PRO power plant considering RSP, ICP and ECP is then analysed under different operational conditions.

Furthermore, an existing full-scale PRO power plant is investigated and analysed under non-ideal operating conditions. Performance of the PRO process in a full-scale module is different to that in a flat-sheet laboratory scale unit. Salinity gradient experiences dynamic changes in the full-scale PRO element due to the continuous dilution and concentration of the draw and feed solutions, respectively [9, 29]. Moreover, the pressure vessel may contain several PRO elements packed in a series and operates under a constant hydraulic pressure while the concentrations of the feed and the draw solution undergo continuous changing along the PRO module and in each module in the pressure vessel. In this work, four different types of gradient resources (Dead Sea(DS)-seawater, Dead Sea-Reverse Osmosis brine(ROb),

seawater-wastewater effluent, Rob-wastewater effluent) were investigated for PRO power generation models.

Performance of the PRO process in a full-scale module is different to that in a flat-sheet laboratory scale unit. Salinity gradient experiences dynamic changes in the full-scale PRO element due to the continuous dilution and concentration of the draw and feed solutions, respectively [9, 29]. Furthermore, the pressure vessel may contain several PRO elements packed in a series and operates under a constant hydraulic pressure while the concentrations of the feed and the draw solution undergo continuous changing along the PRO module and in each module in the pressure vessel.

2.2 Modelling of the Pressure Retarded Osmosis System

Four types of salinity gradient resources (Dead Sea-seawater, Dead Sea-Reverse Osmosis brine (ROb), seawater-wastewater effluent, and ROb-wastewater effluent) were evaluated for power generation in the PRO process. These salinity gradients were commonly investigated in literature and represented as Dead Sea (~5M NaCl), seawater (~0.6M NaCl), Reverse Osmosis brine (~1.2M NaCl), and wastewater effluent (~0.02M NaCl) [8, 29, 75]. In chapter 4, A computer model was applied to predict the performance of the PRO process and the system optimisation was performed using GWO algorithms.

A pre-developed computer model was applied to estimate water flux in the PRO module [4]. Water flux in the PRO membrane was calculated using Eq 2.1 [4, 29]:

$$J_{w,nx} = A_w\left(\frac{(\phi RTC_{Di,nx}(1+\frac{Q_{Di,nx}}{Q_{Do,nx}})/2)\exp(\frac{-J_w}{k_d}) - (\phi RTC_{Fi,nx}(1-\frac{Q_{Fi,nx}}{Q_{Fo,nx}})/2)\exp(J_wK+\frac{J_w}{k_f})}{1+\frac{B}{J_{w-x}}(\exp(J_wK+\frac{J_w}{k_f})-\exp(\frac{-J_w}{k_d}))} - \Delta P\right) \quad (2.1)$$

where, $\emptyset$ is number of ions in the solution, R is the gas constant, and T is the temperature in Kelvin. A_w and B were assumed to be 1.23 L/hm^2·bar and 2.6 kg/hm^2 respectively, $k_d = k_f = 0.18$ m/h, and $K = 31$ h/m [6]. Equation 2.1 accounts for

concentration polarization and external resistance in the PRO membrane [9], [73]. It calculates the water flux in a PRO membrane operating in the PRO model (draw solution faces the membrane active layer; DS-AL). Detailed information about the derivation of Equation (2.1) is found in literature [29]. The fractions of draw and feed volumes, θ_D and θ_F respectively, in the mixture were calculated from the following equations:

$$\theta_D = \frac{v_D}{v_D + v_F} \tag{2.2}$$

$$\theta_F = \frac{v_F}{v_D + v_F} \tag{2.3}$$

where, V_D and V_F are the volumetric flow rate of draw and feed solutions. Different θ_D and θ_F ratios were tested and their effects on the PRO performance were investigated. Furthermore, in a full-scale PRO process, the specific energy output E_S can be calculated at different operating conditions using the following expression [8, 30]:

$$Es = \frac{\Delta P * Q_p}{Q_D + Q_F} \tag{2.4}$$

where, ΔP is the hydraulic pressure of the draw solution entering the hydroturbine (bar) and Q_p, Q_D, Q_F are the permeate, draw solution and feed solution flow rates, respectively. Specific energy output from the optimised PRO system was compared with that from the unoptimised PRO process. In practice, internal and external concentration polarizations, ICP and ECP respectively, can be mitigated by varying the feed and flow rates in the PRO module [21, 22]. However, this would also compromise the specific energy output in the PRO process according to Equation 4 unless the flow rates are carefully optimised. In the following study, optimised method was applied to find the optimum flow rates in the PRO system comprising a single and multi-module.

2.3 Characteristics of a Pressure Retarded Osmosis System

The complete mechanism of a typical module-scale PRO salinity power plant is shown in Fig.2.1 [74]. Here, the PRO membrane model is connected to the external

devices, the pressure of the high-pressure pump is controlled by the MPPT controller. The overall PRO process is presented in Fig. 2.1.

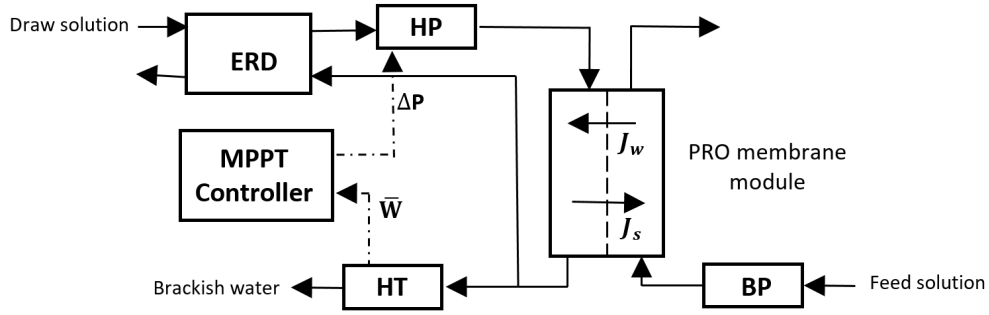

Figure 2.1: Block diagram of the PRO system with MPPT controller

In above block diagram,

ERD: energy recovery device;

HP: high-pressure pump;

BP: boost pump;

HT: hydro-turbine.

In the previous research, various PRO models incorporating detrimental effects (D-PRO) of external polarization concentration (ECP), reverse salt permeation (RSP) and internal polarization concentration (ICP) are studied [75]. In this section, the D-PRO model is implemented and used to derive the MPPT algorithm. This model is analogous to an equivalent circuit model with purely resistive elements in the circuit, albeit nonlinear in general. This implies that we have used purely a quasi-static model. The authors [22, 78, 79] developed the model based on the following assumptions: i) to simplify, a constant density is assumed for both draw and feed solution [75]; ii) the difference of osmotic pressure is assumed based on the van't Hoff law [22]; iii) constant hydraulic pressure difference owing to neglected pressure loss [76]. The mathematical formulation of the power density in a PRO system is described as following [12]:

$$W = J_w \Delta P \tag{2.5}$$

In (2.5) ΔP is the hydraulic pressure and J_w is the water permeation flux in $L \cdot m^{-2} \cdot h^{-1}$. The water permeation flux J_w for the D-PRO model incorporating the detrimental effects of ECP, RSP and ICP is defined as following using experimentally measurable parameters [77]:

$$J_w = A\left(\left\{\frac{\pi_D e^{-Jw/k} - \pi_F e^{-JwS/D}}{1 + B/J_w\left[e^{-JwS/D} - e^{-Jw/k}\right]}\right\} - \Delta P\right) \tag{2.6}$$

In (2.6) A, B, S and D are the membrane water permeability, salt permeability, substrate structural parameter and the bulk diffusion coefficient, respectively. π_D and π_F are the osmotic pressure of the draw solution and the feed solution, respectively. k is the boundary layer mass transfer coefficient which is represented as $k = D/\delta$, where δ is the boundary layer thickness. The actual power density can be formulated as

$$W = A\left(\left\{\frac{\pi_D e^{-Jw/k} - \pi_F e^{-JwS/D}}{1 + B/J_w\left[e^{-JwS/D} - e^{-Jw/k}\right]}\right\} - \Delta P\right) \times \Delta P \tag{2.7}$$

The solution on the draw side is diluted while the concentration of the feed water increases along the flow direction owing to the direct and the reverse water permeation. The reverse solute flux J_s in $L \cdot m^{-2} \cdot h^{-1}$ regarding the detrimental effects is represented as[77]

$$J_s = B\left(\left\{\frac{c_D e^{-Jw/k} - c_F e^{-JwS/D_s}}{1 + Be^{-JwS/D}/J_w - e^{-Jw/k}}\right\} - \Delta P\right) \tag{2.8}$$

The water flux can be calculated from the mass balance of the feed solution at the steady state. The mass flow rate of the permeated water,Δm_p is represented as[75]

$$d\left(\Delta m_p\right) = \rho_P J_w d(A_m) \tag{2.9}$$

Similarly, the mass flow rate of the reverse water Δm_s can be expressed as

$$d(\Delta m_s) = \rho_D J_s d(A_m) \tag{2.10}$$

In (2.9)-(2.10) ρ_P and ρ_D denote the density of permeating water and the draw solution in kg/ m^3·. A_m the membrane exposed area. The flow rates of the draw and feed solution can be updated by[21]

$$q_D = q_D^0 + \Delta q_p \tag{2.11}$$

$$q_F = q_F^0 - \Delta q_p \tag{2.12}$$

The superscript 0 specifies the initial value, namely the variables at the inlet. From the mass change between two sides, the flow rates of both solutions are exhibited as

$$c_D = \frac{c_D^0 q_D^0 - \Delta m_s}{q_D^0 + \Delta q_p} \tag{2.13}$$

$$c_F = \frac{c_F^0 q_F^0 + \Delta m_s}{q_F^0 - \Delta q_p} \tag{2.14}$$

In a module-scale PRO system, the average power density (APD) $\overline{W}$ is used to explore the efficiency considering the detrimental effects, which is expressed as the ratio of the specific energy extraction (SEE) E and the membrane area A_m. In the expression, $\Delta V_P / V_F^0$is called dimensionless permeated water volume [22].

$$\mathrm{E} = \frac{\Delta P \Delta V_P}{V_F^0} \tag{2.15}$$

In which E is the extractable energy SEE. V_F^0 presents the flow rate of the feed solution. ΔV_P is the flow rate of the permeated water per volume in m^3/h.

$$\overline{W} = \frac{E}{A_m} \tag{2.16}$$

The SEE is defined to highlight the efficient application of the osmotic energy. From (2.16) it is obvious that when the membrane area is fixed, the operation of APD and SEE is same. Overall, a scaled-up PRO discharge model can be obtained from the above key equations. Furthermore, the APD is used in this paper to evaluate different MPPT algorithms.

2.3.1 System Description

The non-linear characteristics of the PRO system can be achieved from its mathematic model. The performance of the non-linear PRO model is influenced by membrane parameters and

operating conditions. In Table 2.1, all values of parameters utilised in the module-scale PRO system are clearly illustrated.

Table 2.1: Parameters applied in a scaled-up PRO process

Parameter	Symbol	Value
Water permeability	A	1.74 $L \cdot m^{-2} \cdot h^{-1} \cdot bar^{-1}$
Salt permeability	**B**	0.16 $L \cdot m^{-2} \cdot h^{-1}$
Structural parameter	S	307e-6μm
diffusion coefficient	D	3600*1.490*10^-6 m^2 s^1
boundary layer mass transfer coefficient	k	138.6 $m \cdot s^{-1}$
Efficiency of HP	η_{HP}	70%
Efficiency of HT	η_{HT}	90%
Efficiency of ERD	η_{ERD}	95%
draw solution concentration	c_D	35-55g/kg
feed solution concentration	c_F	0.1g/kg
draw solution flow rate	q_D	1-4kg/h
feed solution flow rate	q_F	1kg/h
Membrane area	A_m	0.1m^2 per 1 L/h feed solution

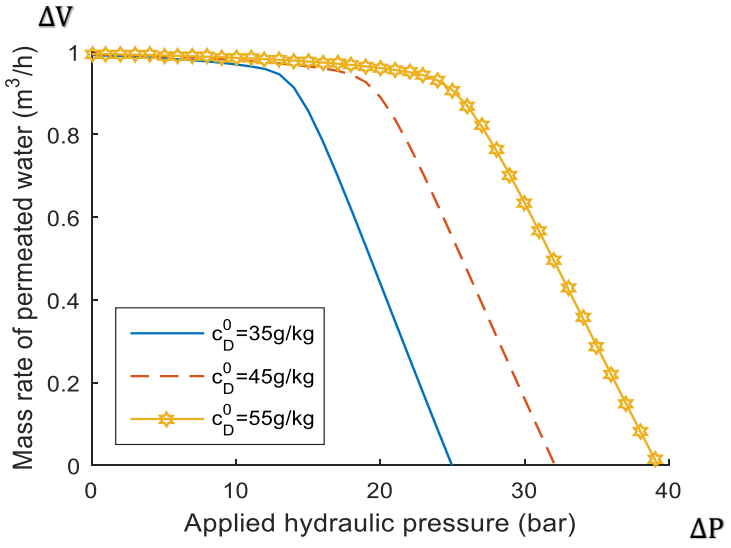
ΔV
Mass rate of permeated water (m3/h)
1
0.8
0.6
0.4
0.2
0
0
10
20
30
40
Applied hydraulic pressure (bar)
ΔP
c0D=35g/kg
c0D=45g/kg
c0D=55g/kg

(a)

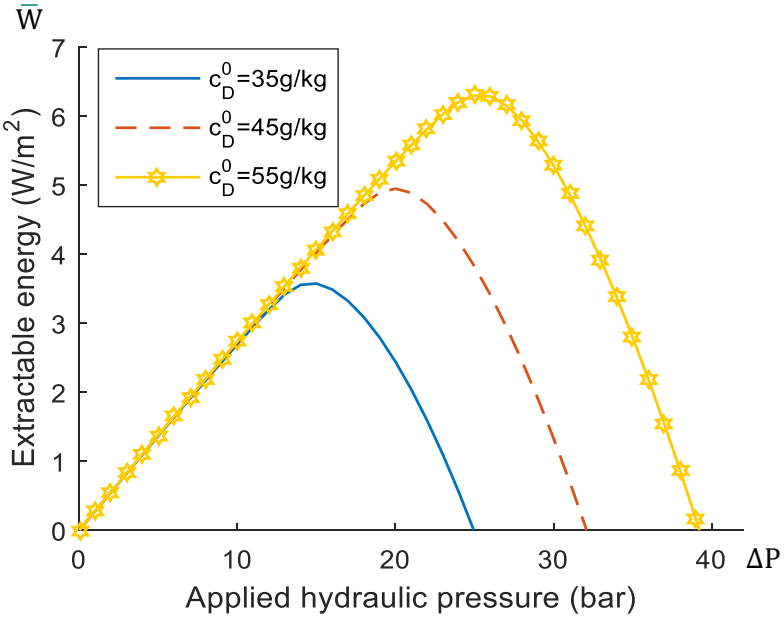
W̄
Extractable energy (W/m2)
7
6
5
4
3
2
1
0
0
10
20
30
40
ΔP
Applied hydraulic pressure (bar)
c0D=35g/kg
c0D=45g/kg
c0D=55g/kg

(b)

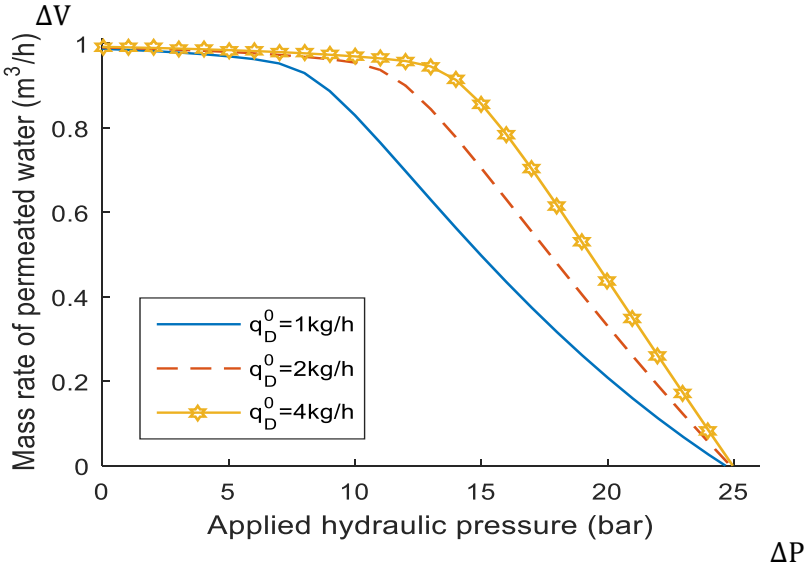

(c)

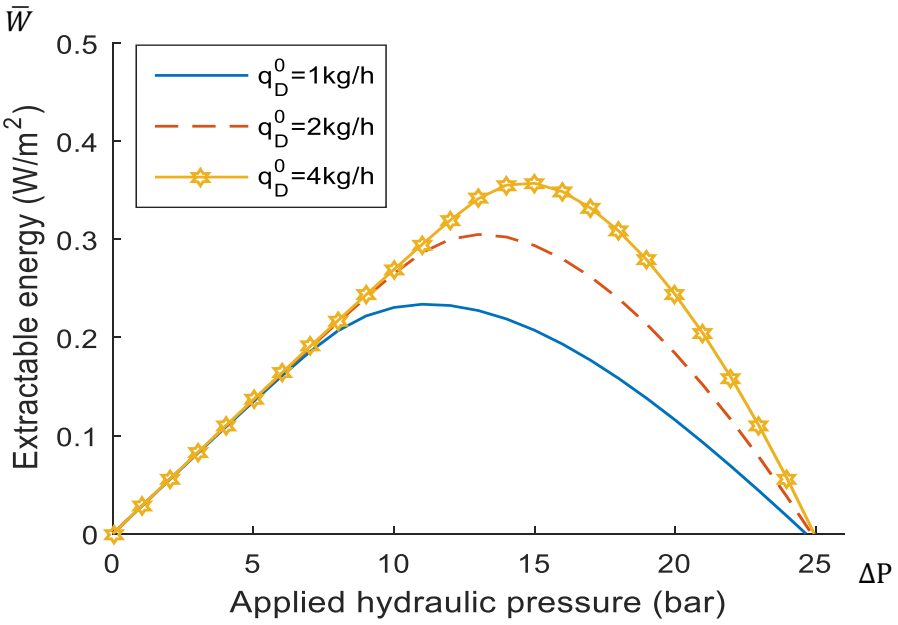

(d)

Figure 2.2: $\Delta V - \Delta P$ characteristics and $\bar{W} - \Delta P$ characteristics of the PRO plant with respect to various concentrations on the draw shown in (a) and (b), respectively; $\Delta V - \Delta P$ characteristics and $\bar{W} - \Delta P$ characteristics of the PRO plant with respect to various flow rate on the draw shown in (c) and (d), respectively.

The performance with different membrane performance is studied in the literature [23, 81]. In this work, the operational conditions, namely the concentration and the flow rate of the salinities are taken into account to test the effectiveness of the proposed method. The concentration on the draw solution is changing during the PRO process, from seawater to the concentrated water. Figure 2.2 (a) and (b) illustrate the permeation-pressure ($\Delta \mathrm{V} - \Delta P$) characteristics and the power-pressure ($\overline{W} - \Delta P$) characteristics of the PRO model with respect to various concentrations on the draw. In Figure 2.2 (c) and (d), the process characteristic curves of PRO with different mass flow rates on the draw side is clearly indicated. The maximum power point is clearly observed from the $\overline{W} - \Delta P$ characteristics in (b) and (d).

2.4 Summary

This chapter presents the analytical model of the PRO system. Firstly, the mathematical modelling and theoretical analysis of a scale-up PRO process is detailed described in this section. The study explored the extractable energy per volume.

Based on the mathematical model, the extractable energy and average power density concepts for a scaled-up PRO model is evaluated which is suitable for capturing nonlinear behaviour of a scaled-up PRO discharge process. Based on a scaled-up PRO process, the non-linear characteristic of the PRO system is achieved and used to explore the osmotic energy efficiency. The energy efficiency and maximum power was investigated in a module-scale PRO system using specific energy extract(SEE), which is calculated by the extractable energy per volume. However, in a full-scaled PRO osmotic energy system, it cannot be used. The volumetric maximum energy is only suitable to low concentrated feed solution [79].

Therefore, the output energy of a full-scale model is developed analytically but encountered challenges in determining an accurate extractable energy [79]. Previous optimisation methods evaluated the extractable energy per volume, which cannot be utilised on a full-scale PRO process.

Chapter 3 Optimisation of a Pressure Retarded Osmosis process using Machine Learning for Maximum Energy Extraction

3.1 Introduction

In recent times, maximum power point tracking (MPPT) for the PRO system have been investigated using incremental mass resistance (IMR) and perturb & observe (P&O) methods [6, 25] widely used to ensure maximum energy harvesting from photovoltaic (PV) systems. The efficiency of a MPPT algorithm is rated using two main criteria: convergence speed and the obtained maximum power level. The less tracking time and higher extracted maximum power result in less power loss in the output, and vice versa. Faster tracking speed may also lead to more steady state oscillations. Both P&O and IMR algorithms have to find a balance between the oscillations and the response speed, which causes more power loss. Therefore, a robust and efficient MPPT method is required for a scaled-up PRO system. It is also observed that the authors in [6, 25] only optimised the hydraulic pressure in a scaled-up PRO system to enhance energy extraction. However, more controlled variables such as the flow rates on the draw side and feed side are also needed to be optimised to yield the maximum energy along the PRO module.

Machine learning based metaheuristic optimisation algorithms offer unique merits in enhancing performance of engineering methods and systems [83-86]. These include i) being nature-inspired, these algorithms result in simple concepts which can be employed easily; ii) they offer derivative-free optimisation method suitable to be used in a wide range of applications; iii) the population-based strategy of these algorithms results in the local optimal stagnation avoidance; iv) they are also well

suited to be implemented in multi-objective problems, for example, the multi-peak MPPT problem.

The Grey Wolf Optimisation (GWO) method, proposed in 2014 by Mirjalili and Lewis [82], is a metaheuristic algorithm inspired by the leadership pyramid mechanism in the hunting process of grey wolves in nature. Although GWO is a relatively new member of the metaheuristic algorithms family, it has attracted significant attention from the scientific community to design efficient control and optimisation techniques in engineering applications including MPPT design. For example, Sultana et. al. [83] used a GWO algorithm for the optimisation of system components in power plants. Later, a GWO algorithm was applied for a multi-objective problem in the electric power systems by Aziziyahed et. al. [84]. Researchers [83-85] proposed a GWO combined with Maximum Power Point Tracking (MPPT) algorithms for PV system. Also, a GWO is used to solve the MPPT problem in the Wind Turbine (WT) system [83]. However, GWO-based MPPT design for a PRO system has not yet been reported in the literature to utilise the unique merits of this optimisation mechanism in extracting the maximum power from a scaled-up PRO process.

The current study proposes a GWO based novel MPPT design for a scaled-up PRO system comprising multiple modules. The GWO was applied not only to identify the optimum hydraulic pressure but also to find the optimum feed and draw solution fractions in the mixture for a number of salinity gradient resources. Impact of adding PRO modules and concentration polarization on the energy yield in the PRO process was evaluated by the GWO. The optimum hydraulic pressure and feed and draw fractions in the mixture was obtained for each salinity gradient resource.

3.2 Grey Wolf Optimiser

The Grey Wolf Optimisation (GWO) is a metaheuristic method proposed by Mirjalili and Lewis [82]. It mimics the leadership hierarchy and the hunting process of the grey wolves in nature. The social dominant hierarchy includes three different types of grey wolves in GWO: the leader, namely α, the second level grey wolf, namely β and the third level grey wolf, namely γ. The grey wolf α is the leader of the navigation whereas α, β and γ are responsible for providing promising solutions.

The hunting and navigating behaviour for every grey wolf is the same. When the hunting mechanism is introduced in designing the GWO technique, three main characteristics of grey wolves are taken into consideration: tracking prey, encircling prey and attacking towards prey.

In the mathematical GWO model, the prey is considered as the optimum. The above hunting strategy is simulated as the optimisation process. The three-dominant hierarchy α, β and γ are considered as the best solution, the second fittest solution and the third fittest solution, respectively. The next move of the current search agent is decided based on the current best solution and the global best three candidate solutions α, β and γ.

3.2.1 Encircling mechanism

In the encircling model, the grey wolves encircle the prey during the hunting. The updating position is estimated with respect to $\overrightarrow{D_\iota}$, which is the distance between the position of the i^{th} searching grey wolves and the prey. This is an exploitation phase; the search agents sense the prey and start to encircle with a circular motion. The mathematic model of this motion is formulated as [82].

$$\overrightarrow{D_\iota} = |\vec{C}.\overrightarrow{X_\iota}(k) - \vec{X}(k)| \tag{3.1}$$

$$\vec{X}(k+1) = \overrightarrow{X_\iota}(k) - \vec{A}.\overrightarrow{D_\iota} \tag{3.2}$$

In which k is the current iteration. $\vec{A}$ and $\vec{C}$ donate coefficient vectors, $\vec{X}$ is the positon vector, $\overrightarrow{X_p}$ depicts the position vector of the prey. The coefficient vectors $\vec{A}$, $\vec{C}$ are calculated in each iteration as

$$\vec{A} = 2 * \vec{a}.\overrightarrow{r_1} - \vec{a} \tag{3.3}$$

$$\vec{C} = 2 * \overrightarrow{r_2} \tag{3.4}$$

$$\vec{a} = 2 - k * \frac{2}{iter} \tag{3.5}$$

where 'iter' is the maximum iteration. $\overrightarrow{r_1}$ and $\overrightarrow{r_2}$ are random vectors in [0, 1].

The position around the prey is adjusted based on the components $\vec{A}$ and $\vec{C}$. The purpose of the parameter $\vec{A}$ is emphasizing the searching phase and the attacking phase which is analyzed further in the following section. The random vector $\vec{C}$ is employed to define the weight of the prey in the interval [0,2]. This coefficient vector provides a stochastic behaviour during the optimisation. When the weight $\vec{C} > 1$, the effect of the prey is emphasized in calculating the distance between the prey and the search agent. In contrast if $\vec{C} < 1$, the effect is deemphasized.

The random parameters of GWO mentioned above is utilised to force search agents reach any location in the search space.

3.2.2 Searching and attacking phase

It can be obtained from equation (3.3) that the vector $\vec{A}$ is decreasing with the parameter $\vec{a}$ in $[-\vec{a}, \vec{a}]$. As previously discussed, this vector is used to emphasize the searching and attacking phase as Fig.3.1 depicts [82].

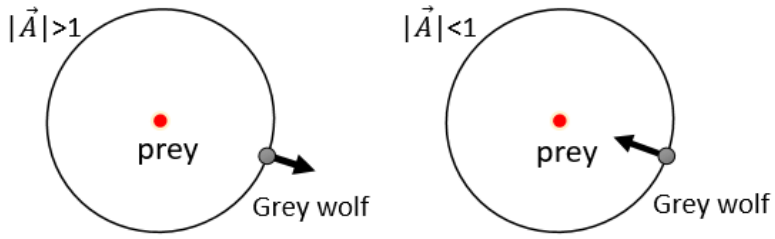

(a) (b)

Figure 3.1: Searching mode and attacking mode with respect to the vector $\vec{A}$

If the value of the coefficient parameter $\vec{A}$ is greater than 1 or less than -1, the next position of the current grey wolf is set to do the searching job stochastically as Fig.3.1(a) illustrates. The searching mode is an exploration phase which is very useful to avoid trap in the local solutions.

Consequently, when the absolute value of the coefficient vector $\vec{A}$ is less than 1, the current search agent converges to the prey and attack it as shown in Fig.3.1(b). The

coefficient parameter $\vec{a}$ is an iteration dependent value range in [0, 2] derived from equation (3.5). It linearly decreases from 2 to 0 during the iterations in order to mimic the grey wolf approaching the prey.

It is significant to point out that the operators, such as the coefficient vector $\vec{A}$ and $\vec{C}$, are utilised to assist solving the MPP tracking problems resulting in the local optima stagnation avoidance in the GWO-based MPPT algorithm. Furthermore, it can be implemented for the multi-peak control systems.

3.2.3 Hunting strategy

The hunting process is the main optimisation procedure. It is supposed that the three best searching wolves, namely α, β and γ have better knowledge about the prey position. Thus, the hunting behaviour of the grey wolves mainly depends on α, β and γ. Take the grey wolf α as an example, the position is updated by the following equations [82]:

$$\overrightarrow{D_\alpha} = |\overrightarrow{C_1}.\overrightarrow{X_\alpha}(k) - \vec{X}(k)| \tag{3.6}$$

$$\overrightarrow{X_1}(k+1) = \overrightarrow{X_\alpha}(k) - \overrightarrow{A_1}.\overrightarrow{D_\alpha} \tag{3.7}$$

The positions guided by β and γ follow the same regard. As mentioned above, the position of prey is defined by these three candidate positions which is the three best solutions of the problem obtained so far. In the next iteration, each grey wolf estimates the prey position and update its position randomly within a circle with respect to the potential location of the prey. The mathematical model of this hunting strategy are formulated in this regard [82].

$$\vec{X}(k+1) = \frac{\overrightarrow{X_1}(k+1)+\overrightarrow{X_2}(k+1)+\overrightarrow{X_3}(k+1)}{3} \tag{3.8}$$

It is important to point out that for each grey wolf, all the random parameters and the coefficient vectors are independent.

3.3 Grey Wolf based MPPT Application

3.3.1 Overview of the Proposed MPPT Method

The objective of the problem investigated in this section is the MPPT design which is specifically for a scaled-up PRO plant. Varying operating environment, such as the concentration and the flow rate of the saline water, yield different properties of the PRO system as illustrated in Fig. 3.2. The power generated from the PRO module come from HT and is sensed by the GWO-based MPPT controller. The controller is assumed to be able to sense the parameters including the instantaneous flow rate and concentration value from the PRO module. Then the MPPT algorithm is executed to generate the pressure signals to the HP. The high-pressure pump works on the draw solution and the pressure is assumed to be instantaneous values at this stage. In this work, the specific problem and the application of GWO for the MPPT design is clearly depicted in the following section.

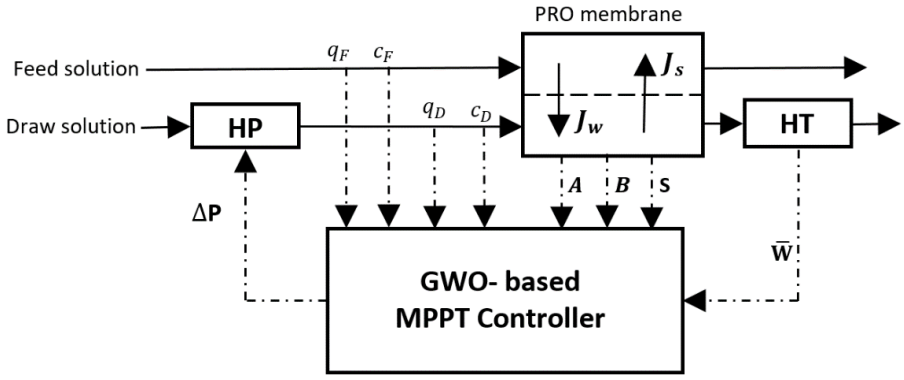

Figure 3.2: The operation of the PRO system with GWO algorithm

3.3.2 Problem Description

The maximization process is subject to the constraints as below. The problem is mathematically formulated as follows:

Consider: $x = [x_1 x_2, x_3]$

Objective function: $f(x) = \max(E(x))$

Constraints: $x \geq lower\ boundary$

$x \leq higher\ boundary$

3.3.3 Application of GWO in MPPT Design

The fitness function of the GWO algorithm is defined to find three best solutions values α, β and γ as

$$E\left((\vec{x})_i^k\right) > E\left((\vec{x})_i^{k-1}\right) \tag{3.9}$$

In the mathematical optimisation model, the solution of the current search agent is defined as

$$\overrightarrow{D_\alpha} = |\overrightarrow{C_1}.\overrightarrow{X_\alpha}(k) - \vec{X}(k)| \tag{3.10}$$

$$\overrightarrow{X_1}(k+1) = \overrightarrow{X_\alpha}(k) - \overrightarrow{A_1}.\overrightarrow{D_\alpha} \tag{3.11}$$

$$\overrightarrow{D_\beta} = |\overrightarrow{C_2}.\overrightarrow{X_\beta}(k) - \vec{X}(k)| \tag{3.12}$$

$$\overrightarrow{X_2}(k+1) = \overrightarrow{X_\beta}(k) - \overrightarrow{A_2}.\overrightarrow{D_\beta} \tag{3.13}$$

$$\overrightarrow{D_\gamma} = |\overrightarrow{C_3}.\overrightarrow{X_\gamma}(k) - \vec{X}(k)| \tag{3.14}$$

$$\overrightarrow{X_3}(k+1) = \overrightarrow{X_\gamma}(k) - \overrightarrow{A_3}.\overrightarrow{D_\gamma} \tag{3.15}$$

$$\vec{X}(k+1) = \frac{\overrightarrow{X_1}(k+1)+\overrightarrow{X_2}(k+1)+\overrightarrow{X_3}(k+1)}{3} \tag{3.16}$$

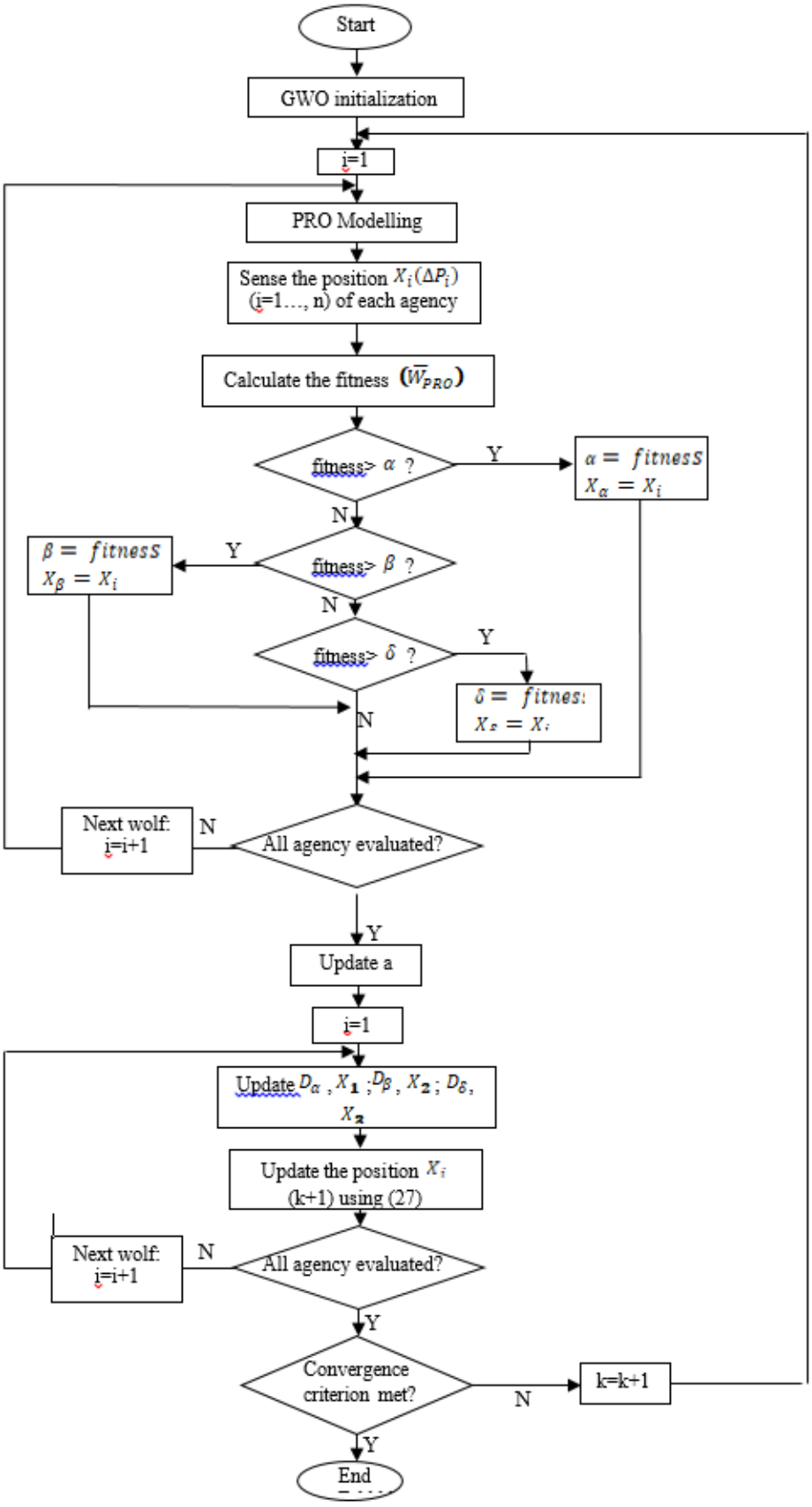

Figure 3.3: Flowchart of the proposed GWO-MPPT algorithm

The random parameter $\vec{C}$ is utilised to weight the distance between the search agent and the prey in [0,2]. The random coefficient vector $\vec{A}$ of GWO is decreasing as the decline of $\vec{a}$, which is employed to define the searching mode and the attacking mode. During the process, the correlated vector $\vec{a}$ declines following the equation

$$\vec{a} = 2 - k * \frac{2}{iter} \tag{3.17}$$

When the global optimum is reached, and hunting process finished, the parameter $\vec{a}$ is decreased to 0.

To sum up, the procedure of the implementation is as follows. First, the grey wolf algorithm is initialized. The PRO model is initialized. The initial fitness values are set to infinitely small. Then the loop starts. The position of the current grey wolf is updated according to the GWO algorithm with respect to the cost function (3.9) at each iteration. Then its fitness is updated and compared with the three candidate solutions. If the current fitness solution i^{i} is larger than the fittest solution α^{α}, both the fitness and the position of α are replaced by which of the current search agent. Similarly, if its fitness is less than the best solution but fitter than the second-best solution, the second-best solution β is replaced by the current grey wolf i. Consequently, the third best solution γ will be replaced if the current fitness is less than the solutions α and β but fitter than γ. All search agents are employed to find the global best three solutions in the search space. After this, α, β and γ as well as their corresponding positions are updated at each iteration. Finally, the GWO parameter is updated with regard of the GWO algorithm using equations (3.10)-(3.15). The probable prey position is estimated according to α, β and γ using equation (3.16). The process is then repeated with respect to the potential prey location obtained from the previous iteration. At the end of the iterations, the solution obtained by the leader grey wolf α is considered as the optimum solution in the GWO-MPPT design.

This GWO-based MPPT algorithm utilises multiple grey wolves to chase the prey position guided by the best three grey wolves. In other word, the hunting

(optimisation) of every search agent considers their own fittest solution as well as the best three fitness α, β and γ from the group. It is significant to point out that both $\vec{A}$ and $\vec{C}$ are generated stochastically, so they vary at each calculation. These random values which are generated over the course of iterations favours avoiding the local optima. For each study, the GWO algorithm was utilised on the problem and the statistical results obtained by the GWO-MPPT controller are reported.

3.4 Application of GWO to PRO Optimisation

GWO was applied for the optimisation of the PRO process and identifying the optimum operation conditions. For a given salinity gradient resource, hydraulic pressure and flow rates are the most critical operating parameters that affect the energy output of the process. These parameters were considered in the optimisation of the PRO process.

In the optimisation process for the full-scale PRO process, parameters implemented in the model are listed in Table 3.1.

Table 3.1: Selected parameters applied in a full-scale PRO system

Parameter	Symbol	Value
number of ionic species in solution	n	2
universal gas constant	**R**	8.314e-2J/mol K
Structural parameter	T	293K
distance	x	0.1m
mass transfer coefficient	k	0.0026 $m \cdot s^{-1}$
water permeation coefficient	Aw	1.23e-3 $L/m^2h.bar$
Membrane area	A_m	$24m^2$

3.4.1 Optimisation of Hydraulic Pressure

As reported in the literatures, the hydraulic pressure is the most critical operating parameter that controls the efficiency of the PRO process [8, 30]. Most studies agreed that the maximum power generation in the PRO process occurs at $\Delta P = \Delta\pi/2$ [8, 12]. However, this conclusion was based on a laboratory scale PRO unit or an ideal PRO system (ignoring the effects of concentration polarizations) [8]12]. We performed GWO optimisation to identify the optimum operating pressure for a PRO system comprising multi-modules packed in a pressure vessel and results were compared with a conventional PRO system. The assumptions made here are i) PRO module length is 1 metre and ii) 1 to 4 modules are packed in the pressure vessel. Energy output in the PRO system consisting of 1 to 4 PRO modules was calculated at $Q_F = Q_D$ and $\Delta P = \Delta\pi/2$ and compared with that of the optimised PRO system at $Q_F = Q_D$ and optimal ΔP. GWO results show 1 to 4.5% increase in the specific energy output was achieved by adjusting the hydraulic pressure (Figure 3.4). Most interestingly, maximum specific energy output occurred at a hydraulic pressure less than $\Delta\pi/2$ and that was for all salinity gradients (Figure 3.4A). It is also observed that the maximum specific energy increased by increasing number of the PRO modules (Figure 3.4B). Adding extra PRO modules improves the process of chemical potential conversion into a hydraulic energy and hence maximized the amount of energy yield from the salinity gradient resource.

Figure 3.4A shows that the optimum hydraulic pressure was 12 bar for 0.6M-0.02M salinity gradient and the number of PRO modules in the pressure vessel did not significantly affect it. For the rest salinity gradients, the optimum hydraulic pressure decreased with the increase of PRO modules in the pressure vessel. In a four-modules system, 5M-0.6M salinity gradient showed the largest difference in the hydraulic pressure between the optimised and unoptimised PRO process followed by 2M-0.02M, 5M-1.2M and 0.6M-0.02M salinity gradients, respectively.

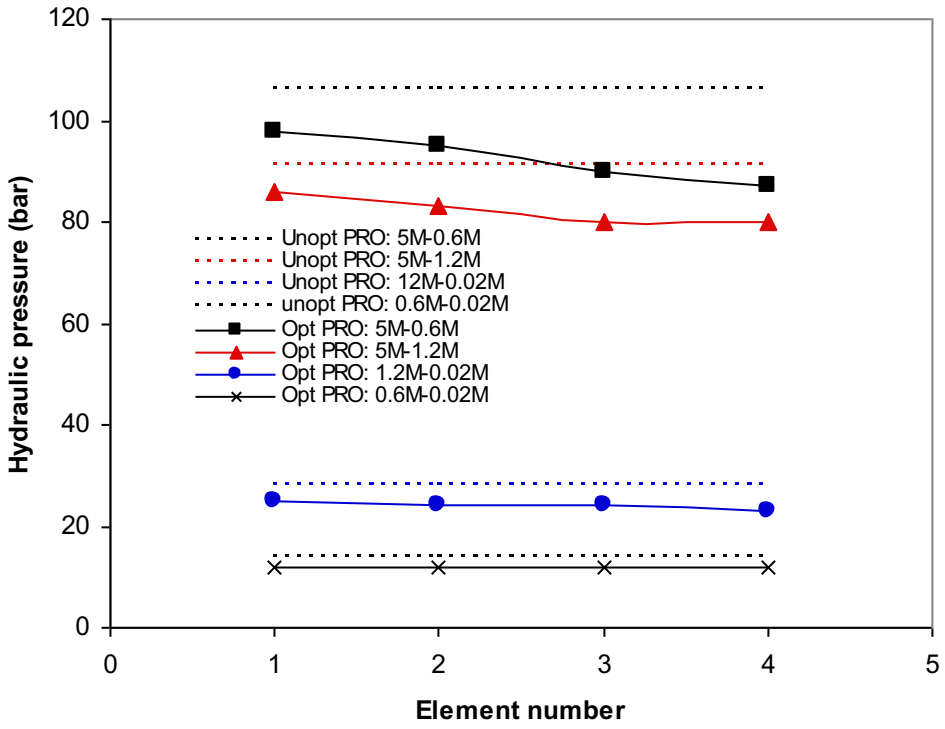
Hydraulic pressure (bar)
Element number
0
20
40
60
80
100
120
0
1
2
3
4
5
Unopt PRO: 5M-0.6M
Unopt PRO: 5M-1.2M
Unopt PRO: 12M-0.02M
unopt PRO: 0.6M-0.02M
Opt PRO: 5M-0.6M
Opt PRO: 5M-1.2M
Opt PRO: 1.2M-0.02M
Opt PRO: 0.6M-0.02M

(A)

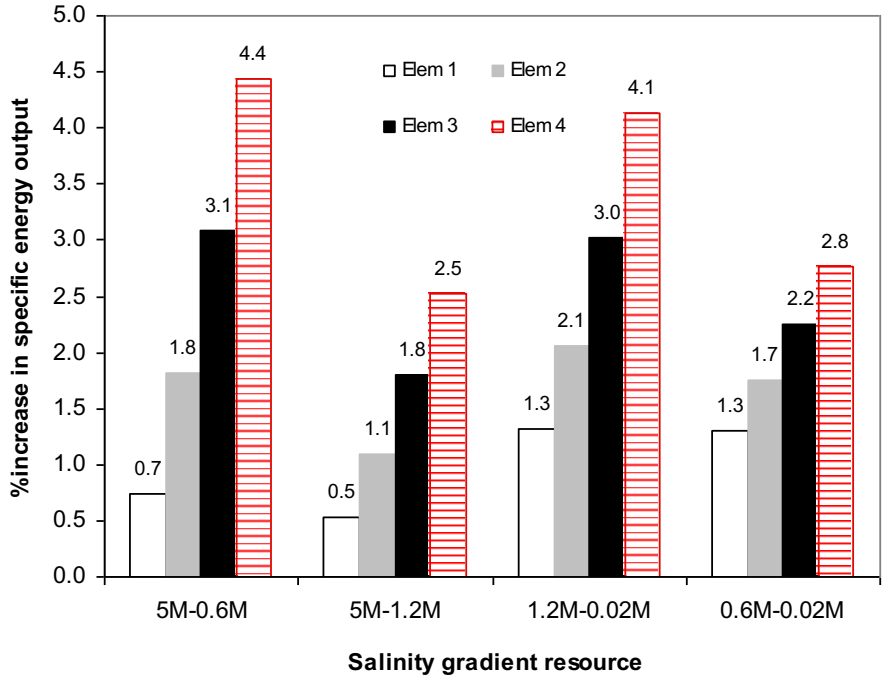

(B)

Figure 3.4: GWO optimisation of hydraulic pressure in the PRO process consisting of 1 to 4 modules in the pressure vessel A) hydraulic pressure in optimised PRO and PRO process B) percentage increase in specific energy output in the optimised PRO compared to PRO process. PRO element is 1 meter long, unoptimised PRO process operates at $\Delta P = \Delta\pi/2$.

For 5M-0.6M salinity gradient, the optimum hydraulic pressure in a PRO system consisting of four modules packed in series was 87 bar and the maximum specific energy output was 0.99 kWh/m^3. The corresponding hydraulic pressure and maximum specific energy output in the normal PRO process (without optimisation) were 106 bar and 0.94 kWh/m^3 respectively. The optimisation of the PRO process resulted in a slight improvement in the energy output (~4.5%) but there was also a tangible drop in the optimum operating pressure. In practice, this suggests that optimised PRO system require lower pressure and pumping energy than a normal system for operation. Furthermore, characteristics of the membrane, such as mechanical strength, are different in the optimised and unoptimised PRO process since the former is operating at lower hydraulic pressure. Experimental works demonstrated that a high hydraulic pressure promotes membrane fouling [85]; hence it can be reservedly assumed that the fouling propensity of the optimised PRO system would be also less than that of normal PRO system.

3.4.2 Optimisation of draw solution flow rate

Mixing ratio of feed and draw solutions has significant impact on the performance of the PRO process [30]. Elimelech and co-workers demonstrated that a maximum energy output in irreversible PRO process is achieved at 50% mixing ratio and a hydraulic pressure equal to $\Delta P = \Delta\pi/2$ [8]. The study ignored the effects of concentration polarization in the PRO module, which questions its applicability on field studies. Laboratory scale experiments demonstrated that performance of the osmotically driven processes were highly dependent on the flow rates of draw and feed solutions [30]. We performed a GWO process to determine the optimum flow rate of the draw solution that results in a maximum output in a non-ideal PRO process operated at $\Delta P = \Delta\pi/2$.

Figure 3.5 shows the optimum volumetric flow rate of the draw solution to maximize the energy yield of the PRO process. For all salinity gradients, the fraction of draw solution, θ_D, increased with the number of the PRO modules in the pressure vessel (Figure 3.5A). Technically, this is to offset the dilution of draw solution in subsequent PRO module and maintain permeation flow across the membrane. The optimum θ_D was less than 0.5 for all salinity gradients and number of PRO modules in the pressure vessel. This contradicts with the findings of previous studies that assumed an ideal PRO process (ignored concentration polarization) or the impact of feed and draw solution dilution and concentration, respectively, along the PRO module [8, 12, 89]. θ_D optimisation maximized the energy output in the PRO process as shown in Figure 4B. Compared of a normal PRO process, GWO maximized the specific energy output in the PRO process and resulted in up to 21.9% higher energy yield in the case of four modules 0.6M-0.02M salinity gradient (Figure 3.5B). Compared of an unoptimised PRO process, GWO maximized the specific energy output in the PRO process and resulted in up to 21.9% higher energy yield in the case of a single module and 0.6M-0.02M salinity gradient (Figure 3.5B). 0.6M-0.02M salinity gradient demonstrated the largest percentage increase in the energy yield due to process optimisation followed by 1.2M-0.02M, 5M-1.2M, and 5M-0.6M salinity gradient, respectively. Apparently, 5M-0.6M salinity gradient was less affected by the optimisation process than other salinity gradients with 9.9% increase in a single module PRO process. This was due to the significant osmotic pressure driving force in the 5M-0.6M PRO process, which rendered the increase of the draw solution flow rate less effective in enhancing the osmosis flux. Furthermore, the

optimisation process had insignificant impact on the energy output in a four-modules PRO process particularly for 5M-0.6M and 5M-1.2M salinity gradients. It is apparent from Figure 4A that θ_D values for 5M-0.6M and 5M-1.2M salinity gradients using four modules was 0.5 and 0.49, which make the operating conditions similar to that in an unoptimised PRO process. Optimisation process resulted in a 2.4% and 0.1% increase in the energy output in 0.6M-0.02M and 1.2M-0.02M salinity gradients, respectively. For a given salinity gradient, increasing the number of PRO modules results in a larger permeation flow. This requires a higher flow rate to compensate the dilution of draw solution and maintain water flux.

The results suggest that energy yield in the PRO process increases with the number of PRO modules (Figure 3.5C) because of the larger permeation flow. However, this depends on the quality of feed and draw solutions to avoid membrane fouling [88, 90]. Good pre-treatment is required to ensure the quality of feed and draw solutions in a closed-loop PRO process that recycles the draw and feed solutions. Larger water flux may cause the membrane fouling in osmotically driven membrane processes if the pre-treatment was insufficient in the removal of fouling materials. However, multi PRO modules can be used in series in the pressure vessel when the feed and draw solutions are of good quality or in a closed loop PRO process when the pure draw and feed solution are recycled.

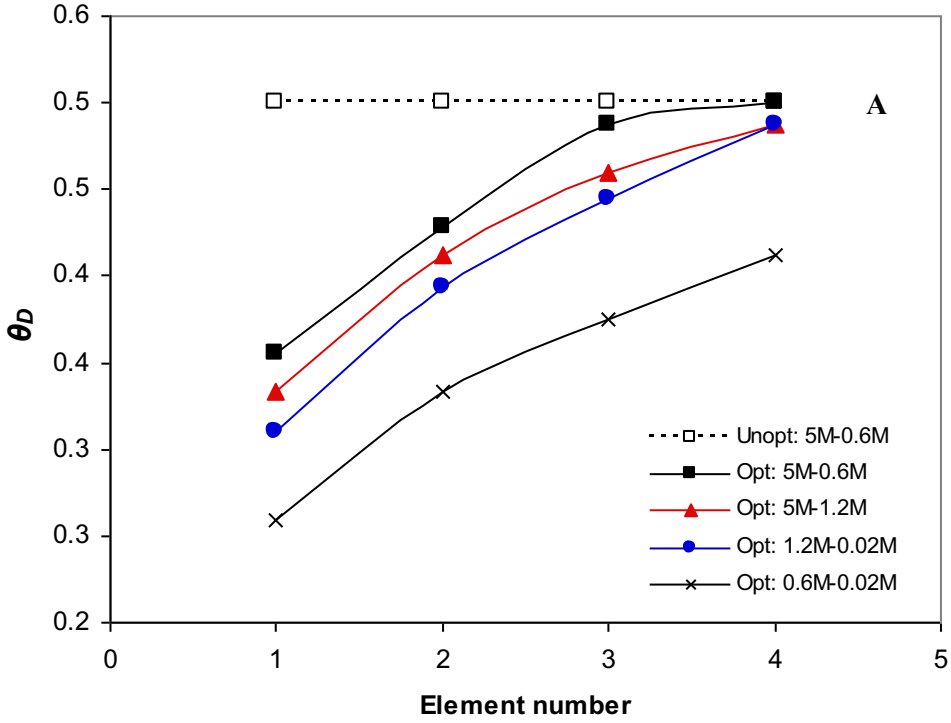
A
θD
Element number
Unopt: 5M-0.6M
Opt: 5M-0.6M
Opt: 5M-1.2M
Opt: 1.2M-0.02M
Opt: 0.6M-0.02M

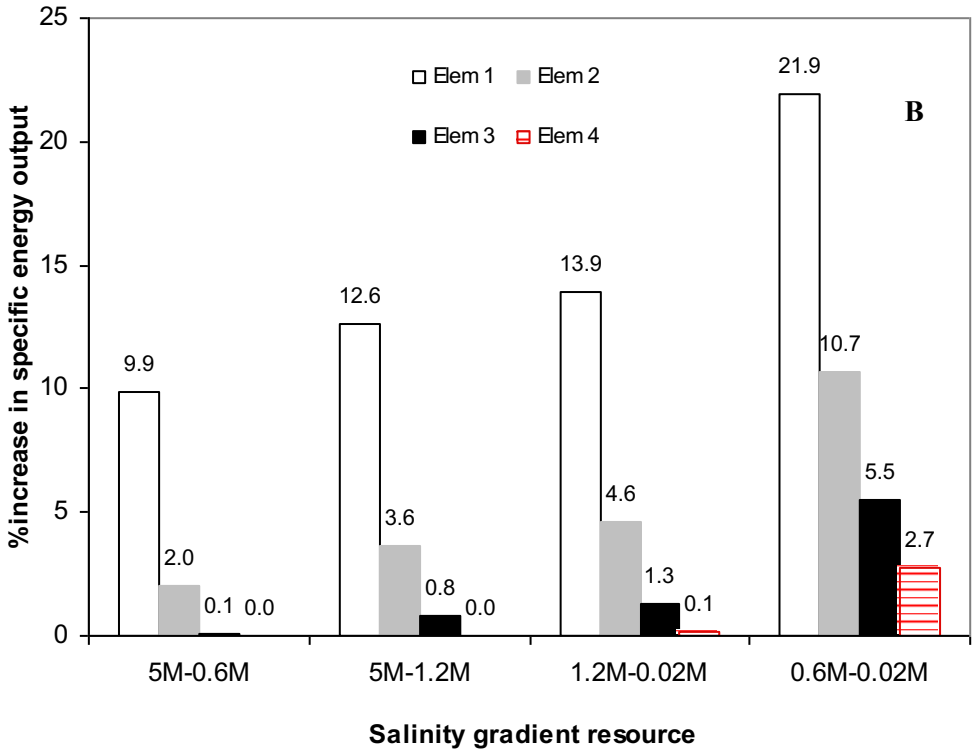
B
%increase in specific energy output
Elem 1
Elem 2
Elem 3
Elem 4
9.9
2.0
0.1
0.0
12.6
3.6
0.8
0.0
13.9
4.6
1.3
0.1
21.9
10.7
5.5
2.7
5M-0.6M
5M-1.2M
1.2M-0.02M
0.6M-0.02M
Salinity gradient resource

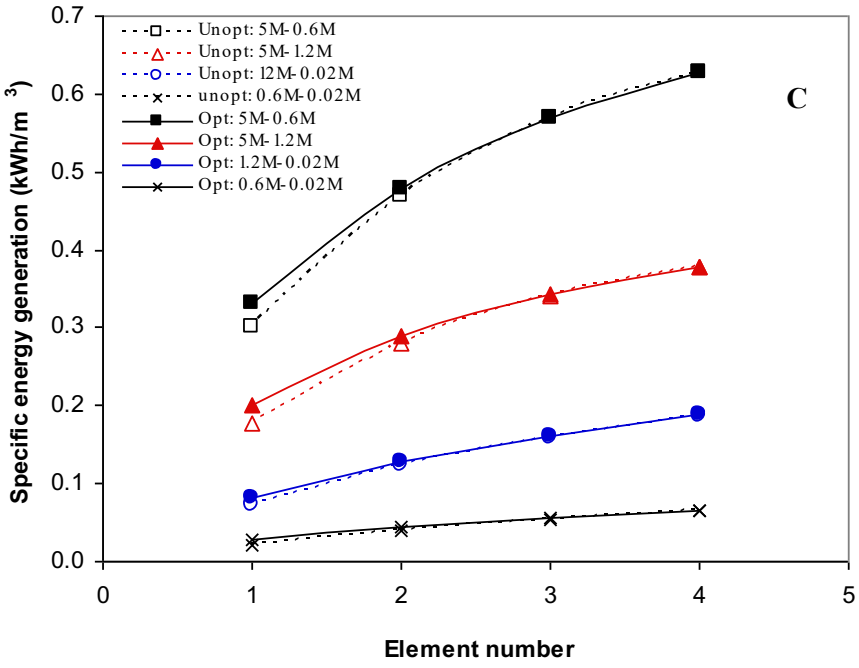

Figure 3.5: GWO optimisation of draw solution fraction in the PRO process A) optimised draw solution fraction θ_D, in PRO system consists of 1 to 4 elements B) percentage increase in specific energy in the optimised PRO compared to a normal PRO process C) impact of number of modules in the PRO process on the specific energy generation. PRO element is 1 meter long, hydraulic feed pressure is $\Delta P = \Delta\pi/2$.

3.4.3 Optimisation of feed solution flow rate

Feed solution is an important parameter that affects the performance of the PRO process. Recent studies demonstrated that ICP could be mitigated by changing the flow rate of feed solution [73]. Similarly, the volumetric flow rate of the feed solution needs to be optimised to maximize the energy output of the PRO process. The optimisation of feed solution flow rate was carried out using GWO method (Figure 3.6). Compared to unoptimised PRO operating at $\Delta P = \Delta\pi/2$and 0.5 feed solution fraction in the mixture, θ_F was less than 50% in the optimised process for all salinity gradient resources (Figure 3.6A). For 5M-0.6M and 5M-1.2M salinity gradients, θ_F increased with the number of PRO modules in the pressure vessel but was higher in the 5M-0.6M salinity gradient (Figure 3.6A). The optimised θ_F in the 1.2M-0.02M was equal to that in the 0.6M-0.02M salinity gradient but lower than that in the 5M-0.6M and 5M-1.2M salinity gradients. In fact, the optimised θ_F value was 9% in a single PRO module system and increased to 13% in two to four PRO modules system.

Optimisation of θ_F resulted in a considerable improvement in the energy output in the PRO process (Figure 3.6B). Between 9.4% and 70.2% higher energy yield was achieved in the PRO process due to the optimisation of θ_F. The maximum energy yield in the PRO process decreased with the number of PRO modules in the pressure vessel. This was probably due to the higher ICP effects in the subsequent PRO modules in the pressure vessel. The largest percentage increase in the specific energy was 70.2% in a single module PRO process and 0.6M-0.02M salinity gradient followed by 69%, 33.6% and 28.3% for 1.2M-0.02M, 5M-0.6M, and 5M-1.2M salinity gradient resource, respectively. 5M-1.2M salinity gradient had the lowest percentage of energy output increase due to θ_F optimisation because of the high concentration of feed solution. In contrast, 1.2M-0.02M and 0.6M-0.02M salinity gradients demonstrated a large improvement in the energy yield due to the low feed concentration that can be relatively easy to alleviate. Technically, ICP can be decreased by increasing the flow rate of the feed solution but it is less effective at high feed concentrations due to the intensive ICP. θ_F optimisation has a greater impact than θ_D on the extractable specific energy from salinity gradients. Therefore, in the optimisation process of the PRO the impact of θ_F on the specific energy generation should to be considered seriously.

θ_F optimisation increased the energy output in the PRO process. The maximum specific energy generation in four modules PRO process was 0.73, 0.41, 0.29, and 0.098 kWh/m^3 for 0.5M-0.6M, 5M-1.2M, 1.2M-0.02M, and 0.6M-0.02M salinity gradients, respectively. The corresponding θ_F ratios were 31, 35, 13, and 13%, respectively (Figure 3.6C). Theoretically, it was possible to use low feed flow rates in order to maximize the energy output but that will strongly depend on the quality of feed solution and the pre-treatment method.

The results show that θ_F was more effective than θ_D to improving the specific energy output in the PRO process due to the complicated nature of the ICP that occurs in the support layer and affect the permeation flow in the PRO process [4, 87]. Mitigation of ICP is possible through increasing the feed flow rate as indicated in recent studies [30, 76]. Furthermore, comparing Figures 3.5A and 3.6A shows that θ_F was lower than θ_D for all salinity gradient resources; i.e. lower feed to draw solution ratio. At low θ_F ratio, the concentration of draw solution would be sufficiently highly in the subsequent PRO modules to maintain the permeation flow

and specific energy generation. Using low feed flow rates, however, is not always practically feasible and it depends on the quality of feed solution. With low quality feed flow rates, the propensity of membrane fouling would be high and there is a risk to apply low feed flow rates. Though, it is possible to apply low feed flow rates in a closed-loop PRO process in which a pure feed and draw solutions are recycled in the PRO process or when good pre-treatment facilities are available.

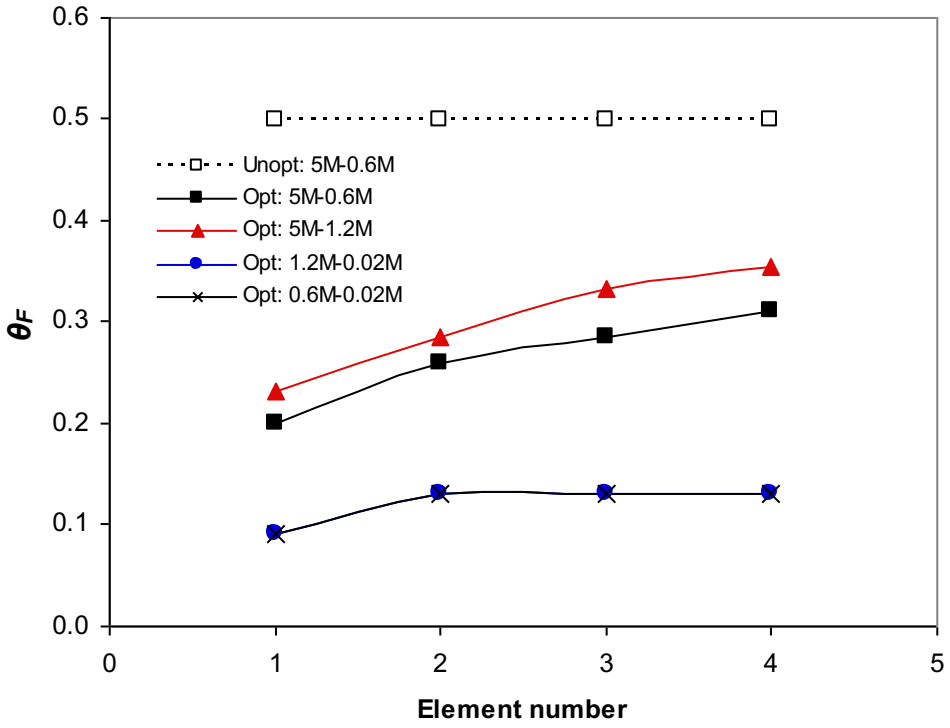

A

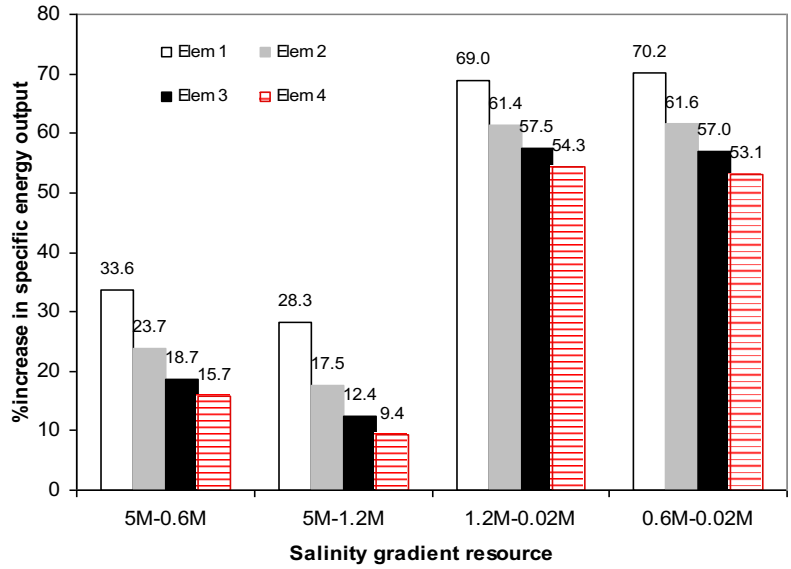

B

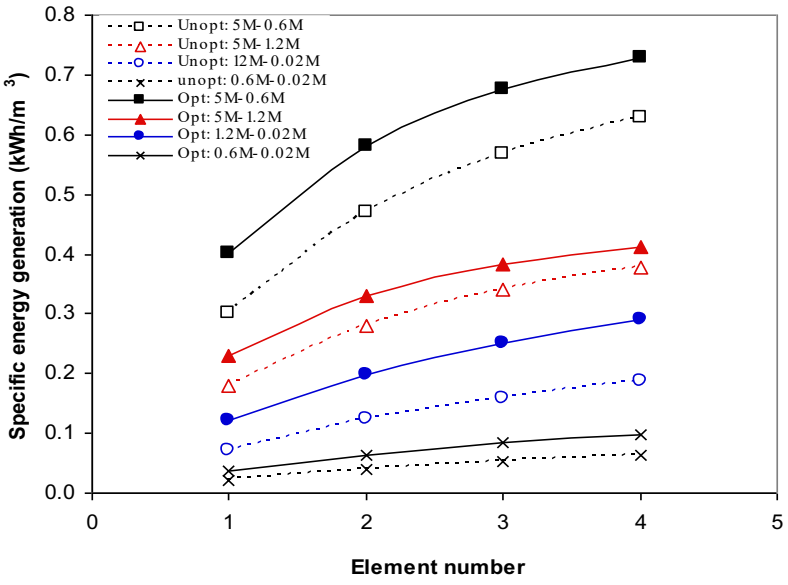

C

Figure 3.6: Optimisation of feed flow rate, θ_F, in PRO system consists of 1 to 4 elements A) optimised feed solution fraction θ_F, in PRO system B) percentage increase in specific energy in the optimised PRO compared to a normal PRO process C) impact of number of modules in the PRO process on the specific energy generation. PRO element is 1 meter long and all results were obtained at $\Delta P = \Delta\pi/2$.

3.4.4 Optimisation hydraulic pressure and feed flow rate

Results reveal that the optimisation of θ_F was more effective than θ_D in improving the specific energy generation in the PRO process. Therefore, results from section 3.2 were further evaluated to determine the optimum hydraulic pressure in the PRO process. Optimisation was performed for all salinity gradient resources using the optimum θ_F from section 3.2 and the optimum hydraulic pressure was obtained in PRO processes consisting of one to four modules in the pressure vessel (Figure 3.7). Results in Figure 3.7A show that the specific energy generation increased with the number of modules in the optimised PRO process and was higher than that in the unoptimised PRO process. The maximum specific energy generation in an optimised PRO process consisting of four modules was 0.75, 0.42, 0.29, 0.10 kWh/m^3 for 5M-0.6M, 5M-1.2M, 1.2M-0.02M, and 0.6M-0.02M salinity gradients, respectively. This was 11.6% to 58.2% higher than the specific energy that can be harvested from the same salinity gradients in unoptimised four-modules PRO processes (Figure 3.7B).

Figure 3.7C shows that the percentage increase of the specific energy generation decreased with the number of modules in the PRO process. For example, there was 45% increase of the maximum energy generation from 5M-0.06M salinity gradient by increasing number of modules from 1 to 2 modules (Figure 3.7A). Adding a third PRO module, however, resulted in 17% increase in the energy generation while increasing the number of PRO modules to four brought out only 9% increase in the energy generation. Furthermore, the optimised PRO process was operated at a hydraulic pressure lower than $\Delta P = \Delta\pi/2$ that is recommended in an unoptimised PRO process (Figure 3.7C). The optimum hydraulic pressure predicted by GWO was 2.2 to 16 bar lower than $\Delta P = \Delta\pi/2$ and always decreases with the number of modules in the PRO process (Figure 3.6C). The optimum pressure for 5M-0.6M salinity gradient was decreased from 100 bar to 89 bar as the number of modules increased from 1 to 4 modules. Compared to an unoptimised PRO process operated at 106 bar, an optimised PRO process consisting of 4 modules required 16% less hydraulic pressure. 5M-0.6M salinity gradient with four PRO modules demonstrated the largest decrease in the operating pressure, from 106 to 89 bar, followed by 0.6M-0.02M, 1.2M-0.02M, and 5M-1.2M salinity gradient, respectively. For 0.6M-0.02M and 5M-1.2M salinity gradients, there was no change in the optimum operating pressure when the number of modules decreased from 4 to 3 modules. As mentioned

before, reducing the operating hydraulic pressure would reduce the size of high-pressure pump and pumping energy. Practically, the net energy output in the PRO process should account for all energy input that includes pumping and pre-treatment energy of feed and draw solutions.

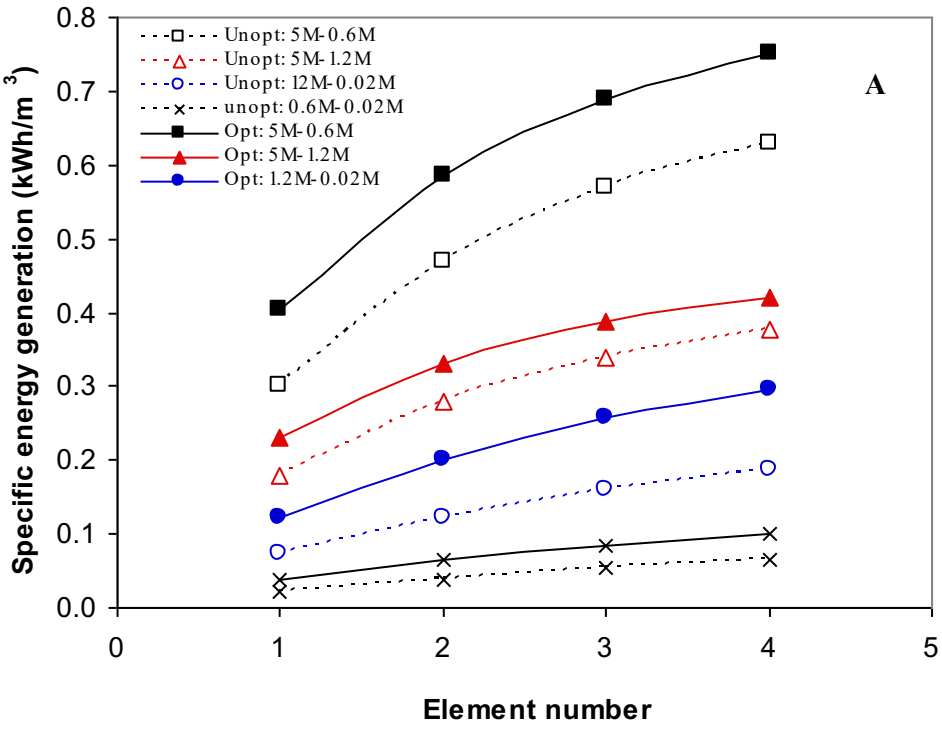

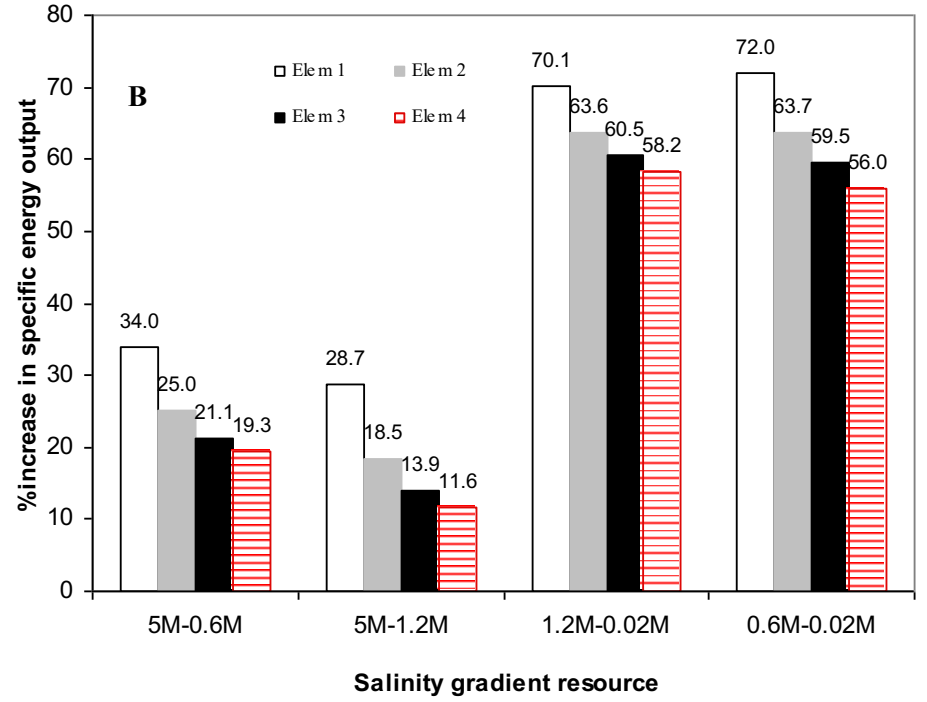

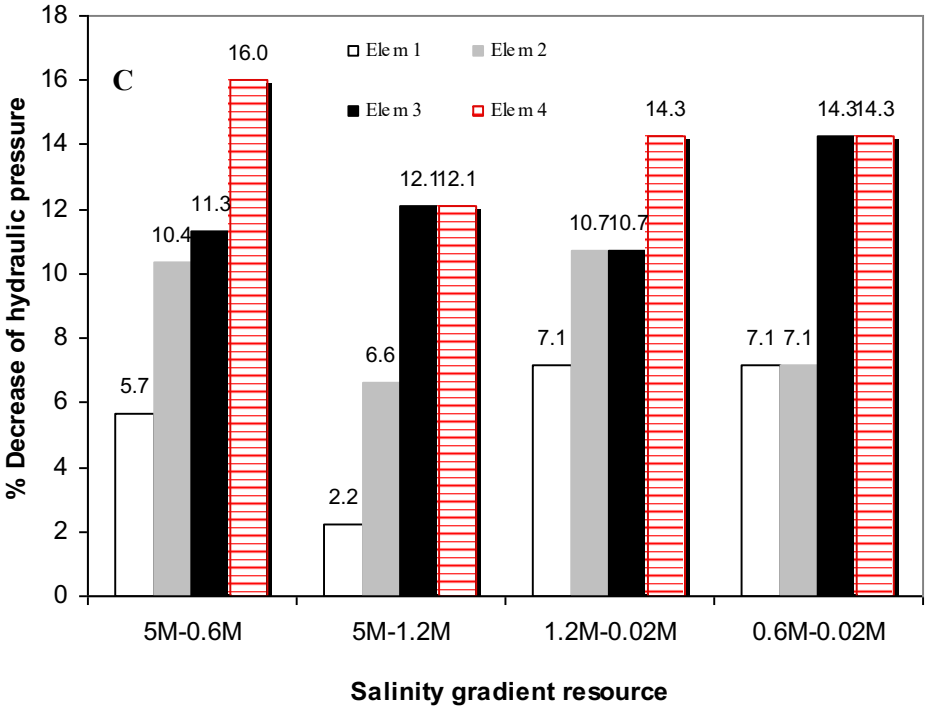

Figure 3.7: Optimisation of hydraulic pressure, ΔP, in PRO system consists of 1 to 4 elements A) impact of number of PRO modules on the specific energy generation B) percentage increase in specific energy in the optimised PRO compared to a normal PRO process C) optimised hydraulic pressure in the PRO process compared to a normal PRO process. PRO element is 1 meter long, results are already optimised for feed flow rate fraction, θ_F.

3.4.4 Application of Whale Optimisation to PRO

Another nature-inspired metaheuristic technique called Whale Optimisation with Differential Evolution algorithm is introduced and compared in Chapter 4. The above optimisation performances and results are double confirmed using whale optimisation algorithm. All of the optimal values in this chapter are validated by whale optimisation methods.

3.5 Net power generation in optimised PRO process

Net power generation in the PRO process is, normally, less than the amount of energy output from the process since there is an energy incurred for the pretreatment of feed and draw solution, pumping, and loss in the pressure exchanger (PX). Thermodynamically, energy input in a feasible PRO process should be less than the energy output. The amount of energy input varies and depends on the type of salinity gradient resources. Previous works identified the amount of energy required for pretreatment, pumping from source, pumping into the module and lost in the PX [4, 91]. In general, the specific energy for the pretreatment of Dead Sea (5M NaCl) and seawater (0.6M NaCl) is 0.3 kWh/m^3 [4], [91-92]. Wastewater effluent requires a minimum pretreatment with estimate power consumption equal to 0.1 [4**,** 93]. ROb (1.2M) is already pretreated for the RO process and hence no further pretreatment is required in the PRO process [4]. Previous studies suggested that pumping from the source to the PRO plant consumes **0.03** kWh/m^3, assuming 1 bar pumping pressure [91]. Studies also proposed that ROB is slightly pressurized when it leaves the energy recovery device and hence does not require an extra energy for pumping from the source to the PRO plant [4], [88]. There is also a small energy equal to 0.05 kWh/m^3 for pumping the feed and draw solution into the PRO module [4]. Furthermore, there is an energy loss in the PX, which operates at 98% efficiency. This energy varies from a salinity gradient to another and it depends on the operating pressure [4].

Table 3.1 shows the energy input in the PRO process represented by pre-treatment, pumping from source, pumping in module, and loss in PX in the optimised and unoptimised PRO process. The total energy input in the optimised PRO process was slightly lower than that in the unoptimised process due to the lower operating

pressure in the former process (Table 3.1). In practical terms, this will reduce operating and capital cost of the PRO process since the high-pressure pump and membrane are made to lower specifications. Table 3.2 shows that the net energy output in the optimised PRO process consisting of four modules in the pressure vessel is higher than that in the unoptimised PRO process. The energy output was 67% higher in the optimised 5M-0.6M PRO process compared to the unoptimised PRO process; 0.32 kWh/m^3 and 0.191 kWh/m^3, respectively. 5M-1.2M salinity gradient showed 14.5% increase in the energy output upon the optimisation. For 1.2M-0.02M, the net energy output was almost doubled in the optimised PRO process compared to unoptimised PRO process. Unfortunately, 0.6M-0.02M salinity gradient requires more energy input than output for both optimised and normal PRO process and hence I may be unsuitable for the PRO process.

Table 3.2**:** Net energy generation in the optimised and normal (unoptimised) PRO processes

Process Description	*Energy kWh/m^3*			
	5M-0.6M	**5M-1.2M**	**1.2M-0.02M**	**0.6M-0.02M**
Pretreatment	0.3	0.15	0.05	0.225
Pumping from source	0.03	0.015	0.015	0.03
Pumping in module	0.05	0.05	0.05	0.05
Loss in PX (unopt)	0.059	0.051	0.016	0.008
Loss in PX (opt)	0.050	0.04	0.01	0.007
Total energy input (unopt)	0.439	0.266	0.131	0.313
Total energy input (opt)	0.43	0.255	0.125	0.312
Energy output (unopt)	0.63	0.38	0.19	0.064
Energy output (opt)	0.75	0.42	0.30	0.1
Net Energy output (unopt)	**0.191**	**0.144**	**0.059**	**-**
Net energy input (opt)	**0.32**	**0.165**	**0.175**	**-**
%Diff in net energy	**67.5**	**14.5**	**200%**	
Pressure bar (unopt)	106	91	28	14
Pressure bar (opt)	89	80	24	12

In general, optimisation of the operating parameters effectively improved the energy output in the PRO process. Depending on the type of the salinity gradient recourse, optimisation of the PRO process resulted in up to 200% increase of the energy output. Furthermore, the optimised PRO process can be operated at hydraulic pressures lower than that in the unoptimised PRO process. The results also revealed that the operating pressure and mixing ratio of feed or draw solution in the mixture to achieve a maximum energy output in a full scale optimised PRO process are different to that in a laboratory scale PRO unit or an ideal PRO process. As such, the optimum pressure of $\Delta P = \Delta\pi/2$ and feed or draw solution fraction of 50% in the mixture is only valid for a laboratory scale PRO unit or an ideal PRO process. It is noteworthy that upon using low feed flow rates as suggested by the GWO caution should be paid as membrane fouling may occur. However, such concerns are less likely in a closed-loop PRO process or when the pretreatment process is well designed.

3.6 Summary

In a full-scale PRO system, the study evaluated the performance of the PRO process using GWO method to optimise key operating parameters for a number of common salinity gradient resources. The optimised PRO process demonstrated a higher energy output increase from 14.5% to 200% compared to the unoptimised PRO process. This shows the significance of performing process optimisation in engineering fields. The study revealed that the optimum operating pressure and mixing ratios in the laboratory-scale PRO process are not valid in an ideal and full-scale PRO process. The optimised PRO process can be operated at lower pressure and feed or draw solution fractions in mixture than an ideal PRO system. The energy output in the PRO process also increased with increasing the number of the PRO module from 1 to 3 modules but a slight improvement in the energy output was achieved by adding a fourth module. Most of the investigated salinity gradients showed potential for commercial applications apart from 0.6M-0.02M because of the insufficient energy generation. The study also reveals the importance of applying machine learning approaches such as GWO method in the optimisation of engineering systems.

Chapter 4 Enhanced Energy Extraction from a scaled-up Pressure Retarded Osmosis process with a Whale Optimisation based Maximum Power Point Tracking

4.1 Introduction

As stated in chapter 1, the MPPT strategies that have been proposed to improve the efficiency of the PRO module include the Perturb & Observe (P&O), the Incremental Mass Resistance (IMR) and the Mass Feedback Controller (MFC) method [6]. Similar to the P&O methods for the PV system, the P&O for PRO system introduces a perturbation in the draw solution pressure of the PRO system. However, it results in oscillations at the maximum power point (MPP) due to the variations in the perturbations around the MPP. The IMR was subsequently proposed to reduce the oscillation as well as the power loss by calculating the slope of the PRO power curve. The idea was inspired by the Incremental Conductance (IC) technique for the PV system [25]. The performance of the PRO system using IMR depends on the incremental pressure. The merit of the IMR method is that it is more flexible and stable compared to the P&O method. Yet the accompanying oscillations persist. Furthermore, a feedback control-based technique, the MFC was proposed to improve the efficiency of energy extraction from a PRO system. Inspired by the PID controller, the MFC is implemented to minimize the error of the power slope. The weighted sum of both the slope and the change of the slope is utilised to determine the error, resulting in fast convergence and lower power loss. The challenge is to balance three designed PID gains under the disturbances and uncertainties from the system. When the system encounters the variation in the operating environment such as salinity and temperature, the IMR method may present low robustness. Therefore, there is a need for a novel and robust MPPT controller for a PRO process that can

offer (i) no or very limited oscillations at the maximum power point, (ii) more flexibility and stability in the face of disturbance and uncertainties, and (iii) faster convergence and less power loss. The controller also needs to be easy to design and implement for a scaled-up PRO system. It is noted that in a PRO based osmotic power plant, under rapidly changing salinity and operation conditions, the need for a trade-off between oscillation and the tracking speed is an unavoidable complication that reduces the efficiency of the overall system significantly. Therefore, the MPPT method will require to find the global maximum power point as fast as possible.

With these in view, a novel MPPT control method for a scale-up PRO process is designed in this work based on the Whale Optimisation with Differential evolution (WODE) algorithm proposed by Mirjalili et al. [26] and is known as the Whale Optimisation Algorithm (WOA). This algorithm uses an evolutionary computing approach inspired by the hunting strategy of humpback whales in the ocean and is able to handle the non-linear objective functions and performs well as an optimising tool for the design of closed loop control systems. To design the MPPT controller for a PRO plant, based on this algorithm, first the permeation-pressure ($\Delta V - \Delta P$) relations and the average power density-pressure ($\overline{\mathrm{W}} - \Delta P$) characteristics of the PRO process, including the primary detrimental effects, is studied. Then the WODE algorithm, developed on the basis of humpback whales' unique bubble-net feeding behaviour during hunting, is introduced and modelled. Finally, the WODE-based MPPT controller is implemented on a scaled-up PRO process and its performance is assessed through a sequence of simulation-based study.

The developed WODE-based MPPT controller is found to be able to track the best-peak position in a few steps with oscillation-free convergence. Additionally, the controller requires fewer iterations, converges faster and has less computational burden owing to fewer search particles being needed to find the best solution. This has resulted in lower steady state oscillation as well as less power loss in the output. The findings are found to be in conformity with that of the WODE-based MPPT methods in the case of PV [27, 28]. The developed method is easy to implement on a scaled-up PRO process with various physical constraints and salinity profiles. Moreover, the development of the proposed method for a scaled-up PRO process indicates that the method is suitable to be implemented on PRO processes of different sizes.

4.2 Whale optimisation with differential evolution algorithm

4.2.1 Mathematic Model of the Whale Optimisation Algorithm

The WODE imitates the unique hunting mechanism of humpback whale's bubble-net feeding behaviour in the ocean, which is a meta-heuristic method proposed by Mirjalili and Lewis and is represented in Figure 4.1 [26].

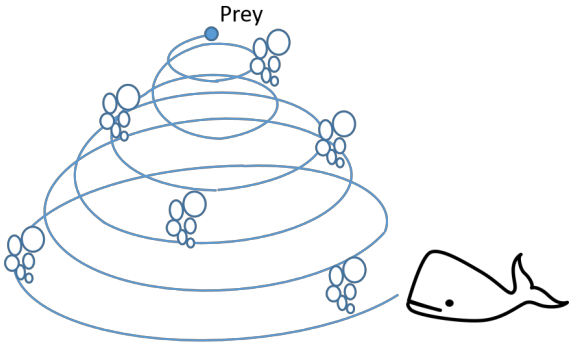

(a)

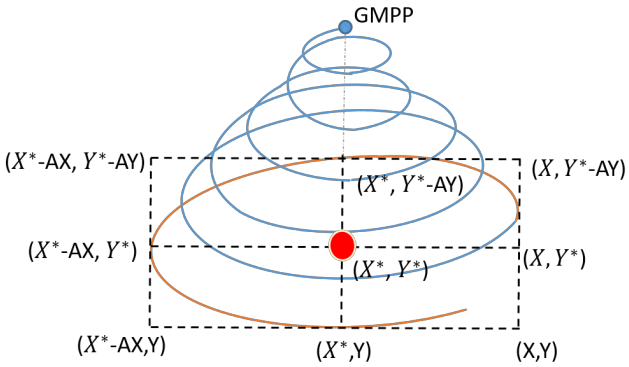

(b)

Figure 4.1: (a) The humpback whale's bubble-net feeding behaviour; (b) Strategy of a whale during hunting process.

In the mathematical model of the WODE, the search agents are considered to be the whales. In each iteration, all search agents find the fittest solution within the constraints in the same way as the whales find the prey during hunting. The fitness function comes from the PRO model aiming to tracking the maximum power point.

Figure 4.1 shows the bubble-net behaviour of the whales when they swim around the prey, namely upward-spirals and the double-loop behaviour which consist of a spiral model and the encircling model, respectively. These two phases are utilised to design the WODE for performing optimisation. Figure 4.1 (b) illustrates a simple rationale of the hunting strategy in the research space. In which $\mathbf{X}^*$, $\mathbf{Y}^*$ denote the current best position of a search agency. GMPP is the global maximum power point. The spiral position model and the encircling model are both constantly updated. The two differential evolutions of the whale optimisation are introduced in the following sections.

4.2.2 Spiral Model

In the spiral model, the whale swim along a helix-shaped path as Fig.3 (a) shows. The spiral updating position is estimated with respect to D_i', which is the distance between the location of the search agent and the prey. This is an exploitation phase, the global best prey is already sensed by the current searching whale with a circular motion. The mathematic model of this motion is formulated as [26]

$$\overrightarrow{D_i'} = \left|\overrightarrow{X^*}(k) - \vec{X}(k)\right| \tag{4.1}$$

$$\vec{X}(k+1) = \overrightarrow{D_i'}.e^{bl}.cos(2\pi l) + \overrightarrow{X^*}(k) \tag{4.2}$$

Where $\overrightarrow{X^*}, \overrightarrow{Y^*}$ denote the current best position of a search agent, b is a constant value, i is a random constant in [-1, 1] and $\overrightarrow{X^*}(t)$ specifies the current global best position**.** The hunt is usually guided by the best positions achieved so far.

4.2.3 Searching Mechanism

As the whale swims around the prey within a shrinking circle, two phases including: the exploration phase and the exploitation phase [26]. These two phases are determined by a coefficient vectors $\vec{A}$**.** If $|\vec{A}| \geq \mathbf{1}$**,** the performance is utilised to emphasize the global search as the whale move far away from the reference position. In contrast, the vector $|\vec{A}| < 1$ indicates the shrinking encircling movement. In the exploration phase, the whales perform a global search randomly. The position can be updated by the following equations [26]:

$$\vec{D} = |\vec{C}.\overrightarrow{X_{rand}} - \vec{X}| \tag{4.3}$$

$$\vec{X}(k+1) = |\overrightarrow{X_{rand}} - \vec{A}.\vec{D}| \tag{4.4}$$

In (4.1) k is the current iteration. $\vec{A}$, $\vec{C}$ and $\vec{D}$ represent coefficient vectors, $\vec{X}$ is the positon vector, $\overrightarrow{X_{rand}}$ is a random position vector (a random whale) from the population. The coefficient vectors $\vec{A}$, $\vec{C}$ are updated in each iteration [26]

$$\vec{A} = 2\vec{a}.\overrightarrow{r_1} - \vec{a} \tag{4.5}$$

$$\vec{C} = 2\overrightarrow{r_2} \tag{4.6}$$

$$\vec{a} = 2 - t * \frac{2}{iter} \tag{4.7}$$

where 'iter' is the maximum iteration. The value of the coefficient vector $\vec{a}$ is linearly decreased from 2 to 0 as (4.7) depicts. r_1 and r_2 are random vectors in [0, 1]. The positions around the prey are adjusted based on the values of $\vec{A}$ and $\vec{C}$.

4.2.3 Encircling Mechanism

When the coefficient value $|\vec{A}| < 1$, the current searching agent recognize the prey and start the exploitation phase. The current best prey is known to it and force the whale towards to this global best prey instead of a random prey. Therefore, (4.8) and (4.9) can be modified as follows [26]:

$$\vec{D} = \left|\vec{C}.\overrightarrow{X^*}(k) - \vec{X}(k)\right| \quad (4.10)$$

$$\vec{X}(k+1) = \left|\overrightarrow{X^*}(k) - \vec{A}.\vec{D}\right| \quad (4.11)$$

The new position of a search agent is updated with respect to the best solution obtained at the current iteration. The two phases of the humpback whales go simultaneously. Thus, the probability of each phase is considered as 50%. During the optimisation, the position is updated as follows:

$$\vec{X}(k+1) = \begin{cases} \overrightarrow{D_i'}.e^{bl}.cos(2\pi l) + \overrightarrow{X^*}(k), & \rho < 0.5 \\ \left|\vec{X}(k) - \vec{A}.\vec{D}\right|, & \rho > 0.5 \end{cases} \quad (4.12)$$

where ρ is a random constant in [0, 1].

4.3 The Proposed WODE-based MPPT Method

4.3.1 Problem Description

The objective of this problem is to maximum the total cost (average power density) of the PRO module. The WODE is then be equipped with a constraint handling method. It is challenging because the fitness function directly effects the updating position of the search agents. The optimum design must satisfy constraints on the searching domain.

The design variable is the actuated pressure (Δp). The optimisation problem is formulated as follows:

Consider $\vec{x} = [x_1] = [\Delta p]$,

Maximum $f(\vec{x}) = f(\Delta p) = \overline{W}(\Delta p)$

Variable range $\Delta p_{min} \leq \Delta p \leq \Delta p_{max}$

where Δp represents the pressure of the high-pressure pump, $\overline{W}(\Delta p)$ specifies the average power density of the PRO module.

This optimisation problem was solved by He et al.[6, 25] with an improved P&O controller and also by employing a PID controller. The proposed WODE was employed on this problem, the optimisation results are provided in the following section.

4.3.2 Application of WODE for MPPT Design

WODE is a metaheuristic method inspired by hunting strategies adopted by whales. The whales search the best position within a range of variables, while the differential evolution (DE) enhances the performance of the search. The block diagram of the proposed WODE-based MPPT design for the PRO system is shown in Figure 4.2 [6]. At every time interval, variables of the PRO system such as the membrane states, the concentration and the flow rate of the saline water are sensed by the MPPT-WODE controller. To implement the WODE-based nature-inspired MPPT method, the MPPT controller evaluates the average power density extracted from the hydro-turbine (HT) and actuates the hydraulic pressure. The actuated pressure ΔP is playing the same role as a whale. The target pressure transition on the draw solution can be obtained by the variable frequency drive [95, 96]. In the proposed method, WODE is combined with the direct instantaneous hydraulic pressure with the MPPT controller.

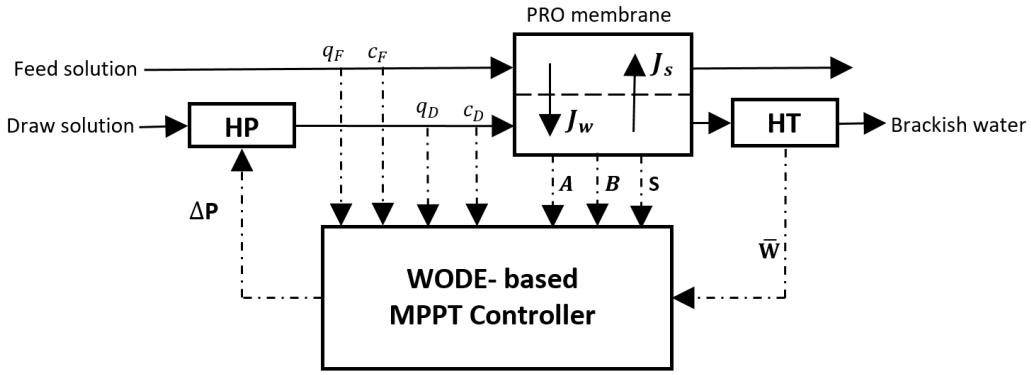

Figure 4.2: The operation of the PRO system with WODE algorithm

At the spiral moving stage, the whale i swimming around the best solution is expressed as the following equations [26]:

$$D_i' = |\Delta P_i^*(k) - \Delta P_i(k)| \tag{4.13}$$

$$\Delta P_i(k+1) = D_i'.e^{bl}.cos(2\pi l) + \Delta P_i^*(k) \tag{4.14}$$

where i donates the number of the current whale. D_i' represents the distance between the whale i and the best solution at the current iteration.

During the exploration phase, the whale i searches for the best solution with the following equations:

$$\mathrm{D} = |C.(\Delta P_i)_{rand} - \Delta P_i(k)| \tag{4.15}$$

$$\Delta P_i(k+1) = |(\Delta P_i)_{rand} - \mathrm{A.D}| \tag{4.16}$$

Similarly, when the whale i encircling the best solution at the exploitation phase, the mathematic model is defined as[26]

$$\mathrm{D} = |\mathrm{C}.\Delta P_i^*(k) - \Delta P_i(k)| \tag{4.17}$$

$$\Delta P_i(k+1) = |\Delta P_i^*(k) - \mathrm{A.D}| \tag{4.18}$$

Consequently, the fitness function of the WODE algorithm is defined as

$$\bar{W}(\Delta p)_i^k > \bar{W}(\Delta p)_i^{k-1} \tag{4.19}$$

When the MPP is found by the search agent, the correlated coefficient vector $\vec{a}$ reduces to zero. Fig. 4.3 illustrates the flow chart of the proposed MPPT algorithm. The MPPT control starts from the initial setting of both the WODE algorithm and the PRO profile. The initial pressure of the hydro-turbine pressure is set to 1 bar. At every iteration *k*, all search agents are used to find the optimum solution. For each search agent i, the fitness function is calculated and compared with the current global best solution. The position of each agent is updated with respect to the WODE algorithm, which contains three position-updated strategies inspired by the natural hunting behaviour of whales.

The position updating strategy is defined by the random value ρ. If $\rho > 0.5$, the position updating method for the current whale i is the spiral model. On the contrary, if the random value $\rho < 0.5$, the current whale i follows the spiral encircling model. In terms of the encircling mechanism, the phase of the current search agent is defined by the random coefficient vector $\vec{A}$. If the coefficient vectors $|\vec{A}| \geq \mathbf{1}$, the search agent i is in the exploration phase; conversely the search agent follows the exploitation phase.

For every search agent, if the calculated power density deviates from the previous power density, the current best fitness value and the global best solution are compared. If the current optimum position performs better than the previous best position, the current solution is set to be the global best position. At the current iteration, the whale i finds its best position following the above steps. In the mathematic model, the current best MPP for the PRO system is found by the search agent i. Then turn to next iteration and repeat the process.

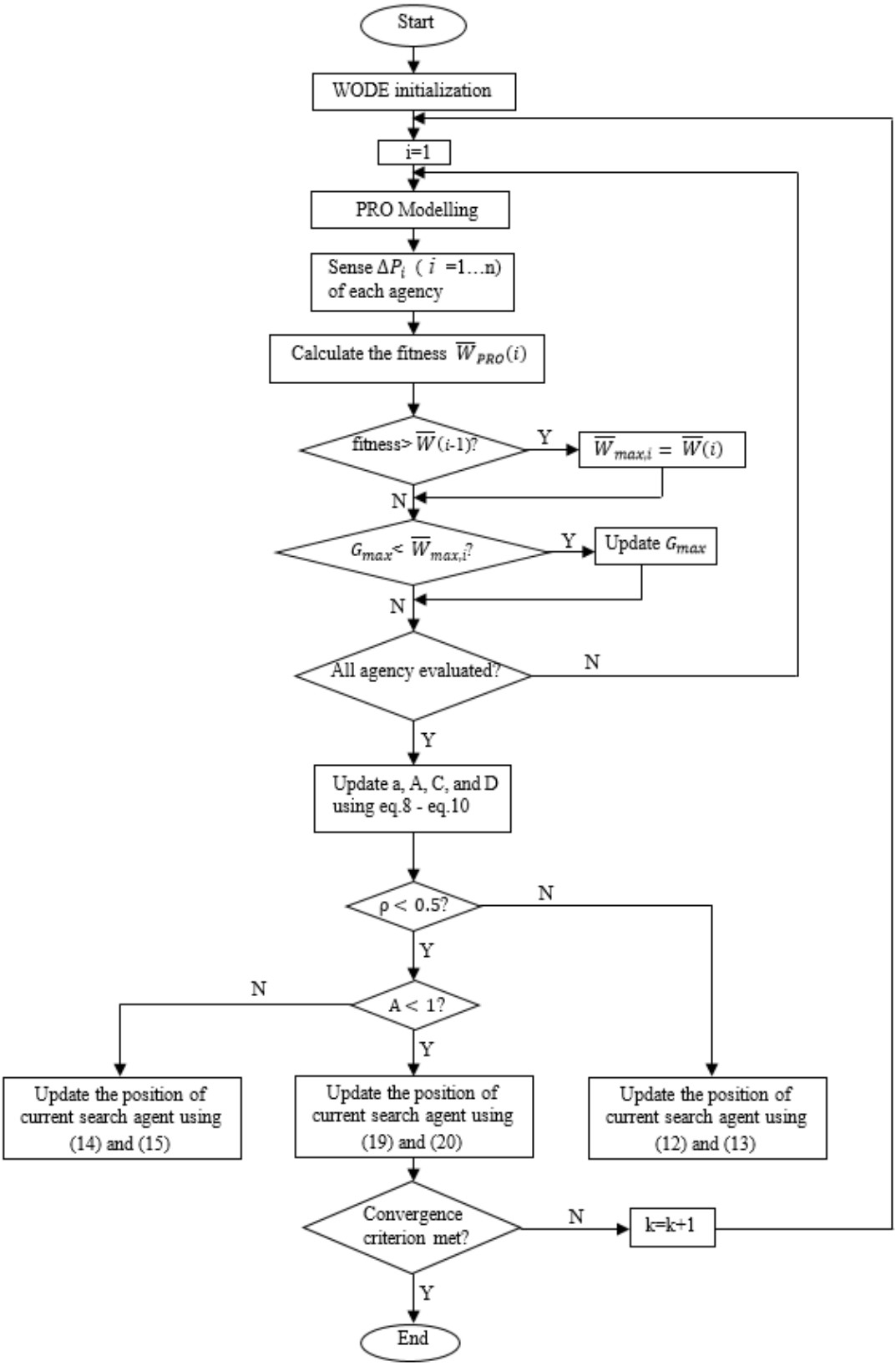

Figure 4.3: Flowchart of the proposed WODE-MPPT algorithm

4.4 Results and analysis

The purpose of the proposed MPPT method is to ensure the maximum power is derived from the PRO process at any operational condition. The performance of the PRO system using the proposed WODE-MPPT method has been compared with other typical and popularly used methods, namely the Perturb & Observe (P&O), the Incremental Mass Resistance (IMR), the Mass Feedback Controller (MFC) MPPT algorithms investigated by He et al [6, 25]. All these methods are model-free methods, where the instantaneous variables are used to produce the control signals. MPPT based P&O, IMR and MFC strategies for the PRO system are presented as those techniques have already demonstrated their merit in the control performance. In addition, among the meta-heuristic techniques to extract optimum power from different renewable energy sources, the Particle Swarm Optimisation (PSO) method is employed extensively. Therefore, the PSO has been evaluated and compared in the work to validate the efficacy of the proposed method. Thus, four methods, P&O, IMR, PSO and WODE, have been implemented in this study to find the MPP under fluctuation of operating conditions. It is noted here that the P&O and IMR are classic MPPT algorithms, while PSO is a conventional evolutionary computation technique simulating the social behaviour.

4.4.1 Case1: Start-up

The WODE-MPPT method are tested and compared with the conventional methods for tracking the maximum power of PRO. At the beginning, the pressure on the draw side is set to an initial value for the control system, then different algorithms are employed to the MPPT controller to track the maximum power density. The initial value of the pressure in the simulation setup is 1 bar. For the P&O and IMR algorithms, the increment is set to be 0.1 bar. In the PSO algorithm, inertia Weight and inertia Weight Damping Ratio are set to be 1 and 0.99, respectively; personal learning coefficient C_1 and global learning coefficient C_2 are set as 1.2 and 2.0, respectively; applied hydraulic pressure is employed as the particle. The WODE algorithm with 70 search agents under two case studies has been evaluated on the problem.

Fig. 4.4 shows comparison of results obtained with the P&O, IMR, MFC, PSO and WODE methods operating from the initial pressure. All of these five techniques are all parameter dependent methods. As shown in Fig. 4.4, the proposed WODE algorithm provides a better result. It is inferred that the oscillation reduces significantly using the proposed WODE-MPPT controller, also the tracking time is shorten notably compared with other four MPPT methods.

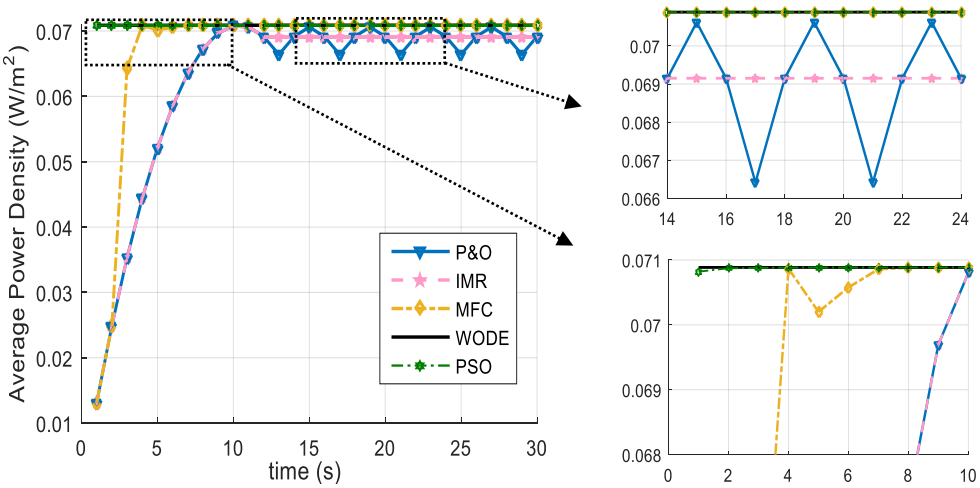

Figure 4.4: The osmotic power of PRO system with different MPPT algorithms

Table 4.1: Comparison of Five MPPT Techniques

Methods	Convergence (W/m^2)	Tracking time (s)
P&O	0.070804	10.2
IMR	0.070872	9.8
MFC	0.070885	4.1
PSO	0.070885	3.6
WODE	0.070885	1.1

Specifically, the detailed average power density is shown in Table 4.1. It is clear that the proposed method is able to locate the MPP of more than 0.07 W/m^2 with the fastest respond time, then the same value is found by PSO-MPPT and MFC-MPPT algorithm with oscillations. Simultaneously, both P&O and IMR miss the maximum power point as they are not that precise to find the MPP resulting in steady-state oscillations. This is because both methods need to balance the trade-off between the convergence speed and the oscillation.

The specific maximum values of the generated osmotic power investigated by all methods are presented in Table I. The data depicts that both the MFC-MPPT, PSO-MPPT and the WODE-MPPT methods are capable to converge to the MPP of 0.070885 W/m^2, where WODE is more stable and faster than the MFC and PSO methods. The P&O and the IMR get the maximum values to be around 0.07080395 W/m^2 and 0.07087187 W/m^2 due to the chosen perturbation or increment. The trade-off between the tracking speed and the oscillations have to be considered. As a result, these conventional techniques cannot get rid of the steady-state oscillations. However, at the MPP, the best applied pressure found by the search agent is constant at the steady state using the oscillation-free WODE algorithm. Furthermore, the reduced power loss from the reduced oscillation provides a higher system efficiency. It is important to point out that more power can be extracted from a two-stage PRO process compared to a single-stage process [97, 98]. In that case the proposed MPPT algorithm will be able to harvest more energy due to its higher efficiency compared with other methods. Overall, the maximum power density evaluated from the proposed method for the PRO system performs better compared to other techniques. WODE-MPPT controller for the PRO system is proved not only robust and efficient to track the MPP, but also capable to mitigate the oscillation around the MPP for the PRO system.

4.4.2 Case2: Variations of concentrates

Moreover, the implementation of the proposed strategy is presented at the operations with fluctuation in the saline water. Firstly, a simple variation of the concentration on the draw solution is shown in Fig. 4.5. At the beginning, the initial concentration on the draw side is set to 35g/kg and increases to 40g/kg at 40s. Then the draw concentration rises to 55g/kg from 70s. This case study is evaluated to test the

performance of the WODE-MPPT strategy. The proposed method is compared with P&O, IMR and PSO techniques in this section.

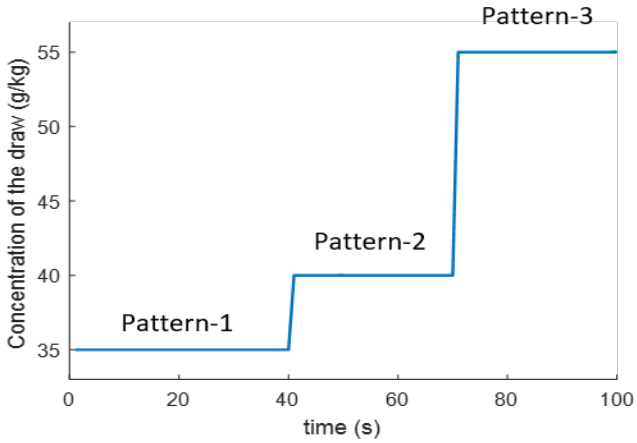

Figure 4.5: Fluctuation profiles of the concentration on the draw solution

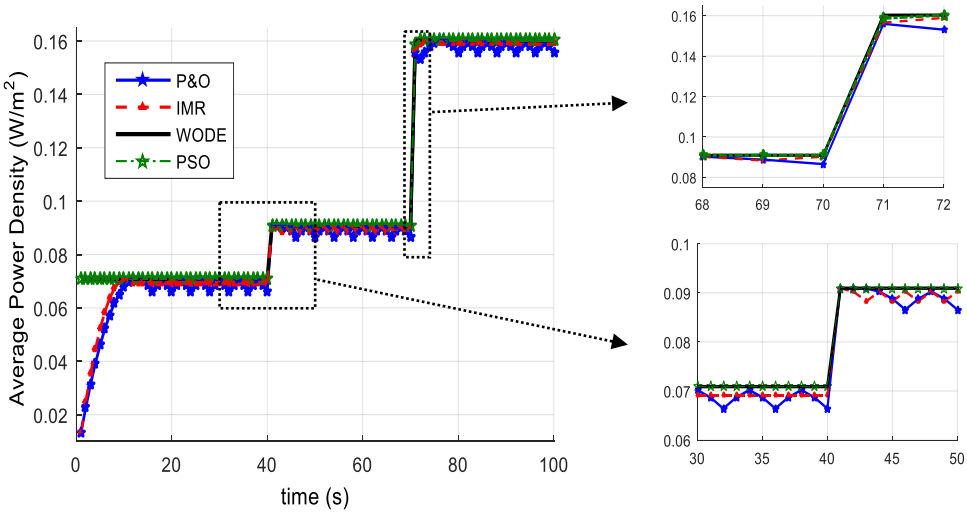

Figure 4.6: The osmotic power of PRO system with P&O, IMR, PSO and WODE based MPPT algorithm under rapidly changing flow rate on the draw solution of the salinities

The convergence process characteristics are shown in Fig. 4.5 in which the P&O, IMR, PSO and WODE strategies are evaluated. In the simulation, the characteristics indicate that the WODE algorithm outperforms over the other three algorithms under rapidly varying saline conditions. The proposed algorithm provides a shorter respond time period to the variations of the PRO plant, whereas P&O and IMR require a long respond time to catch the MPP, followed by PSO. The operating point oscillations around the MPP increase power loss of the system; additionally, the slow response of the techniques under rapidly variation results in a lower efficiency of the PRO system. Furthermore, the specific maximum power density derived from the plant is

shown in Fig. 4.6. According to the results, the faster convergence to the MPP subject to various operating conditions is obtained by the WODE-MPPT method. It is clear that the WODE strategy is capable to find the maximum power compared to the general methods. Moreover, the proposed method is robust and stable around the MPP. From Table II, it is observed that the WODE method is better in terms of both tracking speed and tracking efficiency than that of the conventional methods.

Table 4.2: Performance Comparison of Results Operating with Variations of Salinities

Method	Convergence (W/m^2)			Tracking time (s)		
	Pattern-1	Pattern-2	Pattern-3	Pattern-1	Pattern-2	Pattern-3
P&O	0.070804	0.090832	0.160233	13.7	4.8	7.6
IMR	0.070872	0.090903	0.160206	10.8	4.2	5.9
PSO	0.070885	0.090948	0.160304	5.2	3.9	5.7
WODE	0.070885	0.090948	0.160815	2.1	1.3	1.8

Pattern 1 to 3 are the three different concentration conditions on the draw side.
Pattern-1: 35kg/g; Pattern-2: 40kg/g; Pattern-3: 55kg/g.

4.4.3 Case3: Variations of concentrations and flow rates

In addition, the simulation is repeated for a more complex operational configuration, namely co-varied flow rate and concentration of salinities. Both the varied concentration and the flow rate shown in Fig. 4.7 are considered as the operating conditions. The proposed algorithm is compared to two conventional techniques. In this case study, the draw concentration at the start is set to 35g/kg while the flow rate is set to 1kg/h in pattern-1. At 25s, the draw concentration jumped to 50g/kg and the draw flow rate decreases to 0.5kg/h simultaneously in pattern-2 as illustrated in Fig. 4.7.

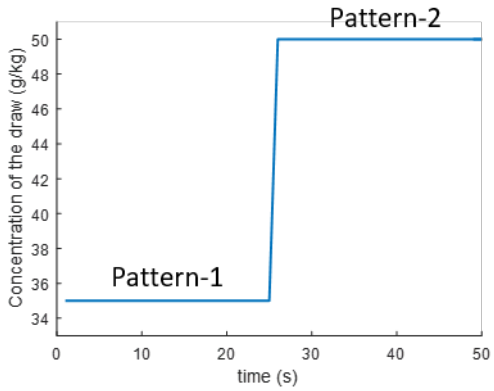

(a)

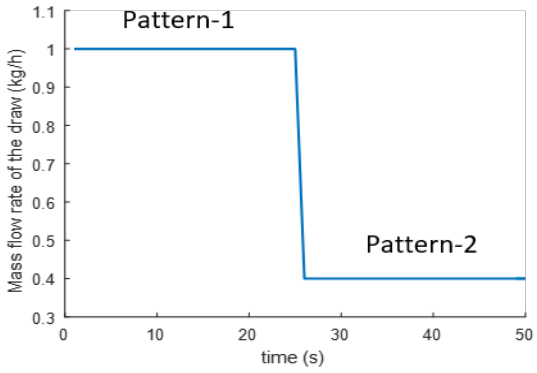

(b)

Figure 4.7: (a) Fluctuation profiles of the draw concentration; (b) Fluctuation profiles of the draw flow rate

The results are shown in Fig. 4.8 in which the WODE-MPPT controller is capable to yield higher tracking speed under the variations of the saline water in a PRO plant. The results indicate that the associated WODE-based MPPT technique can be readily utilised to more complex variation problems. In this case, the variation is both concentration and mass flow rate on the draw side. The results also indicate that the proposed method has ability to deal with other complex variation problems.

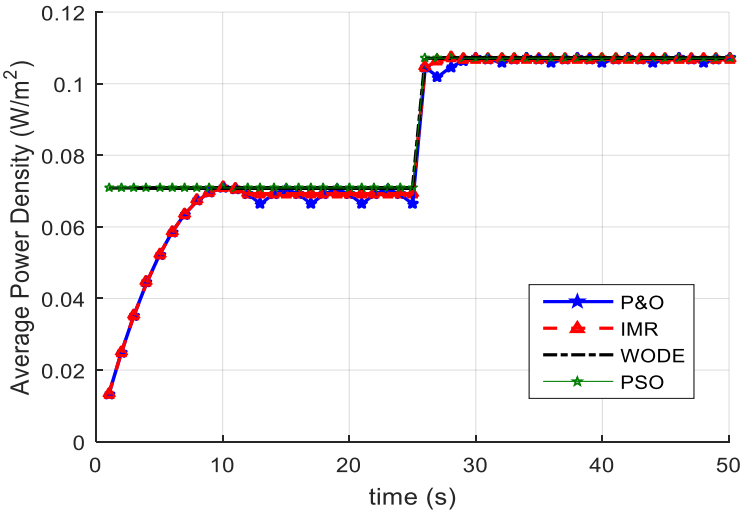

Figure 4.8: The osmotic power of PRO system implementing i) P&O, ii) IMR, iii) PSO, iv) WODE based MPPT algorithm under the co-variant of the flow rate and the concentration of the salinities.

Table 4.3 depicts the detailed quality of the maximum power density obtained by the four algorithms. It is observed from the results that the value achieved is higher at the average power density compared to that reached by the conventional methods. When the flow rate and the concentration on the draw side of the salinities changed at 26s, the MPPT strategies get restarted. The WODE-MPPT and PSO-MPPT technique converge to the MPP of 0.107125 W/m^2, while IMR-MPPT and P&O-MPPT fails to reach MPP and get settle under 0.10711 W/m^2, subject to the complex condition. In both patterns, WODE is able to obtain the maximum energy with the fastest tracking speed, followed by the PSO, IMR and P&O. According to the results, it can be summarized that the proposed WODE-MPPT method is capable to track higher power point. Also, the oscillations disappeared quickly compared to the P&O, IMR and PSO algorithms. Therefore, it is essential to consider the impact of the proposed method on loss reduction and PRO profile improvement.

Table 4.3: Performance Comparison of Results Operating with Variations of Salinities

Method	Convergence (W/m^2)		Tracking time (s)	
	Pattern-1	Pattern-2	Pattern-1	Pattern-2
P&O	0.070804	0.107080	11.2	7.8
IMR	0.0708719	0.107108	10.5	6.8
PSO	0.070885	0.107125	4.9	3.2
WODE	0.070885	0.107125	1.1	1.6

Pattern 1 and 2 are different conditions in terms of the DS concentrations and mass flow rates. Pattern-1: 35g/kg, 1kg/h; Pattern-2: 50g/kg, 0.4kg/h.

4.4.4 Case4: Performance comparison under various operational conditions

To assess the efficiency of the proposed WODE-MPPT strategy, various salinity conditions such as the concentration and the co-varied flow rate and the concentration of the PRO system are studied. The simulation results are shown in Figs. 4.6, 4.8 and 4.10 illustrate that the proposed WODE algorithm can handle the MPPT problem for a PRO system effectively and outperforms the general methods with advantage of higher respond speed and steady state oscillation-free. Further, qualitative comparisons among various MPPT techniques are presented in Tables 4.1, 4.2 and 4.3. According to Table 4.1, the maximum power available, as estimated by the WODE method is exactly the same as that obtained by the MFC method. Moreover, according to Table 4.2 and Table 4.3, the maximum power density available, as estimated by the WODE methods, exceeds the same obtained by any other method. Furthermore, more generated energy is considered from a two-stage PRO[97-98]. Thus, the Figures in the tables clearly depict that the proposed method performed better with respect to the reduced power loss resulting in a higher power efficiency. To sum up, the WODE method is generally more stable than all other methods.

In order to show the agreement of the speed and convergence performance of the proposed method in MPPT, the results obtained using WODE for PV systems from

literature are illustrated in Table 4.4. Kumar and Rao [27] and Kumar et al. [28] have compared the performance of WODE with PSO in terms of the extraction of the maximum power and the tracking time as depicted in Table IV. Kumar and Rao [27] evaluated the performance of the method in simulation, while Kumar et al. [28] validate the results through implementation of the method in hardware. In both cases the WODE is proven to extract more power with less tracking time.

Table 4.4: Comparison of MPPT Techniques in Literature

Method	Convergence (W)			Speed (s)		
	Pattern-1	Pattern-2	Pattern-3	Pattern-1	Pattern-2	Pattern-3
PSO [27]	350.72	293.82	352.44	9.6	10.8	13.8
WODE [27]	363.25	300.91	438.79	4.9	4.6	6.2
	Pattern-4	Pattern-5	Pattern-6	Pattern-4	Pattern-5	Pattern-6
PSO [28]	2428.667	2632.032	2177.538	7.57	8.32	8.27
WODE [28]	2430.32	2636.241	2179.29	1.43	1.56	1.41

Pattern 1 to 3 are three different PV configurations in the shading pattern [27]. Pattern-1: 6S; Pattern-2: 3S2P; Pattern-3:2S3P.

Pattern 4 to 6 are different PV curve patterns under shading [28]. Pattern-4: 3 peaks; Pattern-5: 5 peaks; Pattern-6: 4 peaks.

4.5 A MPPT Design Based on Grey Wolf Optimisation Algorithm for a Scaled-up PRO System

4.5.1 Introduction

The overall PRO power plant with the MPPT controller is clearly shown in Fig.4.9. The PRO membrane model is connected to the external devices including an energy recovery device (ERD), a high-pressure pump (HP), a hydro-turbine (HT) and a feed pump (FP). The pressure of the high-pressure pump is controlled by the MPPT

controller. The aim of the MPPT controller is to track the maximum power. Therefore, the input of the MPPT controller measures the power feedback at each time interval. The control variable is the transit pressure from the high-pressure pump.

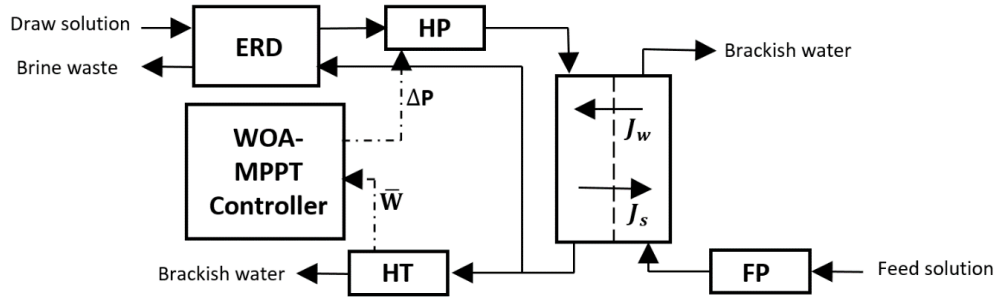

Fig. 4.9: Block diagram of a typical PRO system with MPPT controller I suggest to change BP to feed pump and brackish water may be changed to brine waste (since it will not necessarily be brackish after dilution, TDS>10 g/L)

4.5.2 Application of GWO in MPPT Design

The fitness function of the GWO algorithm is defined to find three best solutions values α, β and γ as

$$\bar{W}\left((\vec{x})_i^k\right) > \bar{W}\left((\vec{x})_i^{k-1}\right) \tag{4.20}$$

In the mathematical optimisation model, the solution of the current search agent is defined as

$$\overrightarrow{D_\alpha} = |\overrightarrow{C_1}.\overrightarrow{X_\alpha}(k) - \vec{X}(k)| \tag{4.21}$$

$$\overrightarrow{X_1}(k+1) = \overrightarrow{X_\alpha}(k) - \overrightarrow{A_1}.\overrightarrow{D_\alpha} \tag{4.22}$$

$$\overrightarrow{D_\beta} = |\overrightarrow{C_2}.\overrightarrow{X_\beta}(k) - \vec{X}(k)| \tag{4.23}$$

$$\overrightarrow{X_2}(k+1) = \overrightarrow{X_\beta}(k) - \overrightarrow{A_2}.\overrightarrow{D_\beta} \tag{4.24}$$

$$\overrightarrow{D_\gamma} = |\overrightarrow{C_3}.\overrightarrow{X_\gamma}(k) - \vec{X}(k)| \quad (4.25)$$

$$\overrightarrow{X_3}(k+1) = \overrightarrow{X_\gamma}(k) - \overrightarrow{A_3}.\overrightarrow{D_\gamma} \quad (4.26)$$

$$\vec{X}(k+1) = \frac{\overrightarrow{X_1}(k+1)+\overrightarrow{X_2}(k+1)+\overrightarrow{X_3}(k+1)}{3} \quad (4.27)$$

The random parameter $\vec{C}$ is utilised to weight the distance between the search agent and the prey in [0,2]. If $\vec{C} > 1$, the effect of the prey is emphasizing in defining the distance, and verse visa.

The random coefficient vector $\vec{A}$, of GWO is decreasing as the decline of $\vec{a}$, which is employed to define the searching mode and the attacking mode. If the absolute value of the coefficient vector $\vec{A} > 1$, the search agent diverges from the current best solution following the exploration phase. If the absolute value of the vector $\vec{A} < 1$, the search agent converges towards the current best solution according to the exploitation phase. During the process, the correlated vector $\vec{a}$ declines following the equation

$$\vec{a} = 2 - k * \frac{2}{iter} \quad (4.28)$$

When the global optimum is reached, and hunting process finished, the parameter $\vec{a}$ decreased to 0.

To sum up, the process of the implementation is as follows: First, the grey wolf algorithm is initialized. The PRO model is initialized. The initial fitness values α, β and γ are set to infinitely small. Then the loop starts. The position of the current grey wolf is updated according to the GWO algorithm with respect to the cost function (4.28) at each iteration k. Then its fitness is updated and compared with the three candidate solutions. If the current fitness solution i is larger than the fittest solution α , both the fitness and the position of α are replaced by which of the current search agent. Similarly, if its fitness is less than the best solution but fitter than the second-best solution, the second-best solution β is replaced by the current grey wolf i.

Consequently, the third best solution γ will be replaced if the current fitness is less than the solutions α and β but fitter than γ. All search agents are employed to find the global best three solutions in the search space. After this, α, β and γ and their corresponding positions are updated at each iteration. Finally, the GWO parameter is updated with regard of the GWO algorithm using (4.21)-(4.27). The probable prey position is estimated according to α, β and γ using (4.28). The process is then repeated with respect to the potential prey location obtained from the previous iteration. At the end of the iterations, the solution obtained by the leader grey wolf is considered as the optimum solution in the GWO-MPPT design.

This GWO-based MPPT algorithm utilises multiple grey wolves to chase the prey position guided by the best three grey wolves. In other word, the hunting (optimisation) of every search agent considers their own fittest solution as well as the best three fitness α, β and γ from the group. It is significant to point out that both A and C are generated stochastically, so they are various at each calculation. These random values which are generated over the course of iterations favors avoiding the local optima. For each case study, the GWO algorithm was run 50 times on the problem and the statistical results obtained by the GWO-MPPT controller are reported for the comparison.

4.5.3 Results and discussion

The proposed MPPT design for the PRO system is object to extract the maximum power under various operational conditions, including the temperature and the salinity profiles. The performance evaluation of the proposed GWO-based MPPT algorithm is performed by using a boost pump which is illustrated above.

To test these three methods, the improvements of the MPPT performance are evaluated by simulations in this section. Two case studies aiming to rapidly changing temperature and salinity operational conditions are then presented in this paper. The performances were probed with the highly popular ‘P&O’ and ‘IMR’ methods to verify the superiority of the proposed technique [6, 25]. These methods are model-free methods, where the instantaneous variables are used to produce the control signals. It is important to point out that there are two assumptions at the early stage:

firstly, the pressure is adjusted by a stable and fast controller. Secondly, the instant sample period is larger than the pressure transition time at each step.

Case study: Rapidly Changing Salinity Levels

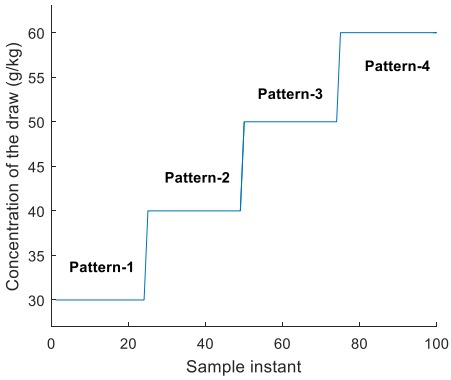

(a)

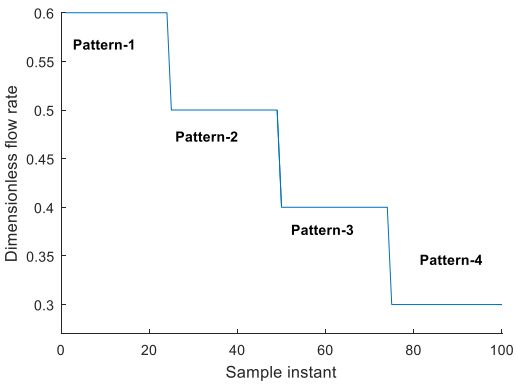

(b)

Figure 4.10: (a) Fluctuation profiles of the draw concentration; (b) Fluctuation profiles of the dimensionless flow rate

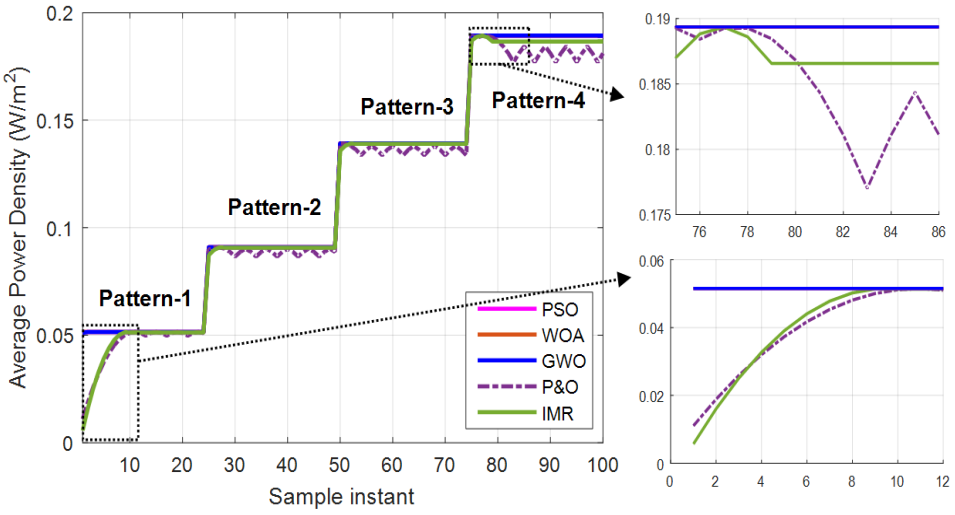

Figure 4.11: Osmotic power of PRO system with P&O, IMR, PSO, WOA and GWO based MPPT algorithms under rapidly changing operating conditions

Table 4.5: Performance Comparison of Results Operating with Variations of Salinities

Method	Convergence (W/m²)				Tracking time (step)			
	Pattern-1	Pattern-2	Pattern-3	Pattern-4	Pattern-1	Pattern-2	Pattern-3	Pattern-4
P&O	0.051493 91786	0.090903 18523	0.139234 53977	0.189261 35716	10	4	2	4
IMR	0.051378 79625	0.090831 96469	0.139199 64890	0.189353 47161	9	3	3	3
PSO	0.051496 4159	0.090947 7604	0.139267 0086	0.189358 7011	1	1	1	1
GWO	0.051496 4163	0.090947 7657	0.139267 01500	0.189358 67846	1	1	1	1
WOA	0.051496 4161	0.090947 7612	0.139267 01357	0.189358 68170	1	1	1	1

Table 4.5: Pattern 1 to 4 are the four different operational conditions.

For better comparing the effectiveness of the proposed methods GWO and WOA, a more complex operational condition is investigated, and the simulation is repeated. In this section, the variations in the concentration and the flow rate on the draw side

of the saline water are both considered, which pattern is shown in Fig.4.10. The MPPT controller using GWO, WOA, PSO, IMR and P&O techniques are all implemented under this operational condition. The result is represented in Figs. 4.10 and 4.11.

In the results of Figure 4.10, under dynamic change condition regarding concentrates and flow rates, classic MPPT algorithms P&O and IMR show limited ability to find the maximum power efficiently. P&O takes 10 intervals at the beginning and 4 intervals for the salinity change from pattern-2 to pattern-3 to reach the MPP. In the case of IMR, the performance is improved for both situations, it takes 9 and 3 time instant to track the MPP. In this situation, the PSO, WOA and GWO performs significantly well and has the capability to catch the MPP only in 1 instant (acceptable error: 0.001%).

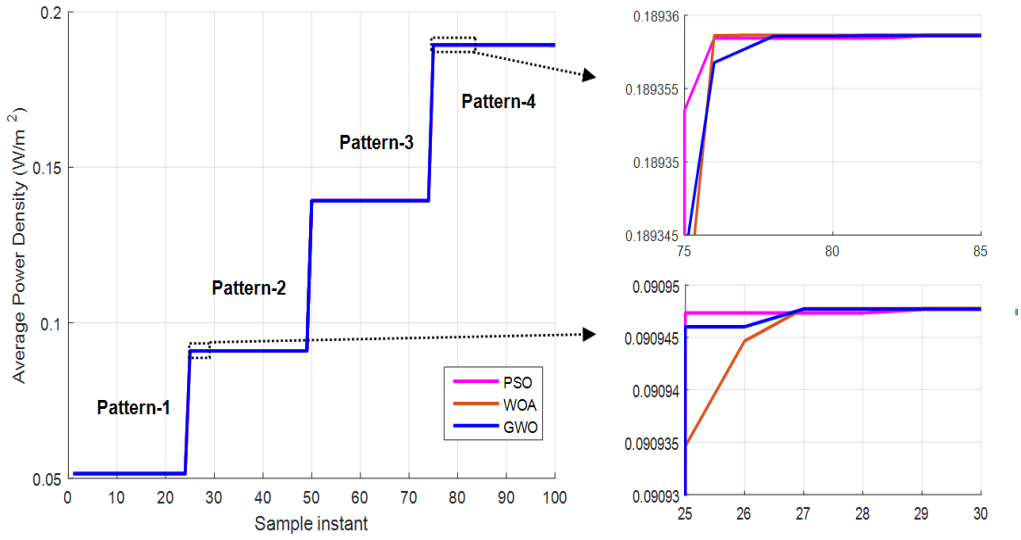

Figure 4.12: Detailed osmotic power of PRO system with PSO, WOA and GWO based MPPT algorithms under rapidly changing operating conditions

The complete comparison of the respond time is shown is Table 4.5. These results again illustrate that the proposed metaheuristic algorithm has the ability to reach the MPP with the fastest speed among the four general techniques, favoring oscillations avoidance and less power loss. Again, the superior performance of the optimisation technique based MPPT method over all methods can be obviously confirmed during the dynamics. At the beginning, the MPP extracted from GWO is 0.0514964161W,

where IMR reaches MPP of 0.05137879625 W and P&O algorithm settled at 0.05149391786 W. It means the tracking ability of the GWO is higher favouring a higher power efficiency.

Moreover, the detailed comparison among PSO. WOA and GWO is presented in Fig. 4.11. The detailed data is also presented in Table4.5. This table shows that there is improvement in tracking the maximum power point utilizing WOA and GWO algorithm, comparing with PSO. GWO performs slightly better than WOA. Furthermore, all of them give a fast-tracking speed under rapidly changing operational conditions. It is important to point out that more power can be extracted from a two-stage PRO process compared to a single-stage process [94].

The simulation results reveal that the GWO-based MPPT metaheuristic algorithm outperforms P&O and IMR techniques with respect to reduced steady state oscillation, faster tracking speed and higher tracking efficiency. Furthermore, the convergence time and the maximum power obtained by the five methods are briefly summarized in Table 4.5 with the purpose of the qualitative comparison. It can be clearly seen that the proposed technique outperformed other methods. From all the results, the proposed GWO-MPPT method is proved to be capable to handle the MPPT problem with efficiency and robustness.

4.6 Summary

In a scaled-up system, a novel evolutionary computing approach, namely whale optimisation with differential evolution method is implemented to track the maximum power in the dynamic as well as the steady state conditions. The superior performance of the proposed WODE-based MPPT algorithm in solving MPPT problem is proved to be efficient for the PRO system. The results also demonstrate that GWO method can show a high performance not only on unconstrained problems but also on constrained problems. Furthermore, this proposed algorithm validates the ability solve the multi-peak MPPT problem. Finally, the results of the design problems also illustrate that the WOA-based and GWO-based MPPT metaheuristic algorithms have high performance in challenging search spaces.

In this chapter, the comprehensive study illustrates that both the proposed WOA-based and GWO-based MPPT metaheuristic algorithm has merit among the current MPPT strategies. The simulation results on the MPPT problem showed a substantial improvement of power efficiency compared to current approaches, showing the applicability of the proposed MPPT method in solving real problems.

For a full-scale PRO power system, GWO algorithm is used to obtain the optimum operating parameters of the PRO process. Optimisation performed on a full-scale module operating under non-ideal conditions. Optimum operating parameters in bench PRO unit are invalid in a full-scale module. For a scaled-up PRO power system, a novel maximum power point tracking approach for a pressure retarded osmosis process is proposed. The method is based on the Whale Optimisation with Differential Evolution algorithm, which is able to overcome lower tracking efficiency and steady state oscillations. Moreover, the technique guarantees maximum power extraction in the face of rapid salinity variation. The efficacy and robustness of the scheme are evaluated with a scaled-up PRO system.

Chapter 5 Design and Development of Model Predictive Controller for a Photovoltaic Power System

5.1 Introduction

From the literature review on the utilisation of MPC algorithm based MPPT controller, it is noted that the methods were generally suitable for controlling the power output of PV panels. However, it was observed that the algorithm had not been validated with noisy variations of the ambient temperature and the local wind speed. It also seemed essential to speed up the algorithm for MPPT applications, particularly in the presence of environmental noise. For this reason, in this section, a new performance index will be proposed and used to develop a variable step size MPC algorithm based MPPT for PV systems. The algorithm with an adaptive droop controller was also coupled to adjust the bus voltage when multiple photovoltaic power supply buses are used, introducing a variable step size MPC method.

5.2 Mathematical modelling of a PV cell

Over the years, several researchers have worked on the PV panel and studied PV characteristics and factors that affect them. It is essential to provide a robust model of PV cells. Sera[32] provides a PV panel model based on manufacturer's data sheets in Standard Test Conditions(STC). However, it depends on only one operating condition. Villalva [13] proposes an effective and straightforward solution to fit the mathematical equation of the nonlinear I-V characteristic with three crucial points of a practical PV array, but it is only suitable for single-diode models. Soto [34] proposes a five-parameter model for four different cell technologies. Though effective, these researches lack the study on the choice of tilt angle. Costa[35] and Armstrong [36] mainly propose the temperature control law and the methodology to

choose the optimum tilt angle for a PV panel respectively. Dolara [38] compares three physical models of PV cells using actual weather data.

There are a few types of equivalent circuit models, such as single diode model, two diode model and dynamic model. Besides, there are five key parameters of single diode which are light generated current (I_{PV}), diode reverse saturation current (I_0), series resistance (R_S), parallel resistance (R_p) and diode ideal factor (a).

5.2.1 Ideal PV Cell

To understand the working principle of this device better, a PV cell equivalent circuit model is required. An ideal PV cell model can be represented as a current source in parallel with a light-sensitive diode. When there is no light generated, the PV cell behaves like a diode. The light photons are absorbed by the materials, if photon energy is higher than the band of materials, the conduction band will excite the electrons. When an external load connects to the output of PV cells, then the electricity will be generated. An ideal single-diode model of PV cell is shown in Fig.5.1.

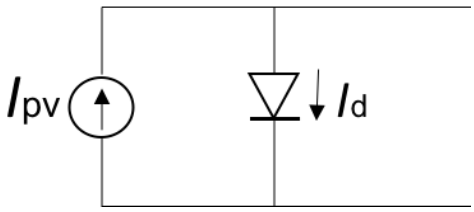

Figure 5.1: Theoretical single-diode model of PV cell

The output current of a theoretical PV cell is acquired by equation [96]

$$I = I_{pv} - I_d \tag{5.1}$$

$$I_d = I_0[exp\left(\frac{qV}{akT}\right) - 1] \tag{5.2}$$

In which I_d stands for current from the diode, I_{pv} stands for the photocurrent, I_0 is the saturation current of the diode, q stands for the electron charge of value 1.6×10^{-19} Coulombs, V stands for the measured cell voltage, a stands for ideal diode constant

(typically between 1 and 2), k stands for the Boltzmann constant with the value of $1.3806503 \times 10^{-23}$, T stands for the p-n junction temperature in Kelvin.

5.2.2 Modelling the PV Array

The ideal model does not consider the internal losses of the current. In practice, the observation of PV characteristics requires the series residence R_S and the parallel residence R_p. Fig.5.2 illustrates the equivalent circuit.

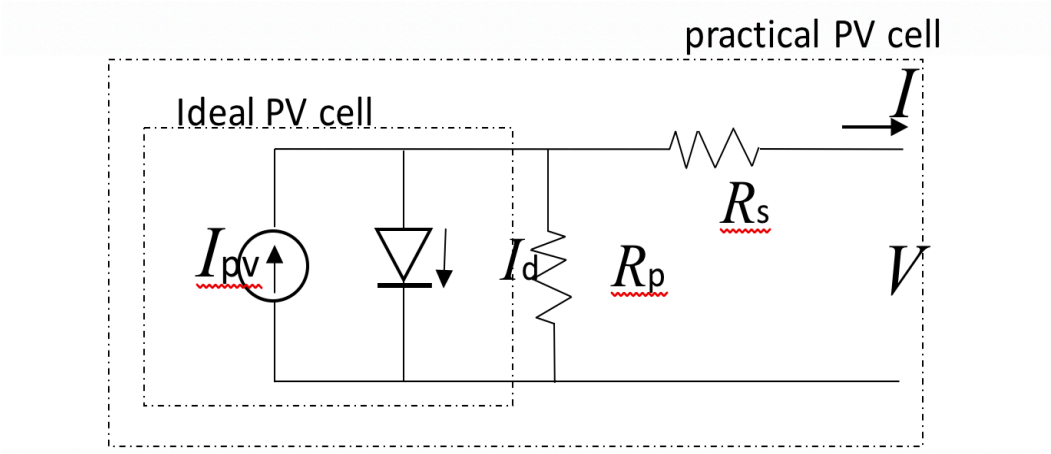

Figure 5.2: Model of a practical PV cell

From Kirchhoff law,

$$I = I_{pv} - I_d - I_p \tag{5.3}$$

The equation that mathematically depict the I-V characteristic of a practical PV array is [32]

$$I = I_{pv} - I_0[exp\left(\frac{V+R_sI}{aV_t}\right) - 1] - \frac{V+R_sI}{R_p} \tag{5.4}$$

Where $V_t = N_skT/q$ is the thermal voltage of PV arrays with N_S being the number of PV cells connected in series. R_S is the equivalent series resistance and R_p is the equivalent parallel resistance.

The I-V characteristics of PV devices is determined by internal influences like R_p and R_S, as well as external factors such as temperature [62].The output current of PV cells are influenced by temperature and solar irradiance according to equation [32]

$$I_{pv} = (I_{pv,n} + K_I \Delta T) \frac{G}{G_n} \quad (5.5)$$

Where $I_{pv,n}$ is the photocurrent in Ampere at nominal conditions (25$^{\circ}C$, 1000 W/m^2), K_I is the short circuit current coefficient in Ampere, $\Delta T = T - T_n$ in Kelvin with T is the actual temperature and T_n is the nominal temperature, G and G_n is the actual irradiance on the device surface and nominal irradiance in watts per square meter respectively.

Table 5.1: KC200GT solar array Parameters at STC [97]

PV Parameter	Symbol	Nominal Value
Nominal short-circuit current	I_{scn}	8.7 amps
Array current at MPP	I_{mp}	8.2 amps
Nominal array open-circuit voltage	V_{oc}	37.7 V
Array voltage at MPP	V_{mp}	30.1 V
Series resistance	R_s	0.221 Ω
Parallel resistance	R_p	415.405 Ω
Voltage-Temperature coefficient	K_V	-0.123 V/K
Current-Temperature coefficient	K_I	0.0032 A/k
Array output peak power	P_{max}	246.82W

5.2.3 Parameter Determination

Chapter 2 The above parameters are normally provided by experimental data or the manufacturer's datasheet. Take the M2543BB solar array as a research plant, the parameters of KC200GT from KYOCERA at Standard Test Conditions (STC) is shown in table 5.1 [97].

Simulations results

By using the mathematical equations and Figures discussed above, the I-V characteristic and P-V characteristic curve is obtained in the MATLAB/Simulink environment (see Appendix). Fig.5.3 and Fig.5.4 illustrates the I-V characteristics and P-V characteristics respectively under different solar irradiance levels.

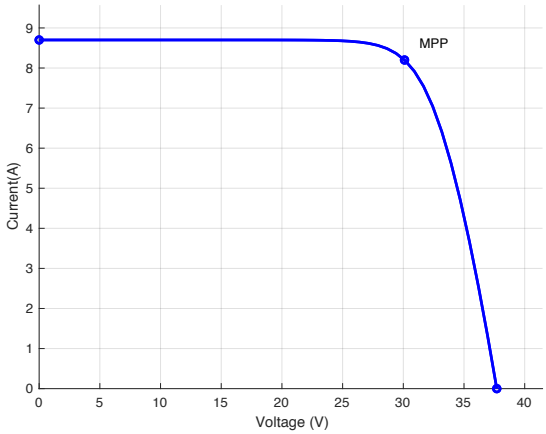

Figure 5.3: I-V model characteristics of the solar array under different irradiance, $25^{\circ}C$

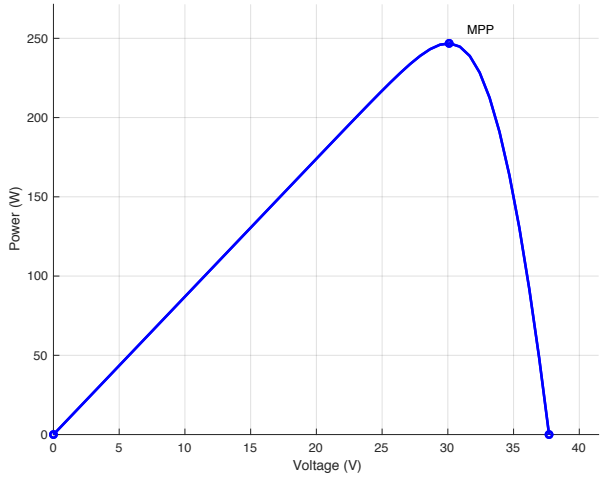

Figure 5.4: P-V model characteristics of the solar array under different irradiance, $25^{\circ}C$

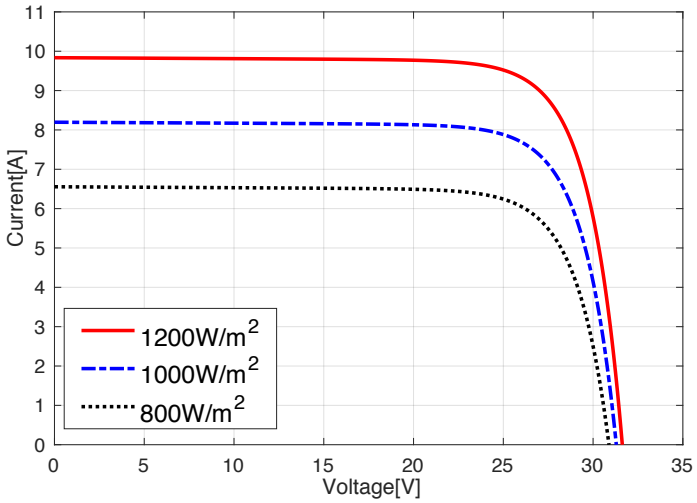

Figure 5.5: PV characteristic curves at different irradiance with constant 25°C temperature

5.3 Modelling of PV panels with environmental disturbances

A typical equivalent circuit of a PV type photovoltaic cell is used, in which use several diodes to simulate the dark current branch. It is generalization of the equivalent circuit of Figure 8.12 of Vepa [98], which is used simulate the single diode dark current flow.

Based on a multi-diode model, we may express the current i in the series resistor R_S as

$$i = i_{pv} - i_{01}\left\{\exp\left(\frac{v_0+R_S i}{n_1 v_T}\right) - 1\right\} - \left(\frac{v_0+R_S i}{Z_P}\right) + i_{noise} \tag{5.6}$$

where the photo-current i_{pv} is calculated as

$$i_{pv} = \lambda_{si}\left(i_{sc} + K_i\left(T_{op} - T_{ref}\right)\right) \tag{5.7}$$

In which i_{pv} depends mainly on the solar irradiance ratio λ_{si} and the operating temperature T_{op}.

The quantity of thermal voltage v_T is related to the *Boltzmann* constant k and the electronic charge q by the relation $v_T = n_s kT_{op}/q$. In which n_s the number of diodes is connected in series. n_i is the diodes ideal factor in parallel line. The quantity of the diodes reverse saturation current i_{0i} is in parallel line and can be expressed as a function of the operating temperature T_{op}. It can be expressed at a reference temperature T_{ref} as

$$i_{0i} = i_{0i,ref}\left(\frac{T_{op}}{T_{ref}}\right)^{\chi} \exp\left(\beta\left(\frac{1}{T_{ref}} - \frac{1}{T_{op}}\right)\right) \tag{5.8}$$

In which χ and β are constants. Furthermore, in the Laplace transform domain, $Z_P = R_P/(1 + sCR_P)$. Assuming C is very small, $Z_P = R_P$.

The cell operating temperature T_{op} is function of the ambient temperature T_a, the solar irradiance ratio and the wind speed W_s.

It is given by [99]

$$T = 273° + \left(T_{op\_ref} + 0.25\lambda_{si} + 0.899T_a - 1.3W_s\right) \tag{5.9a}$$

with

$$T_{op\_ref} = 3.12° \tag{5.9b}$$

The effect 3 different wind speeds on the power output of a PV cell is shown in Fig. 5.6, which clearly indicates that the power output may increase by about 15-20% due to the cooling of the cell. Furthermore, both the wind speed W_s and the ambient temperature T_a are assumed to contain additive noise which generated from a random variable with a Weibull distribution [99]. The reason for choosing a Weibull distribution is not only because the hourly variation of wind speeds follows a Weibull probability density function, but also because the noise generated in this manner can be highly impulsive. The impulsive noise is particularly useful for validating our algorithms with disturbance attenuation and for demonstrating robustness of the control laws.

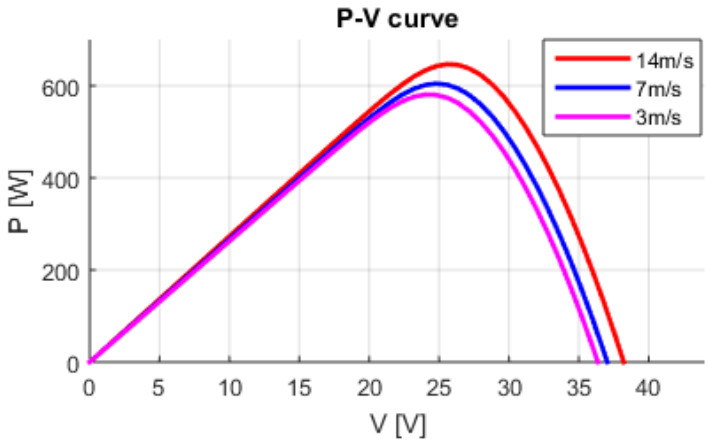

Figure 5.6: Effect of wind speed on the power output of a PV cell

A solar panel is assumed to be constructed from N_P strings of identical cells connected in parallel and with each string having N_S identical solar cells connected in series. The panel output current is given by

$$I = N_p I_{ph} - N_p I_0 \left\{ \exp\left(\frac{(V/N_s) + (I/N_p)R_s}{AV_t} \right) - 1 \right\} - N_p \frac{(V/N_s) + (I/N_p)R_s}{R_{sh}} \quad (5.10)$$

A similar formula is derived for non-identical cells. To solve for the current, we adopt as iterative scheme such as the Newton-Raphson method.

The output of the PV panel simulation was verified by comparing it with the output of a hardware PV simulator, the CHROMA 52000H-150S, and correlates well with it.

5.4 Design of a DC-DC boost converter

DC-DC converter is a typical switching system. It can be composed of four end network modelling, in which the source end by an inductance L connected in series to a PV system. The equivalent circuits with two statuses of idealized switching signal is displayed as Fig.5.7.

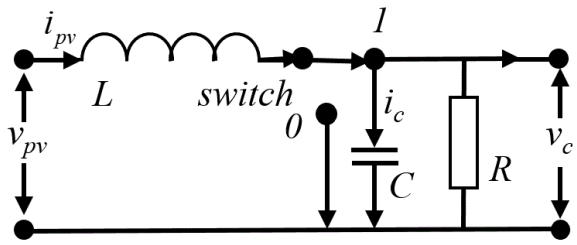

Figure 5.7: Equivalent circuits of DC/DC converter with binary switching status

When s=1, the ideal switch is open; s=0, the ideal switch is closed. Fig.5.8 and Fig.5.9 is demonstrated to make it clear.

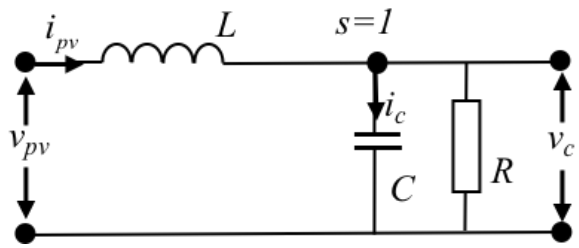

Figure 5.8: Equivalent circuits of DC/DC converter with switch closed

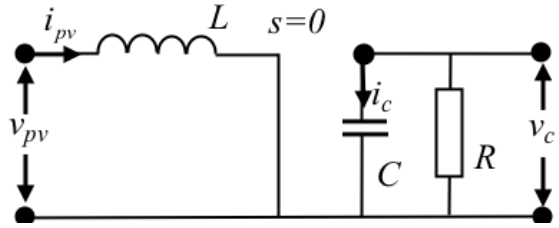

Figure 5.9: Equivalent circuits of DC/DC converter with switch open

The model illustrated above is a boost converter, the principle of a buck converter, buck-boost converter and so on are similar.

From Fig.5.9, the converter operation can be depicted by the systems as equation (5.11) and (5.12) when the switch is open and be considered as equation (5.13) and (5.14) when the switch is closed.

$$\frac{i_{pv}}{dt} = -\frac{1}{L} i_{pv} + \frac{1}{L} v_{pv} \tag{5.11}$$

$$\frac{v_c}{dt} = -\frac{1}{RC} v_c + \frac{1}{C} i_{pv} \tag{5.12}$$

As switch is open, which means s=0 as Fig.11, equation system is of the following form:

$$\frac{i_{pv}}{dt} = -\frac{1}{L} i_{pv} + \frac{1}{L} v_{pv} \tag{5.13}$$

$$\frac{v_c}{dt} = -\frac{1}{RC} v_c \tag{5.14}$$

The discrete time system of equations can be derived as follows with sampling time Ts. By implementing these equations, at sampling time k, controlled variables i_{pv} and v_c can be predicted at the next sampling time k+1. MPC method is utilised to predict the error in next sampling time and is based on minimizing the cost function g so as to get switching state for the present time and a future time.

As switch open and closed:

$$i_{pv}(k+1) = i_{pv}(k) - \frac{T_s}{L} v_c(k) + \frac{T_s}{L} v_{pv}(k) \tag{5.15}$$

$$v_c(k+1) = (1 - \frac{1}{RC}) v_c(k) + \frac{1}{C} i_{pv}(k) \tag{5.16}$$

$$i_{pv}(k+1) = i_{pv}(k) + \frac{T_s}{L} v_{pv}(k) \tag{5.17}$$

$$v_c(k+1) = (1 - \frac{1}{RC}) v_c(k) \tag{5.18}$$

Combining these equations, the following equations are obtained:

$$i_{pv}(k+1) = i_{pv}(k) - s * \frac{T_s}{L} v_c(k) + \frac{T_s}{L} v_{pv}(k) \tag{5.19}$$

$$v_c(k+1) = -\frac{1}{RC} v_c(k) + s * \frac{1}{C} i_{pv}(k) \tag{5.20}$$

In which the switching variable s=1 when the switch is open while s=0 when it is closed and T_s presents sampling time.

The foregoing equation system can be expressed in the following matrix form:

$$\begin{bmatrix} i_{pv}(k+1) \\ v_c(k+1) \end{bmatrix} = \begin{bmatrix} 1 & -s * \frac{T_s}{L} \\ s * \frac{T_s}{C} & 1 - \frac{T_s}{R*C} \end{bmatrix} * \begin{bmatrix} i_{pv}(k) \\ v_c(k) \end{bmatrix} + \begin{bmatrix} \frac{T_s}{L} \\ 0 \end{bmatrix} * v_{pv}(k) \tag{5.21}$$

Furthermore, the discrete time equation system can be extended to n-step horizon. Better performance can be obtained when increasing the step number n [50], which will be accomplished in the next chapter.

$$i_{pv}(k+n+1) = i_{pv}(k+n) - s * \frac{T_S}{L} v_c(k+n) + \frac{T_S}{L} v_{pv}(k+n) \quad (5.22)$$

$$v_c(k+n+1) = -\frac{1}{RC} v_c(k+n) + s * \frac{1}{C} i_{pv}(k+n) \quad (5.23)$$

5.5 MPPT control techniques

5.5.1 P&O MPPT method

The Perturbation and Observation method is the simplest one for MPPT and needs only the value of power. It is also called Hill Climbing technique, while both of them describe the same method on how it is employed. Based on the sampling method, in P & O systems, the current value is confided to the past data that gives the difference in power (ΔP). Considering a light change (perturbation) on the voltage, if (ΔP) is positive, then this change is in the right direction or else it is reversed [100]. Though simple, there are a few drawbacks. Immense perturb values will lead to oscillations. Also, the oscillations around MPP causes the loss of energy at the steady state. Its response to rapid vibrations is poor. To overcome these disadvantages, modified P& O methods is studied in literature. Abdelsalam [101] processes a method of fixed perturb, but the hindrance is to choose a desirable perturb step. Khaehintung [102] proposes the step-size method, which can achieve a faster response.

The P&O method is the most popular MPPT method using in the PV system due to the simplicity [39] [103]. The principle of P&O method is based on the derivation of the output power to voltage is zero at the MPP from the P-V characteristics. When operating at the left side of the MPP with an incrementing voltage, the output power will increase, and verse visa. Therefore, if the perturbation of the voltage and the observation of the output power are in the same direction, it is noted that the operating point is in the left side of the MPP. The subsequent perturbation should be kept and move the operating point towards the MPP.

Similar principle at the right side of the MPP on the P-V curve. When the given perturbation is an increment operating voltage leading to a decreasing output power, the operating point is at the right of the MPP. The P&O method reverse the direction of the perturbation to change the point to reach the MPP. The basic strategies in the P&O method is given as Table 5.2, where the symbols + and – are positive and negative, respectively. The perturb and observe technique is employed reputably until obtained the MPP. The P&O method has a few disadvantages: i) it is not stable under rapidly changing operational conditions; ii) it has to balance the trade-off between the tracking dynamics and the steady state oscillations. Therefore, the improved methods are evaluated in the following sections.

Table 5.2: Strategies in P&O Technique

Perturbation	Change in Power	Next Perturbation
+	+	+
+	-	-
-	+	-
-	-	+

5.5.2 Improved INC MPPT method

The INC method is demonstrated in Fig.5.10. The INC method is utilised widely because of its good stability under rapid changes. However, it requires complex circuits. To solve this problem, improved InC algorithm is studied by researchers. Tey [104] proposes a modified INC to modulate the duty cycle of the dc-dc converter, with the purpose of tracking the global maximum power point (GMPP) under partial shading conditions and load variation. Liu [105] proposes a modified variable step size INC technique to improve the MPPT speed and accuracy. Punitha [45] proposes a neural network based modified InC algorithm, which provides a higher percentage of maximum power with less time.

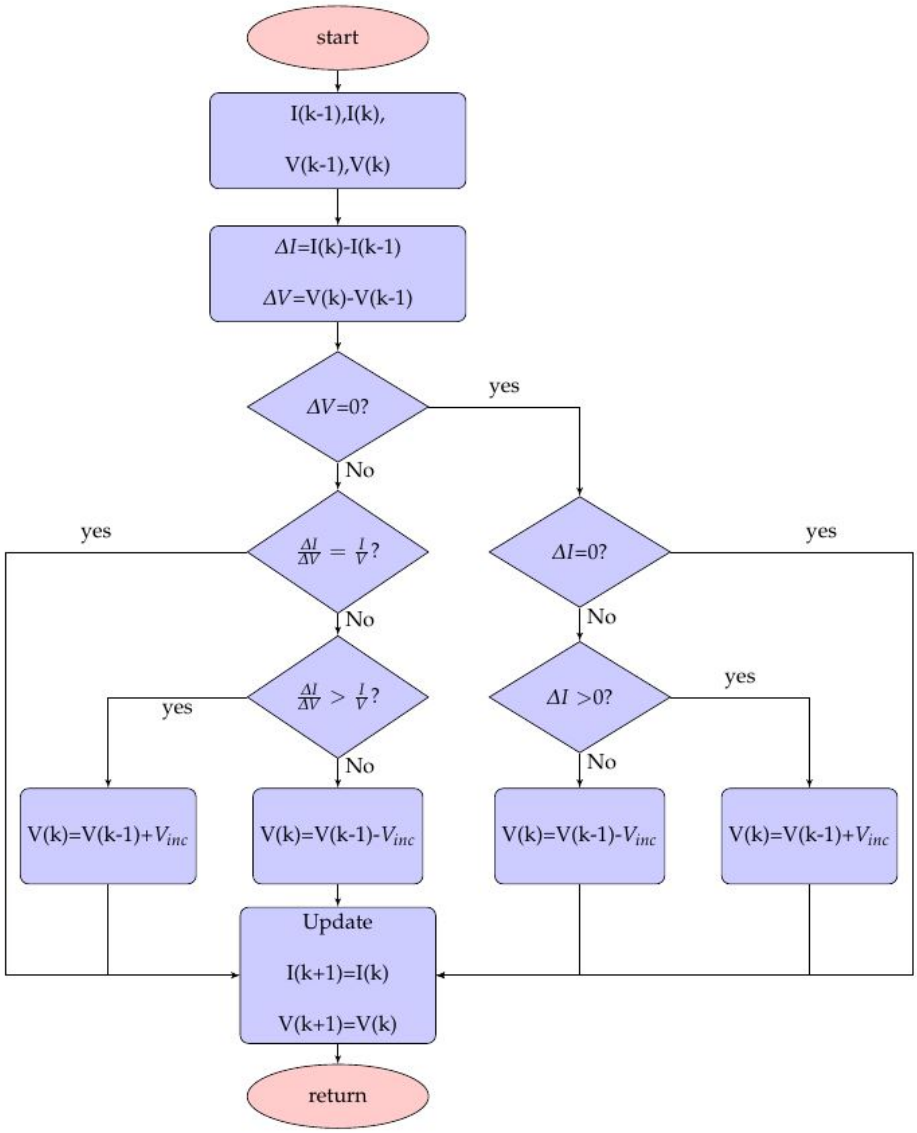

Figure 5.10: Flow chat of classic INC method

The modified INC algorithms utilised in this chapter have two main contributions with MPC technique:

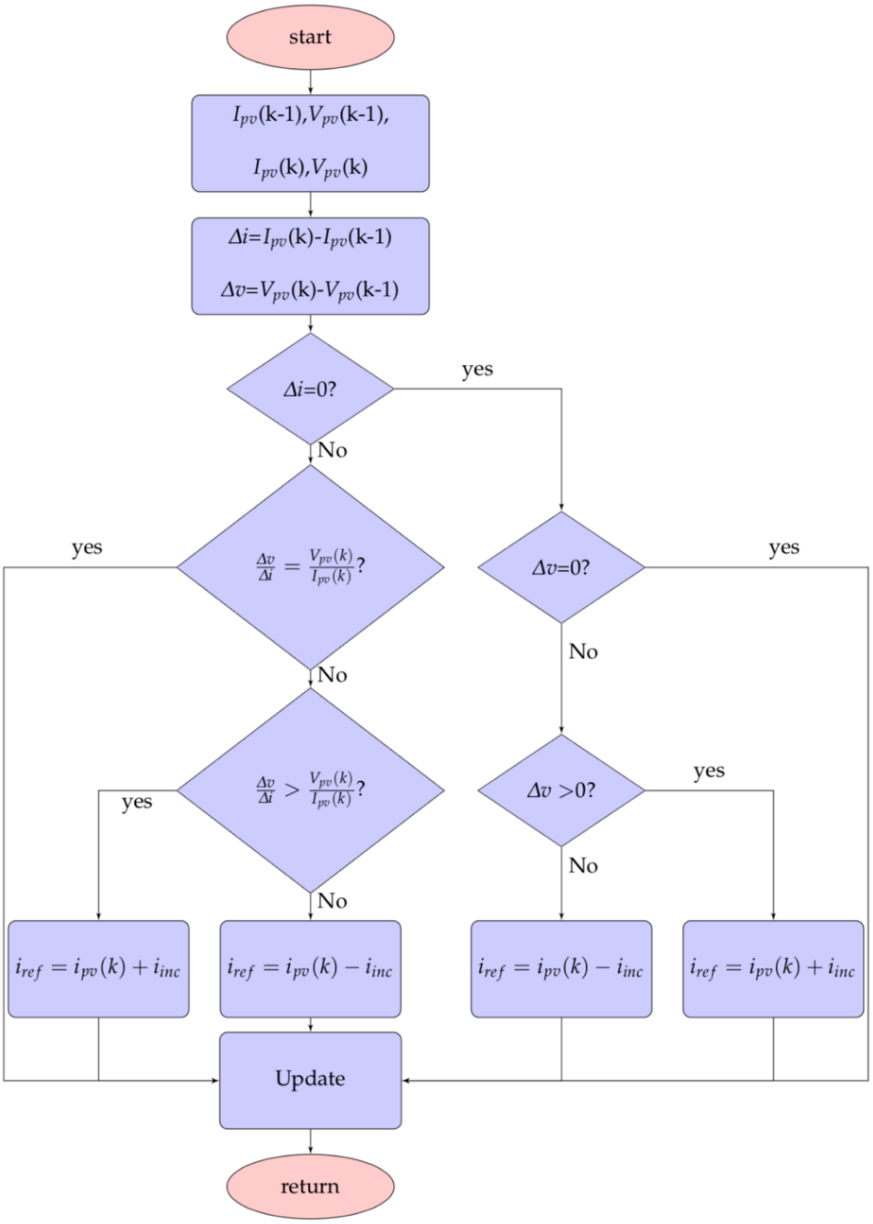

Figure 5.11: Flowchart of improved Incremental conductance algorithm imposing the reference current

1. The INC method aims to regulate the value of reference current to the MPC controller (current based).2. The increments of the reference current are the measured current of the PV system instead of the reference current in previous sampling time. The INC algorithm combined with MPC technique predicts the error one step ahead compared with the formal INC technique.

The output power and the current are taken into consideration in tracking MPP. In the maximum power point, the slope of I-P curve is equal to zero. Fig.5.11 illustrates the proposed INC method that used in this chapter intuitively.

5.5.3 fixed-step size MPC MPPT method

Two main forms of green energy are studied in the literature based on MPC, PV generation and wind power generation [106]. In terms of PV, the MPP tracking with combination of INC and MPC algorithm is implemented, where MPC method gives advantages of fast response under variation and its ability to extract MPP under various conditions [107]. Shadmand [55] proposed a MPP tracking method using modified P & O through a fixed step MPC of a flyback converter. The error is predicted before switching states. Kakosimos [50] proposed an implementation of PV array MPPT through MPC. A modified INC technique combined with two-step horizon MPC is employed in the controller for tracking the MPP. These algorithms contain two stages, first stage is to yield a reference value by modified INC algorithm, then MPC is implemented to control the PV module and to reach the maximum power point.

Overall Frame

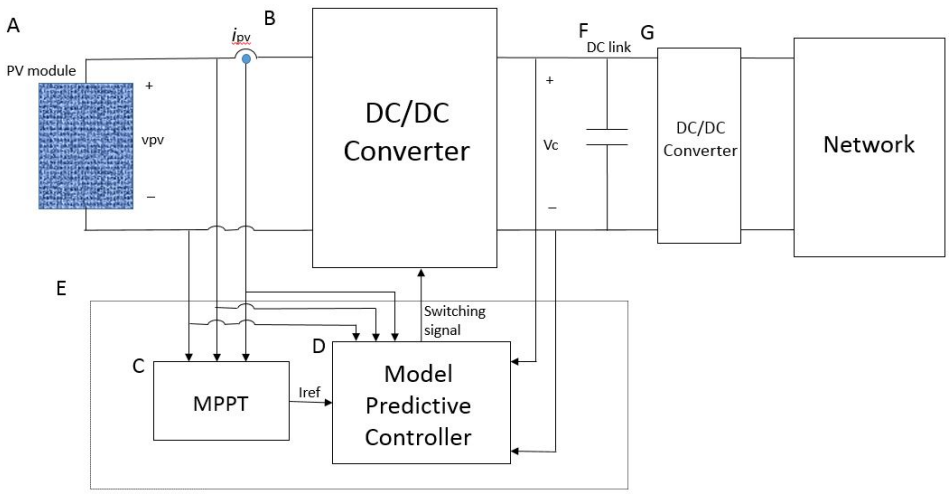

Figure 5.12: Brief outline of PV system structure utilizing MPPT-MPC algorithm

Model predictive control is utilised with MPPT at this stage. MPC is one of the best controllers because addition of MPC in tracking MPP can not only reach steady state faster, but also make a faster response under different condition [41].

Fig.5.12 illustrate the integrated frame using Model Predictive Control based Maximum Power Point(MPC-MPPT) method [50, 110]. It comprises of a few units:

A: PV module which can produce power straight from solar radiation.

B: DC/DC converter which will be defined below.

C: MPPT module gets current and voltage from PV system as inputs. Simultaneously, it determines the MPPT reference output current for predictive controller.

D: The MPC method that used in this study. Current reference from MPPT, DC/DC converter output voltage, current and voltage from PV array are formed as adequate inputs to predict the error in the next sampling time, as well as to decide the switching state for DC/DC converter based on cost function. The switching signal is a binary output, which is believed to be open when it is 1 and equal to 0 when it is closed.

E: The control strategy. It consists of two main components: MPPT and MPC module.

F: DC link.

G: A DC/DC converter.

Principle of Predictive Control

Early application of Model Predictive Control(MPC) dates back to the 1980s with low switching frequency [40]. With the development of high-speed microprocessors, MPC methods have developed greatly [106]. The basic idea of MPC is the receding

method. The model for predictive control used in this research is discrete-time model, with main strategy: 1) At current time, assuming as step k, the future desired control outputs $y(k + i|k)$ is predicted confide to the past input and output, as well as a reference signal $r(k + i|k)$ during the predictive horizon H_p. 2) The cost function used to optimise the switching state is employed as a criterion. 3) Only the first predicted element in the resulting optimal sequence is applied for the process. When finished, repeat the optimisation over the future horizon.

The most obvious merits of MPC are the speed and reliability, which refer to the ability to handle multivariable control problems by assigning different levels of importance to each input and output. Also, this method takes account nonlinearities and constraints. On the contrary, one of the limitations of MPC is the required computational effort [108].

The most significant part in MPC is the cost function, which is used to optimise the switching state. Cost function is given as:

$$g = \lambda_i g_i + \lambda_v g_v \tag{5.24}$$

Where g_i is the absolute error between the reference current and DC voltage predictive value, while g_v is the absolute error between the reference voltage and its predictive value. λ_i and λ_v are the weighting values of g_i and g_v respectively.

The cost function is a linchpin of MPC algorithm which is utilised to constrain the deviation from reference values i_{ref} and $v_{ref,}$ $w_{A,}$ w_B is employed to define the proportion[9].The cost function for the MPC technique is:

$$g = w_A \cdot |i_{pv}(k+1) - i_{ref}| + w_B \cdot |v_{pv}(k+1) - v_{ref}| \tag{5.25}$$

In this study, one-step horizon predictive control is implemented. $I_{pv,}$ $v_{pv,}$ v_c and $i_{ref\,,}$ v_{ref} are considered as inputs for the controller. By evaluating the cost function twice for each switch status, the binary variable s is determined to satisfy the

minimum cost g. Fig.5.13 depicts the process of the control scheme for one step horizon MPC.

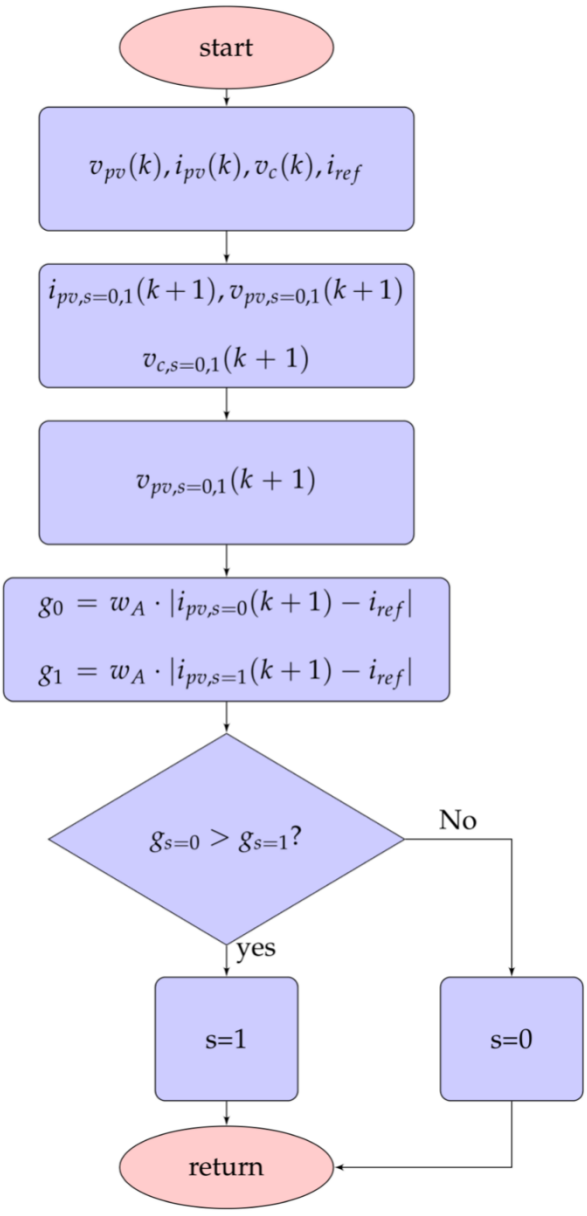

Figure 5.13: 1-step horizon MPC-MPPT procedure

Implementation and discussion

A PV system was developed using MATLAB to confirm the controls. A typical PV system configuration is implemented to test the proposed MPC-MPPT control technique under abrupt solar intensity. The solar configuration in this chapter is shown below:

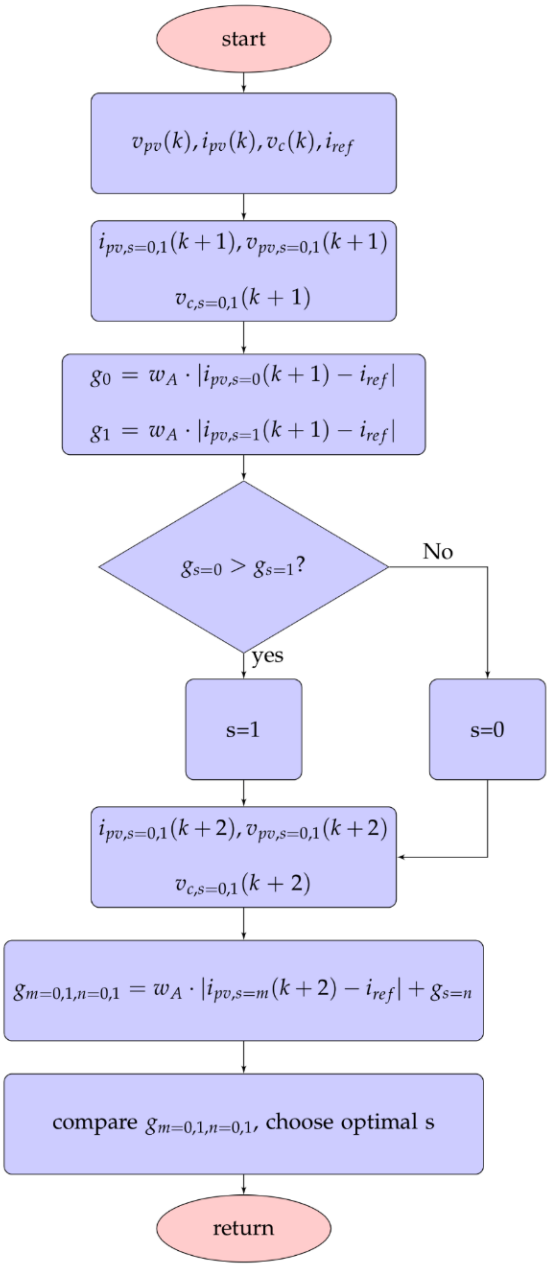

Figure 5.14: 2-step horizon MPC-MPPT procedure

5.5.4 Variable step size INC MPPT method

The incremental conductance controller introduced in the previous section is fixed step size. a smaller step size contributes to relatively less oscillations in the stead state. However, it causes slower dynamics resulting a comparatively low efficiency. Also, under rapidly changing conditions, it may get lost in the wrong direction around the MPP [109]. This conflicting situation can be fixed by a larger step size. Though the speedy tracking achieved, oscillations around the MPP are increased. During the rapid changing operational conditions, the excessive oscillations lead to a high-power loss.

In fact, not only the INC method, other conventional methods such as P&O method are characterized by the dilemmas between the oscillations and the reaction speed, which resulting to a low efficiency. Dedicating to deal with this trade-off between the dynamics and the tracking accuracy, the variable step size INC technique is proposed by researchers [109]-[105]. In the proposed technique, the step size is changed according to the atmospheric conditions, contributing to a faster dynamic, less oscillations and a higher power efficiency.

The MPPT controller is connected with a DC/DC boost buck converter and tune the duty cycle iteration step size of the converter. The V and I are the voltage and the current outputs of the PV array. D is the duty cycle. To simplify the system, the PV power output is adopted directly to control the duty cycle. The variable step size INC MPPT method is given as [108-112]

$$D(k) = D(k-1) + N * \left|\frac{dP_{pv}}{dV_{pv}}\right| \tag{5.26}$$

In which $D(k)$ and $D(k-1)$ are the converter duty cycle at the instant k and k-1, respectively. N is the scaling factor adjusted manually by at the beginning. dP_{pv} and dV_{pv} are the power derivate and the voltage derivate, respectively. They are updated by

$$dP_{pv}(\mathrm{k}) = P_{pv}(\mathrm{k}) - P_{pv}(\mathrm{k}-1) \tag{5.27}$$

$$dV_{pv}(\mathrm{k}) = V_{pv}(\mathrm{k}) - V_{pv}(\mathrm{k}-1) \tag{5.28}$$

The difference between fixed step size law and variable step size is shown in Fig. 5.15.

As shown in Fig 5.15, the derivative of the output power to voltage is used to determine the size of the step for the INC algorithm [105]. Later, an modified variable step size INC algorithm is investigated and verified with experimental by Loukriz [109]. The rule in the proposed variable step size INC technique is updated as

$$D(k) = D(k-1) + N * \left| \frac{dP_{pv}}{dV_{pv} - dI_{pv}} \right| \tag{5.29}$$

In which dI_{pv} is updated by

$$dI_{pv}(\mathrm{k}) = I_{pv}(\mathrm{k}) - I_{pv}(\mathrm{k}-1) \tag{5.30}$$

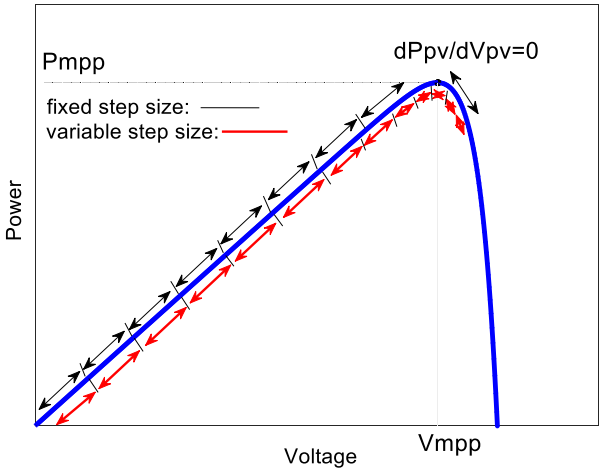

Figure 5.15: Variable size and fixed step size behaviour

5.6 Nonlinear discrete time model in a switching system

By using the state space averaging method proposed in 1970s, the small signal mathematical models of DC power converters are established in the state space average signal equations near rated little change. The product term of any two small signal distributions is ignored. Therefore, the state space average leads to the

equivalent linear dynamic model. Instead of transistor switches technology allows the ideal switches, developing models for their 'ON' state and the 'OFF' state and evaluate ideal equivalents of transistor switches. Moreover, they could also be in the duty ratio and the 'OFF' state of the state is weighted, during a single power cycle.

5.6.1 Improved model in a PV system

Modeling the DC-DC Converter for Stability

A typical generic DC-DC converter is a semiconductor based, PWM controlled, switched state system. It can be modelled a four-terminal network, in which the source end is connected with PV module through a series inductor as illustrated in Fig.5.16. In the boost mode the switch is as shown while in the buck mode, the roles are reversed. The model shown is that of a boost converter. Two parameters may be used to define the operation of the converter, k and α . For the boost operation, $k=1$ and $\alpha=1-T_d$ where T_d is the converter duty cycle time. For buck operations, $k=-1$ and $\alpha=T_d$.

The power supply voltage is v_{pv} . i_{pv} and v_c are input current and output voltage, respectively. The output is connected to a capacitive load. R and C are the load resistance and capacitance connected in parallel. Thus, the voltage across the inductance is given by

$$v_L = L\, di_{pv}/dt = k\left(v_{pv} - \alpha v_c\right) \tag{5.31}$$

The current equation is obtained by applying Kirchhoff's current law on the output side. They are used to derive the discrete time equation for the converter.

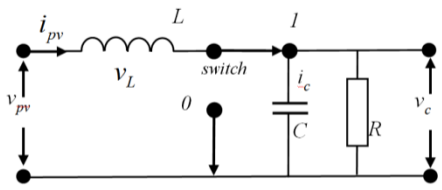

Figure 5.16: Equivalent circuit of a DC-DC converter

In the boost mode, the dynamics is governed by the pair of discrete time recursive equations [40, 47]

$$i_{pv}(k+1) = i_{pv}(k) + (T_s/L)(v_{pv}(k) - sv_c(k)) \tag{5.32a}$$

$$v_c(k+1) = (1 - T_s/RC)v_c(k) + s(T_s/C)i_{pv}(k) \tag{5.32 b}$$

where T_s is the sampling time. In the 'OFF' state, or when the switch is or open, the switching variable $s = 1$; when the switch is in the 'ON' state or closed, $s = 0$.

Bilinear Discrete Time Model and Stability

The equations(5.32) can be expressed in matrix form as follows:

$$\begin{bmatrix} i_{pv}(k+1) \\ v_c(k+1) \end{bmatrix} = \begin{bmatrix} 1 & 0 \\ 0 & 1 - T_s/RC \end{bmatrix} \begin{bmatrix} i_{pv}(k) \\ v_c(k) \end{bmatrix} + \frac{T_s}{L} \begin{bmatrix} 1 \\ 0 \end{bmatrix} v_{pv}(k) + s \begin{bmatrix} 0 & -T_s/L \\ T_s/C & 0 \end{bmatrix} \begin{bmatrix} i_{pv}(k) \\ v_c(k) \end{bmatrix} \tag{5.33}$$

In which s is a binary control variable. There must be adequate stability margins for those roots whose magnitudes are strictly less than unity, which will guarantee the stability and the robustness of the open/closed loop system for any value of the binary control variable s. The binary control variable can be updated based on the following equation:

$$s(k+1) = s(k) + \Delta s(k) \tag{5.34}$$

In which the values of s and Δs will be explained below. The above equations (5.33) are not linear in controlling the state vector Δs with three elements. In addition, the system of equations represent a typical bilinear system, the principle of

the linear control law [47]. The three key controlled variables are i_{pv}, v_c and S. These three variables are predicted for the next sampling instant in order to generate the control action Δs for both the current and future times. A predictive controller that uses a one-step horizon is achieved according to four measured values of i_{pv}, v_{pv}, v_c and s. The control input Δs is Estimated, the performance of the controlled variables in the future are predicted based on the evaluation of a cost function and the current value of s.

5.6.2 Performance Index in Model Predictive Controller

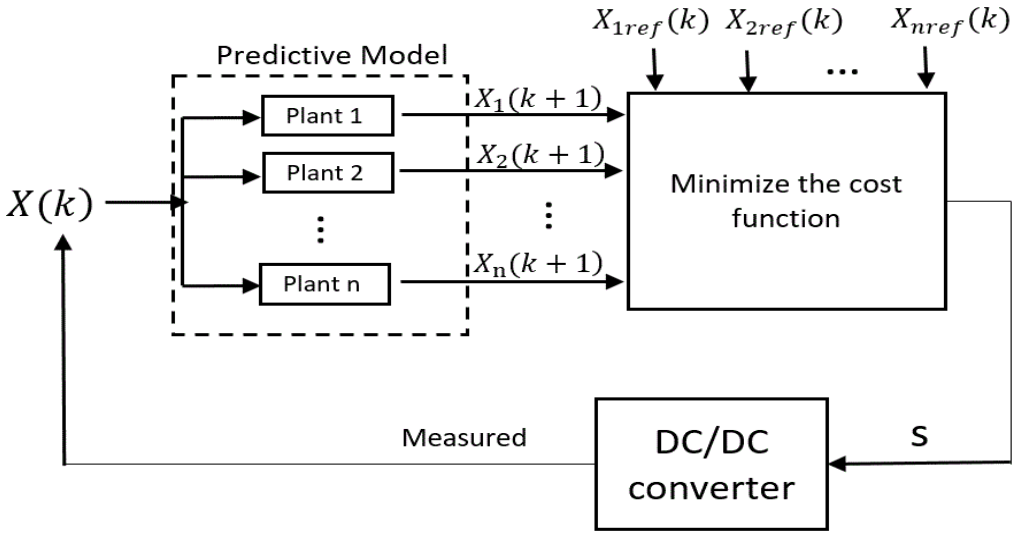

Figure 5.17: General MPC block diagram

Fig. 5.17 depicts the general principle of a predictive controller. The future behaviour of the control variables can be predicted from (8). In terms of PV system, $i_{pv}(k+1)$ and $v_c(k+1)$ are obtained by predictive control law, while $v_{pv}(k)$ is extracted from the I-V characteristics of PV cell from Fig. 5.17.

The predictive variables are compared using the cost function, which is expressed as

$$J = \lambda_1 \left| X_1(k+1) - X_{1ref}(k+1) \right| + \lambda_2 \left| X_2(k+1) - X_{2ref}(k+1) \right|$$

$$+\ldots+\lambda_n\left|X_n(k+1)-X_{nref}(k+1)\right| \tag{5.35}$$

Generally, (5.36) can be extended as a discrete time equation as following:

$$\begin{bmatrix} i_{pv}(k+n+1) \\ v_c(k+n+1) \end{bmatrix} = \begin{bmatrix} 1 & 0 \\ 0 & 1-T_s/RC \end{bmatrix} \begin{bmatrix} i_{pv}(k+n) \\ v_c(k+n) \end{bmatrix} + \frac{T_s}{L} \begin{bmatrix} 1 \\ 0 \end{bmatrix} v_{pv}(k+n)$$

$$+s \begin{bmatrix} 0 & -T_s/L \\ T_s/C & 0 \end{bmatrix} \begin{bmatrix} i_{pv}(k+n) \\ v_c(k+n) \end{bmatrix} \tag{5.36}$$

The system defined in the preceding section is a bilinear system. The control input is Δs . A linear control law can be defined to control the bilinear system without the need to change the bilinear character of the system. To determine the linear control input Δs , a nonlinear MPC synthesis approach is adopted. First a suitable performance index is defined. To this end the cost function $g(k,s)$ is defined as

$$g(k,s)=\left|i_{pv}(k+1)-i_{ref}\right| \tag{5.37}$$

Where i_{ref} is obtained by P&O method using MPPT algorithm. The proposed method will show a faster response than traditional P&O method under rapid changing conditions.

Moreover, the performance variable J is expressed as

$$J = g(k,0) - g(k,1) \tag{5.38}$$

Essentially J is evaluated as the plant which is switched from one state to the other. Therefore, the values of the variables and the current state of the switch based on control Δs is calculated as shown in Table 5.3.

Table 5.3: Choice of Δs

S=1 AND J<0	$\Delta s = -1$
S=0 AND J>0	$\Delta s = 0$
S=1 AND J>0	$\Delta s = 0$
S=0 AND J>0	$\Delta s = 1$

The reference current is estimated at the Maximum Power Point, b increasing or decreasing until the MPP is obtained. In most PV arrays, because insolation varies greatly, better performance variable is required.

Consider the change in the power output of a PV system at a reference operating point, the derivation of output power can be expressed as

$$dP_{pv}(k+1) = v_{pv}(k+1)\left(i_{pv}(k+1) - i_{ref}\right) + \left(v_{pv}(k+1) - v_{pv}(k)\right)i_{ref} \tag{5.39}$$

Thus,

$$\frac{dP_{pv}(k+1)}{v_{pv}(k+1)} = i_{pv}(k+1) - i_{ref} + \left(1 - \frac{v_{pv}(k)}{v_{pv}(k+1)}\right)i_{ref} = i_{pv}(k+1) - \left(\frac{v_{pv}(k)}{v_{pv}(k+1)}\right)i_{ref} \tag{5.40}$$

A modified performance function is then defined as

$$g_{\mathrm{mod}}(k,s) = \left|\frac{dP_{pv}(k+1)}{v_{pv}(k+1)}\right| = \left|i_{pv}(k+1) - \left(\frac{v_{pv}(k)}{v_{pv}(k+1)}\right)i_{ref}\right| \tag{5.41}$$

where it is assumed that $v_{pv}(k+1) \neq 0$. When $v_{pv}(k+1) = 0$, no power is being delivered by the PV system. Thus, $v_{pv}(k)$ is set to zero and

$$g_{\mathrm{mod}}(k,s) = \left|\frac{dP_{pv}(k+1)}{v_{pv}(k+1)}\right| = \left|i_{pv}(k+1) - i_{ref}\right| \tag{5.42a}$$

The corresponding performance variable is

$$J_{\text{mod}} = g_{\text{mod}}(k,0) - g_{\text{mod}}(k,1) \tag{5.43b}$$

The resistance increment is equal to the instantaneous resistance of PV cells at MPP.

Step size adaptation law

Adaptive searching and reduction of appropriate step size can accelerate the speed of the algorithm. The incremental change in the power output of a PV system can be alternately expressed as,

$$\frac{dP_{pv}(k+1)}{di_{pv}(k+1)} = i_{pv}(k+1)\left(\frac{v_{pv}(k+1)}{i_{pv}(k+1)} + \frac{dv_{pv}(k+1)}{di_{pv}(k+1)}\right) = i_{pv}(k+1)\left(r(k+1,s) - R(k+1,s)\right) \tag{5.43a}$$

where

$$r(k+1,s) = v_{pv}(k+1)/i_{pv}(k+1) \tag{5.44b}$$

is known as the incremental resistance while instantaneous array resistance in a PV module is expressed as

$$R(k+1,s) = -dv_{pv}(k+1)/di_{pv}(k+1) \tag{5.44c}$$

Then, a new performance index J_{new} can be defined as

$$J_{new} = r(k+1,s) - R(k+1,s) \tag{5.44}$$

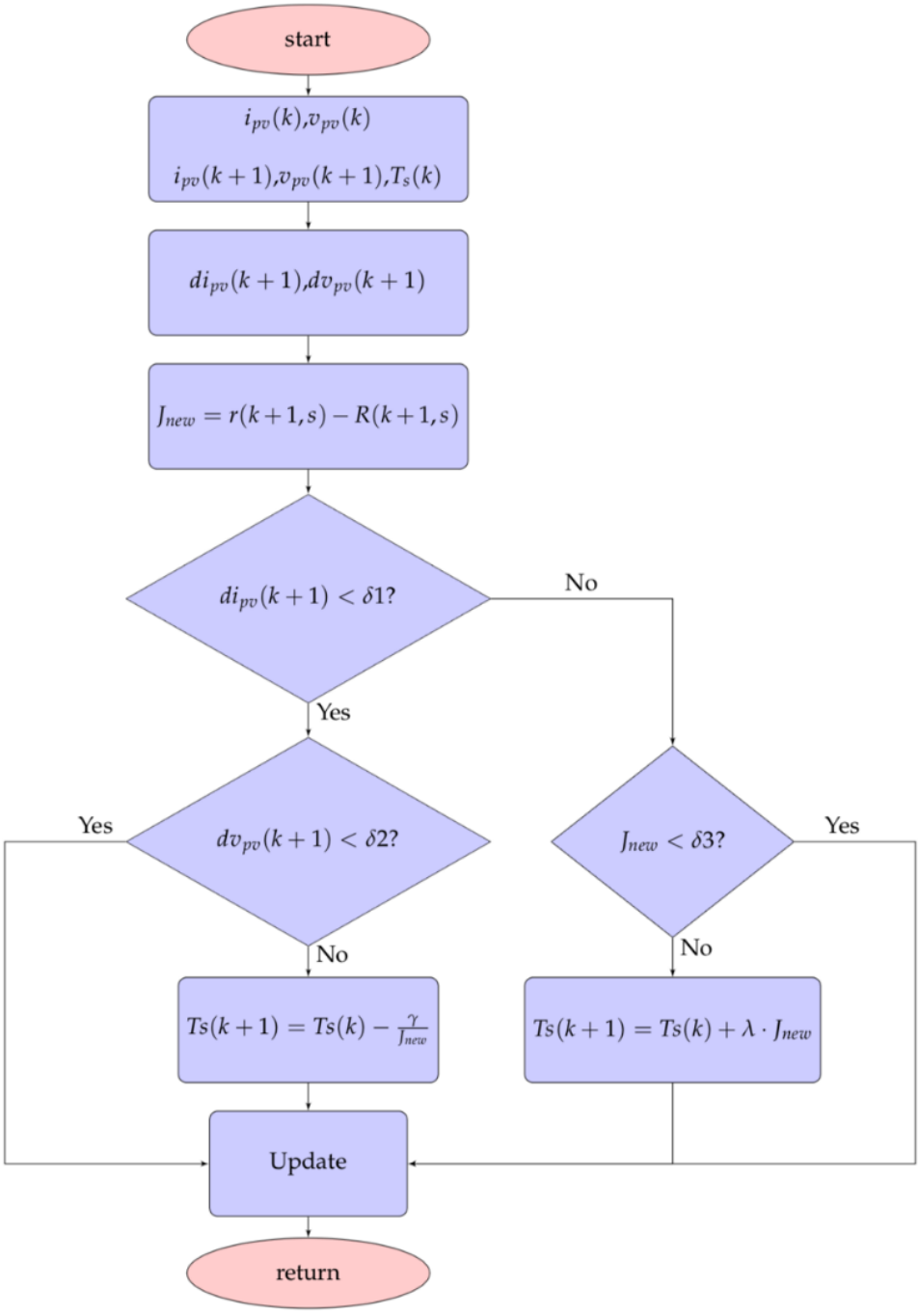

Figure 5.18: Step Size Adaption Control Law

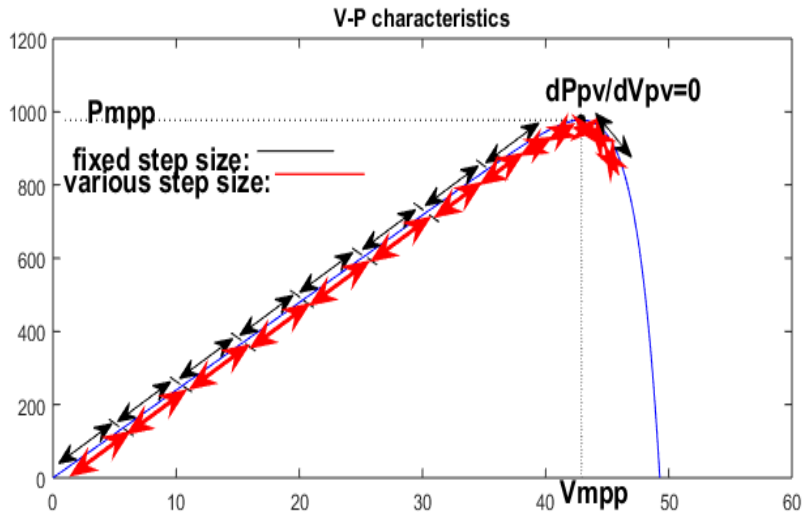

Figure 5.19: Variable size and fixed step size behaviour

When the initial operating point is near the MPP, the speed of this technique is relatively fast. Therefore, the above algorithm is preserved when the operating point is close to the MPP. Otherwise, the best step size is chosen using a second algorithm. As shown in Fig.5.18, the behaviour in a PV module is related to the step size because of its nonlinear characteristics.

In terms of the new performance index J_{new}, the variable step size control law with positive and small constants ε_j, $j = 1,2$ is defined as following:

i) If $di_{pv} > 0$,$J_{new} < \varepsilon_1$, there is no change made to the step size;

ii) If $di_{pv} > 0$,$J_{new} > \varepsilon_1$, the step size is expressed as $dt(k+1) = dt(k) + \lambda J_{new}$ where λ is constant;

iii) $di_{pv} < 0$, $dv_{pv} < \varepsilon_2$, there is no change made to the step size;

iv) $di_{pv} < 0$, $dv_{pv} > \varepsilon_2$, the step size is expressed as $dt(k+1) = dt(k) - \gamma / J_{new}$ where γ is constant, where the variable step size value λ and γ can be found from [109]-[107]. The difference between fixed step size law and variable step size is shown in Fig. 5.18.

Flow chart of variable step MPC method is illustrated in Fig. 5.19. In the following sections, the proposed performance indices based on the model predictive controller will be evaluated and compared with the other algorithms including the fixed step size control law.

Droop Control law

Droop control is implemented to achieve parallel operation of micro-power supply in micro grid. In power system, droop control has been used in control systems for regulating the power output by simulating the droop characteristics or traditional generators. Generally, droop control is used to adjust the converter output impedance to balance the bus voltage when supplied by multiple power sources. In the case of PV systems, when the converter provides a larger current, the technique is utilised to reduce the output voltage in order to achieve a constant bus voltage. The converter can consequently maintain the bus voltage based on the load line equation which is formulated as

$$v_{bus} = v_{ref} - R_{droop} I \tag{5.45}$$

In which R_{droop} is the droop factor. It is designed for a stable bus voltage v_{bus} by regulating bus voltage considering the converter output current [62, 113]. The principle problem is the choice of the droop factor. Here are the solutions: the ratio R^i_{droop} / R_{ci} is assumed to be maintained as a constant between 0.5 to 1. In which R_{ci} and R^i_{droop} are the output resistance of a DC converter and the corresponding droop factor of converter i, respectively. It might be obliging to change the droop coefficient R_{droop} adaptively in practice. It is noted that any increment in R_{droop} will only result in the power loss. Thus, R_{droop} is advised to be small when

increasing its value. While when decreasing, a much larger number should be considered.

Considering two DC converters with output voltages $v_{con,1}$ and $v_{con,2}$,

$$v_{bus} = v_{con,1} - R^1_{droop} I_{con,1} = v_{con,2} - R^2_{droop} \tag{5.46}$$

the adaptation law is expressed as

$$R^1_{droop}(K+1) = R^1_{droop}(k) + sign(v_{con,1} - v_{con,2}) i_{con,1} K \tag{5.47a}$$

where the constant K is chosen based on numerical simulations as follows:

$K = K(v) = 0.0005$ to 0.001 when

$$v = sign\big(v_{con,1} - v_{con,2}\big) > \delta \tag{5.48b}$$

$K(v) = 0.01$ to 0.02 when

$$v = sign\big(v_{con,1} - v_{con,2}\big) < -\delta \tag{5.48c}$$

δ being a small positive number. In practice, in order to make the simulations realistic, Gaussian distributed White noise of appropriate strength has been added to the outputs of the converter $v_{con,1}$ as shown in equations, based on the data provided in [58].

Considering the inherent load-dependent voltage variation of a PI controller is one classic technique to define the control law in a control system. In doing so, the bus voltage level is measured and compared with the desired voltage. The output of the lead filter is introduced to change the droop factor.

Given R_{droop} the controlled bus voltage is obtained by adjusting it and takes the form

$$v_{bus} = v_{con} - \left(R_{droop} - \delta R_c\right) I \tag{5.48a}$$

$$\delta R_c = K_p e + K_I \int e dt \ , \ e = v_{con} - v_{bus} \tag{5.49 b}$$

$$v_{con} = v_{con,ideal} + v_{con,noise} \tag{5.49 c}$$

The proposed adaptive law and performance indices are evaluated independently. They are validated and compared with several traditional methods in the following section. The droop controller lead to a reduction in the output power in a PV system. It is significant to keep this reduction within limits.

5.7 Typical simulation results

The *I–V* characteristic of the PV system used in this paper for different irradiance levels are illustrated in Fig. 5.20.

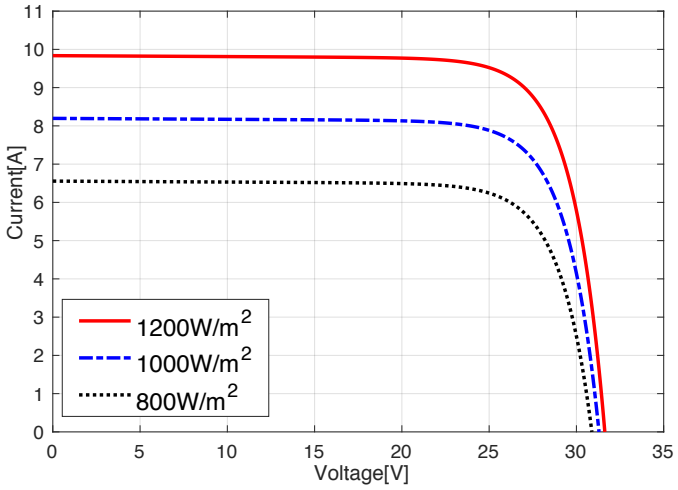

Figure 5.20: I–V characteristics of the PV cell

Table 5.4 illustrated the parameters of the PV cell and a converter/controller system. Some of the other parameters used in the two cases with the performance index J_{mod} and J_{new} are also given for simulating the PV cells in the module. The implementation involving the performance indicator J_{new} including the adaptive adjustment. In this case the time step is considered to be variable.

Table 5.4: Typical Values of the System Parameters

PV Parameter	Nominal Value	Other Parameters	Nominal Value
I_{scn}	8.7 *amps*	I_{mp}	8.2 *amps*
V_{ocn}	37.7 *volts*	V_{mp}	30.1 *volts*
α	1.5	R_p	415.405 Ω
R_s	0.221 Ω	T	298.15 °K
K	-0.12064	K_i	-0.002784

To make simulations realistic, the Gaussian distributed White noise of appropriate strength to the output of the PV cell based on experimental data reported in [40] is also been added. Therefore, the algorithms are tested with noise included. In the results section, the proposed MPC based MPPT algorithm is firstly implemented and compared to the traditional P&O technique. The sampling time is set to be 50μs. The simulation results are shown in Fig. 5.21. In order to make simulation results more practical, the distributed White noise is introduced as the disturbance. Furthermore, the results based on the variable step size with the MPC and those of the P&O method are compared in Fig.5.22. The initial operating power level is 2000 W. The characteristics of the two approaches are summarized in Table 5.4.

In Fig. 5.22, the oscillations in the results from the application of the P&O method are comparatively reduced in the corresponding results obtained by the MPC method. There is a trade-off which has to be considered in all of the conventional approaches, including the P&O method. When the size of the increments is increased in the P&O technique, the speed of response will be faster but there are also more oscillations, and verse visa. Thus, it is difficult to increase the speed of response while also reducing the magnitude of the oscillations. From the comparison results illustrated in Fig. 5.23, it is obvious that the reaction of the variable step size method is significantly superior to the conventional P&O method. Also, it is seen that the disturbances are well attenuated in the presence of White noise in the output of the PV cell.

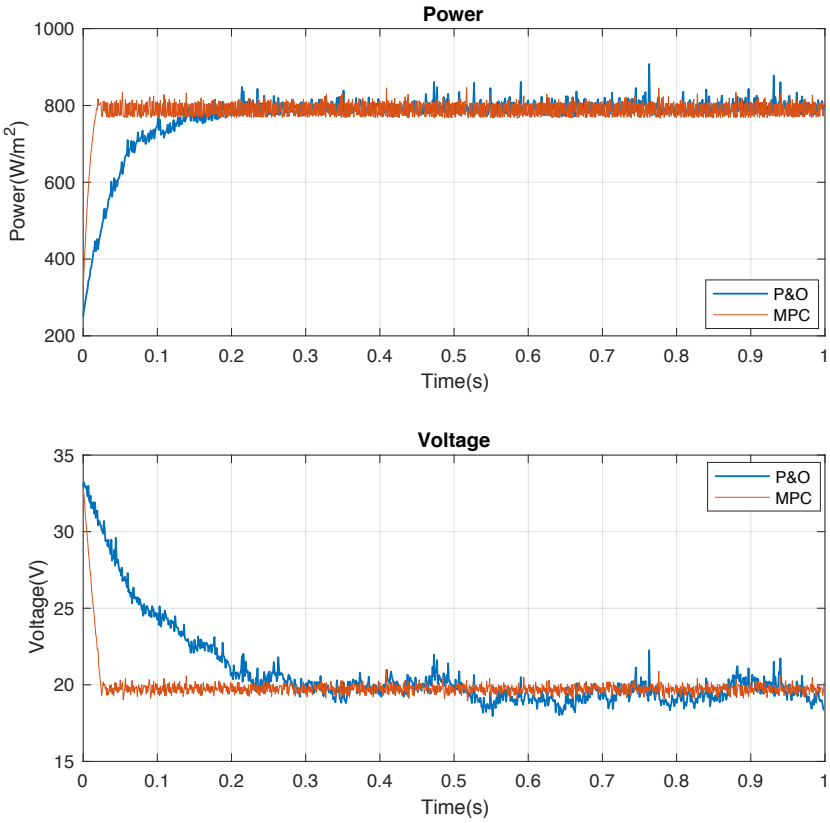

Figure 5.21: Comparison of the power and the voltage output using the P&O and the MPC methods

In order to validate the proposed methods, the model for predicting the air temperature is used to simulate the real environmental conditions [111]. The latitude value used in the model is 51.5074 which is the value of London. The time range is set to from 9am to 4pm. Also, the Gaussian distributed random variable is transformed to simulate a Weibull distributed value of the air temperature. The system is tested for eight maximum operating power levels. The results are illustrated in Figs. 5.23 and 5.24 under the proposed condition. In the two Figures, the powers obtained by using the performance indices J_{mod} and J_{new} are compared with the corresponding results obtained by using the P&O method.

Starting at $t = 0.5s$, the temperature level is set to be rapidly reduced due to the variations of the air temperature in the model. At $t = 3s$ a step increment is involved in the operating temperature level and thus the operating temperature starts to increase. It is seen from the simulation results that the variable adaptive step algorithm based on J_{new} has superiority in response speed under rapidly changing operational conditions. Not only the proposed methods are verified to be more effective in terms of both the speed of response and a reduction in the magnitude of the oscillation, but also show a robust performance particularly with parameter variations, which results in a higher extracted energy for a real PV system.

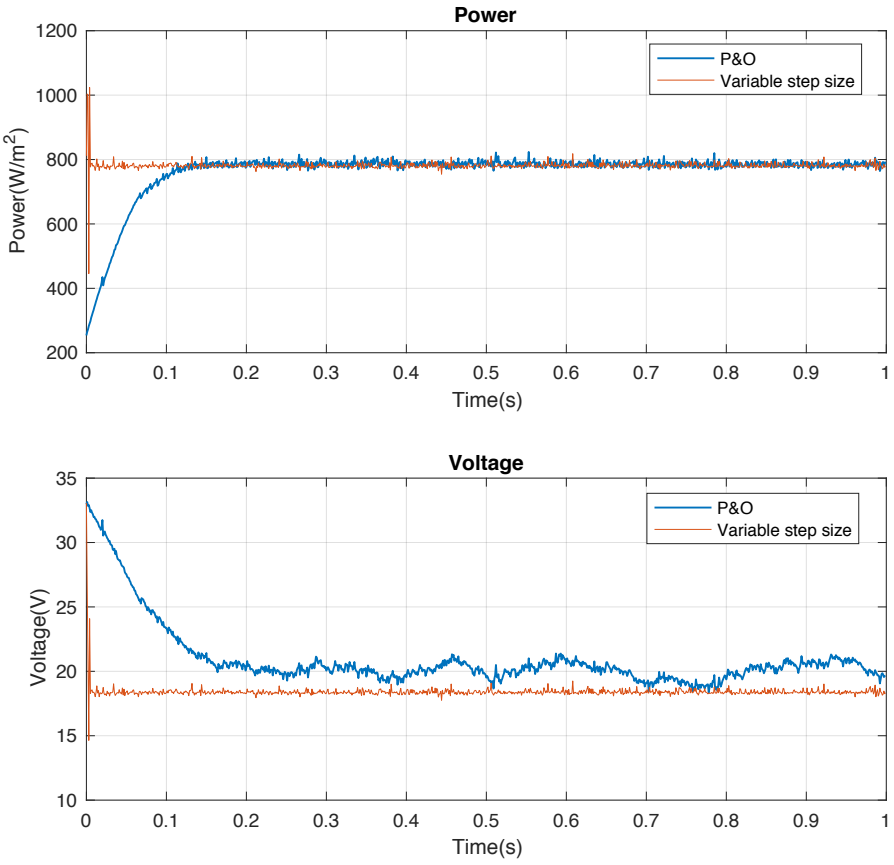

Figure 5.22: Comparison of the power output and the voltage using the P&O and the Step size methods

Table 5.5: Characteristics of Different MPPT Algorithms

	Cost function	Controller	Increment
P&O	None	P&O	Fixed
$\mathbf{J_{mod}}$	$\left\lvert i_{pv}(k+1)-\left(\frac{v_{pv}(k)}{v_{pv}(k+1)}\right)i_{ref}\right\rvert$	MPC	Fixed
$\mathbf{J_{new}}$	$r(k+1,s)-R(k+1,s)$	MPC	Variable

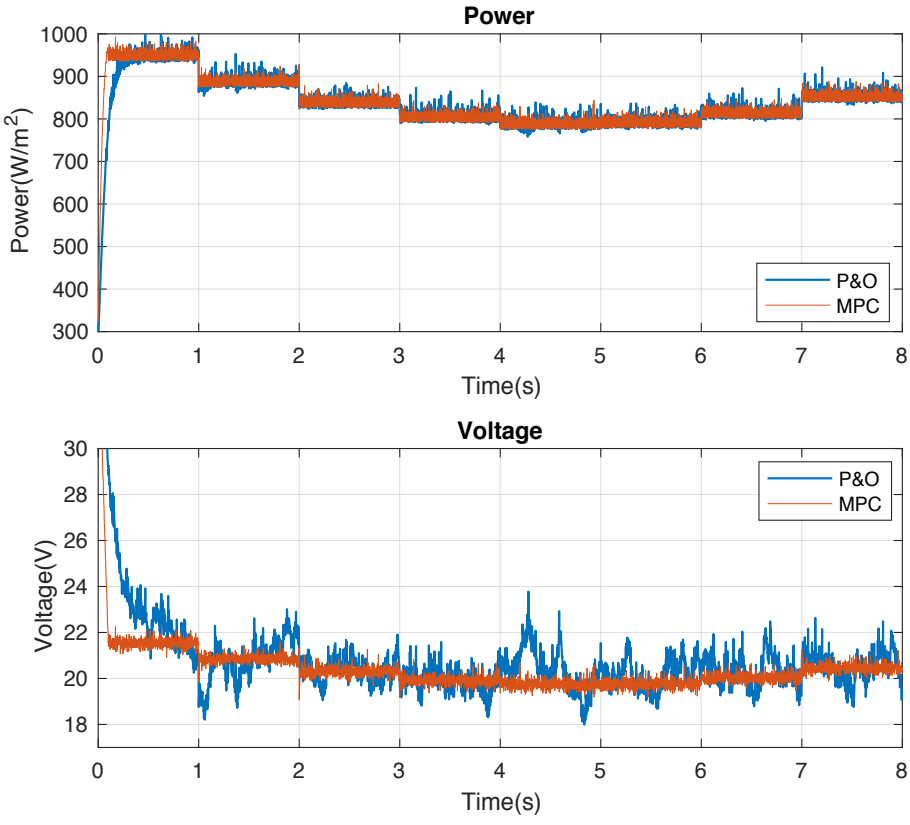

Figure 5.23: Comparison of the power output and the voltage using the P&O algorithm and the MPC method from 9am to 4pm with White noise in temperature and wind speed

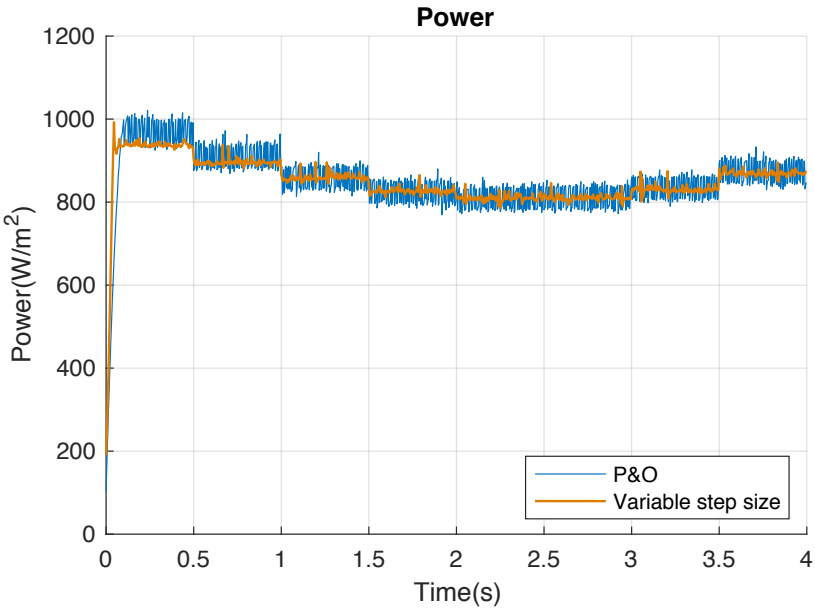

Figure 5.24: Comparison of the power output using the P&O and the Variable step size techniques from 9am to 4pm with White noise in temperature and wind speed

The ability to maintain the bus voltage within limits along with the superior of the proposed droop control method is illustrated in Fig. 5.25. The variations of the converter voltage v_{con} are compared for two converters connected to the bus. The results show how they converge towards each other after a disturbance.

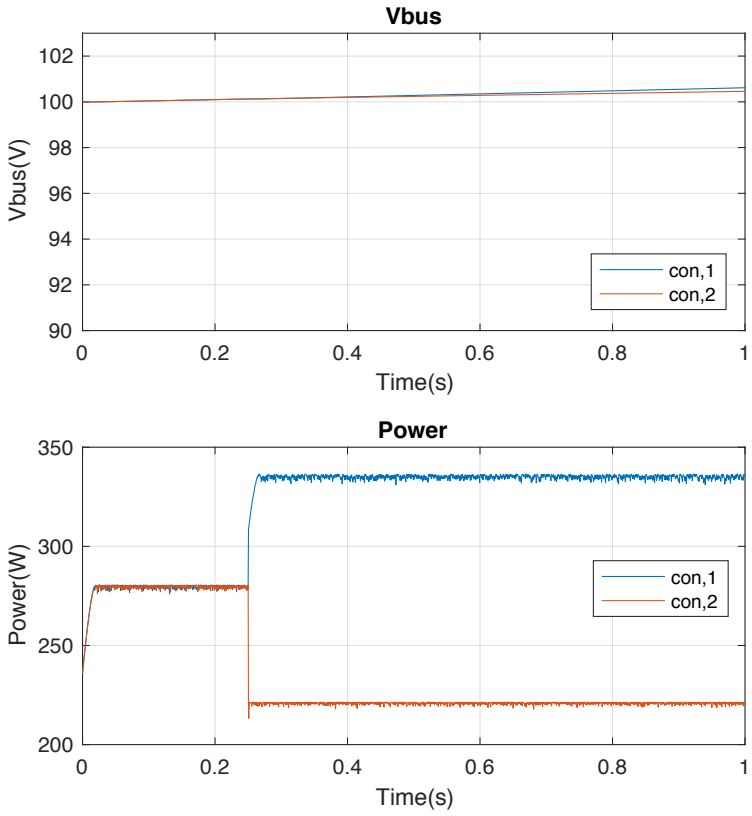

Figure 5.25: The power and the bus voltage of two converters with time, using droop control in operation

5.8 Discussion and Conclusions

In the PV system, two MPPT procedures for photovoltaic applications and another for the droop control of the bus voltage when several solar cell packs are feeding into a single bus are presented. The first MPPT technique is based on a fixed step MPC while the second involves an adaptive variable step MPC. The two techniques were tested and compared. Results shows that the variable time step algorithm is generally faster. A novel feature of the proposed algorithms is that they are both adaptive and can handle variable step sizes. These algorithms have been tested with relatively large additions of process noise to emulate real experimental conditions. The advantages of the proposed techniques are evaluated and verified that they are able to yield the maximum energy under different insolation and environmental conditions. Furthermore, responds to the rapidly variation in case studies such as solar irradiance, the proposed variable step algorithm is confirmed to be more

efficient and stable comparing to the conventional fixed time step algorithms. Moreover, the parameters of the circuit model for the DC-DC converter are chosen to maximize the stability margin within the permissible limits. This ensures that the system is sufficiently robust. Moreover, both disturbance attenuation and the robustness of the controller are validated by simulation. In addition, the performance of a droop control method for parallel DC-DC converters used in standalone photovoltaic systems is also investigated. For different irradiance of multiple PV arrays the droop control system is tested and verified.

Chapter 6 Wind Turbine Modelling and Control

6.1 Introduction

In this chapter, a linearised parameter varying dynamic modelling of the nonlinear wind turbine system including wind disturbances is developed. The stability of the wind turbine system is first considered, and a blade pitch control system is designed, based on the linearised, parameter-varying model. The basis of the controller is model predictive control which is then validated. Thus, the wind turbine is regulated in a way that the generator delivers the desired power to the load. Operation at the maximum power point is also shown to be feasible. Moreover, the blade pitch control system also performs the key function of augmenting the stability of the wind turbine system.

6.2 Dynamic modelling of the PMSG and the Wind Turbine

The simplified block diagram of a wind turbine model is illustrated in Fig.6.1.

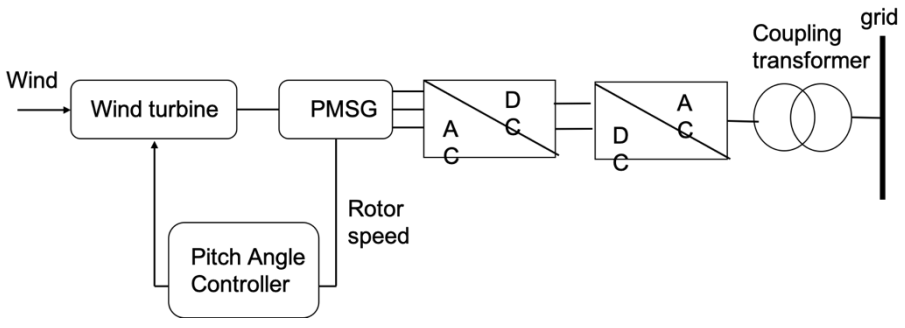

Figure 6.1: Plots of the torque coefficient $C_T = C_p(\lambda, \beta)/\lambda$

The dynamics of the PMSG is modelled in the well-known *d-q* co-ordinates. For example, Vepa [98] and the currents in the *d-q* axes satisfy the differential equations given by

$$\begin{bmatrix} L_d & 0 \\ 0 & L_q \end{bmatrix} \frac{d}{dt} \begin{bmatrix} i_d \\ i_q \end{bmatrix} = \begin{bmatrix} -R_a & L_q p\omega_m \\ -L_d p\omega_m & -R_a \end{bmatrix} \begin{bmatrix} i_d \\ i_q \end{bmatrix} + \begin{bmatrix} 0 \\ -p\omega_m \emptyset_m \end{bmatrix} + \begin{bmatrix} u_d \\ u_q \end{bmatrix} \quad (6.1)$$

The electro-magnetic torque generated is given by [98]

$$T_{em} = \frac{3}{2} p\left(\left(L_d - L_q\right) i_d i_q + \emptyset_m i_q\right) \quad (6.2)$$

Furthermore, the electrical frequency is related to the mechanical speed by the relation $\omega_e = p\omega_m$, where p is the number of generator pole pairs. Thus, given the driving torque generated by the wind turbine, dynamics of the mechanical shaft speed of the turbine is governed by

$$\mathrm{J} \frac{d\omega_m}{dt} + B\omega_m = T_{dr} - T_{em} \quad (6.3)$$

The power output of the wind turbine can be modelled in terms of the power coefficient $C_p(\lambda, \beta)$ which is function of both the tip speed ratio and the blade collective pitch angle β. The wind power output is formulated by

$$P_w = T_{dr}\omega_m = \frac{1}{2}\rho A V_w^3 C_p(\lambda, \beta) \quad (6.4)$$

where $\lambda = \omega_m R / V_w$ which is the tip speed ratio, $C_p(\lambda, \beta)$ is the output power coefficient and the torque driving the PMSG is calculated by

$$T_{dr} = T_{wt} = \frac{P_w}{\omega_m} = \frac{1}{2\omega_m}\rho A V_w^3 C_p(\lambda, \beta) \quad (6.5)$$

In (6.5), the turbine hub atmospheric air density is ρ, which is assumed to be at a height H. R is the outer radius of the rotor. An approximate expression for the power coefficient is given by

$$C_p(\lambda,\beta) = 0.5176\left(\frac{116}{\lambda_i} - 0.4\beta - 5\right)e^{-\frac{21}{\lambda_i}} + 0.006795\lambda_i \qquad (6.6)$$

where λ_i is given by

$$\lambda_i = {}^{1}\Big/_{\frac{1}{\lambda+0.08\beta} - \frac{0.035}{1+\beta^3}} \qquad (6.7)$$

The maximum pitch angle β_{max} is assumed to be 30°.

A generic expression for the power coefficient $C_p(\lambda,\beta)$ is

$$C_p(\lambda,\beta) = C_1\left(\frac{C_2}{\lambda_i} - C_3\beta - C_4\beta^{C_5} - C_6\right)e^{-\frac{C_7}{\lambda_i}} + C_8\lambda_i \qquad (6.8)$$

In which λ_i is calculated as

$$\lambda_i = {}^{1}\Big/_{\frac{1}{\lambda+C_9\beta} - \frac{C_{10}}{1+\beta^3}} \qquad (6.9)$$

Table 6.1 lists the approximations to constant parameters C_i, in the power coefficient $C_p(\lambda,\beta)$ (from Wijewardana, Shaheed and Vepa [114]). Plots of the power coefficient $C_p(\lambda,\beta)$ and the torque coefficient $C_p(\lambda,\beta)/\lambda$ are respectively compared in Figs 6.1 and 6.2, for increasing values of the blade pitch angle.

The blade pitch angle actuator is assumed to be represented by the first order dynamics given by

$$\tau_b\dot{\beta} + \beta = u_c \qquad (6.10)$$

Table 6.1: Approximations to the parameters $C_i, i = 1,2,\ldots,10$ in the expressions for the Power Coefficient $C_p(\lambda, \beta)$

Model	**Our Model**	**Voltolini et al** [112]	**Heier** [113]	**Constant speed operation**	**Variable speed operation**
C_1	0.5176	0.5176	0.5	0.44	0.73
C_2	116	116.0	116.0	125.0	151.0
C_3	0.4	0.4	0.4	0	0.58
C_4	0	0	0	0	0.002
C_5	0	0	0	0	2.14
C_6	5	5	5	6.94	13.2
C_7	21	21	21	16.5	18.4
C_8	0.006795	0.006795	0	0	0
C_9	0.08	0.08	0.08	0	-0.02
C_{10}	0.035	0.035	0.035	-0.002	-0.003

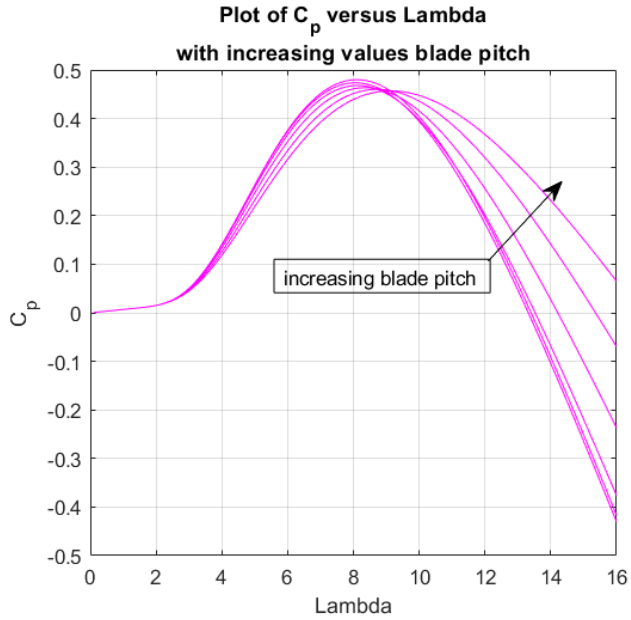

Figure 6.2: Plots of the power coefficient $C_p(\lambda, \beta)$

In which τ_b is the blade actuator time constant, and u_c is the blade angle control input which may be expressed in terms error between the blade angle feedback and the demanded blade angle as $e = \beta - \beta_d$.

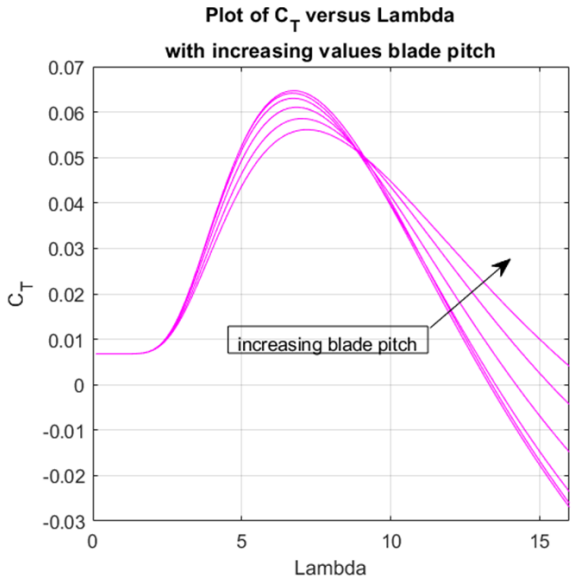

Figure 6.3: Plots of the torque coefficient $C_T = C_p(\lambda, \beta)/\lambda$

At any location on the Earth's surface, the wind is distributed probabilistically. The Weibull distribution best describes the probability distribution of the wind. Since the wind power is proportional to the third power of the wind speed, as a consequence of the fact that the wind is a random variable, the actual mean wind power at a

particular location can be expressed in terms of the parameters of the Weibull distribution and is given by

$$T_{dr}\omega_m = \frac{1}{2}\rho A\overline{V_w}^3 C_p(\lambda,\beta)\frac{1}{\bar{c}^3}\Gamma(1+\frac{3}{k}) \tag{6.11}$$

Where $\bar{c} = \Gamma(1+\frac{3}{k})$. In which $\bar{c}$ and k are the parameters of Weibull distribution, $\overline{V_w}$ is mean wind speed, Γ is the Gamma function.

Finally, one may specify the desired power output as follows:

When $\overline{V_w}$ below cut-off, which is $\overline{V_w}<\overline{V_{cut\_off}}$,

$$P_d = 0;\ \beta = \beta_{max} \tag{6.12}$$

For $\overline{V_{cut\_off}} \le \overline{V_w} < V_{rated}$,

$$P_d = \overline{P_w} = \frac{1}{2}\rho A\overline{V_w}^3 C_p(\lambda,\beta)\frac{1}{\bar{c}^3}\Gamma(1+\frac{3}{k});\beta = 0 \tag{6.13}$$

For $V_{rated} \le \overline{V_w} < V_{max}$,

$$P_d = \frac{1}{2}\rho A{V_{rated}}^3 C_p(\lambda,0)\frac{1}{\bar{c}^3}\Gamma(1+\frac{3}{k});\overline{P_w} = \frac{1}{2}\rho A\overline{V_w}^3 C_p(\lambda,\beta)\frac{1}{\bar{c}^3}\Gamma(1+\frac{3}{k}) \tag{6.14}$$

For $\overline{V_w} \ge V_{max}$,

$$P_d = 0;\ \beta = \beta_{max} \tag{6.15}$$

Hence, given the expression for the rated $C_p(\lambda,\beta) = C_p(\lambda,0)$ $(\frac{{V_{rated}}^3}{\overline{V_w}^3})$ and the actual operational value of the power coefficient $C_p(\lambda,\beta)$, the problem is often reduced to one finding the value to be set for β to achieve the desired value of the power coefficient$C_p(\lambda,\beta)$.

6.3 De-coupling the electrical and mechanical subsystems

To simplify the design of the controller for the wind turbine it is useful to decouple the electrical and mechanical subsystems. Thus, to decouple the electrical and mechanical sub-systems, re-consider the electrical sub-system dynamics given by (6.1)

$$\begin{bmatrix} L_d & 0 \\ 0 & L_q \end{bmatrix} \frac{d}{dt} \begin{bmatrix} i_d \\ i_q \end{bmatrix} = \begin{bmatrix} -R_a & L_q p\omega_m \\ -L_d p\omega_m & -R_a \end{bmatrix} \begin{bmatrix} i_d \\ i_q \end{bmatrix} + \begin{bmatrix} 0 \\ -p\omega_m \emptyset_m \end{bmatrix} + \begin{bmatrix} u_d \\ u_q \end{bmatrix} \tag{6.16}$$

With electrical feedback

$$\begin{bmatrix} u_d \\ u_q \end{bmatrix} = \begin{bmatrix} L_q p\omega_m i_q \\ R_d i_{q0} + p\omega_m \emptyset_m + L_d p\omega_m i_d \end{bmatrix} \tag{6.17}$$

one has

$$\begin{bmatrix} L_d & 0 \\ 0 & L_q \end{bmatrix} \frac{d}{dt} \begin{bmatrix} i_d \\ i_q \end{bmatrix} = \begin{bmatrix} -R_a & 0 \\ 0 & -R_a \end{bmatrix} \begin{bmatrix} i_d \\ i_{q-i_{q0}} \end{bmatrix} \tag{6.18}$$

The electro-magnetic torque generated is given by

$$T_{em} = \frac{3}{2} p\big(\big(L_d - L_q\big) i_d i_q + \emptyset_m i_q\big) \tag{6.19}$$

Thus, the electrical and mechanical subsystems are coupled, and the controllers can be independently synthesized. Moreover, the stability can be independently assessed.

6.4 The State Space Model

The dynamics of the PMSG driven by the wind turbine may now be expressed in state space domain. Define the state vector

$$\mathrm{x} = [i_d \quad i_q \quad \omega_m \quad \beta]^T \tag{6.20}$$

Equation (6.16) can be rewritten as

$$\begin{bmatrix} L_d & 0 \\ 0 & L_q \end{bmatrix} \frac{d}{dt} \begin{bmatrix} x_1 \\ x_2 \end{bmatrix} = \begin{bmatrix} -R_a & L_q p x_3 \\ -L_d p x_3 & -R_a \end{bmatrix} \begin{bmatrix} x_1 \\ x_2 \end{bmatrix} + \begin{bmatrix} 0 \\ -p x_3 \emptyset_m \end{bmatrix} + \begin{bmatrix} u_d \\ u_q \end{bmatrix} \tag{6.21}$$

On the other hand, based on the decoupled model

$$\begin{bmatrix} L_d & 0 \\ 0 & L_q \end{bmatrix} \frac{d}{dt} \begin{bmatrix} x_1 \\ x_2 \end{bmatrix} = \begin{bmatrix} -R_a & 0 \\ 0 & -R_a \end{bmatrix} \begin{bmatrix} x_1 \\ x_2 - x_{20} \end{bmatrix} \tag{6.22}$$

$$T_{em} = \frac{3}{2} p\left(\left(L_d - L_q\right) x_1 x_2 + \emptyset_m x_2\right) \tag{6.23}$$

The mechanical dynamics in terms of the states is,

$$J x_3 + B x_3 = T_{dr} - T_{em} \tag{6.24}$$

In which T_{dr} can be expressed as

$$T_{dr} = T_{wt} = \left(\frac{P_w}{x_3}\right) = \frac{1}{2} x_3 \rho A V_w^3 C_p(\lambda, x_4) = \frac{1}{2} \rho A V_w^2 R C_T \tag{6.25}$$

In which C_T is calculated by

$$_T = C_p(\lambda, x_4)/\lambda \tag{6.26}$$

Where $\lambda = x_3 R / V_w$. (6.10) can be expressed as

$$\tau_b \dot{x_4} = u_c - x_4 \tag{6.27}$$

6.5 Linearised Dynamics of the Wind Turbine

The complete dynamics may now be linearised and the conditions for equilibrium and stability may be established. The derivative of the mechanical torque driving the PMSG is

$$\frac{dC_T}{d\lambda} = \frac{d}{d\lambda}\left(\frac{C_p(\lambda,\beta)}{\lambda}\right) = \frac{1}{\lambda}\left(\frac{dC_p(\lambda,\beta)}{d\lambda} - \frac{C_p(\lambda,\beta)}{\lambda}\right) \tag{6.28}$$

Thus, linearising the expression for T_{dr} gives

$$T_{dr} = \frac{1}{2}\rho A V_w^2 \frac{d}{d\lambda}\left(\frac{C_p(\lambda,\beta)}{\lambda}\right)(\lambda - \lambda_0) + \frac{1}{2}\rho A V_w^2 \frac{d}{d\beta}\left(\frac{C_p(\lambda,\beta)}{\lambda}\right)\beta \tag{6.29}$$

In terms of the states of the system,

$$T_{dr} = \frac{1}{2}\rho A V_w^2 \frac{d}{d\lambda}\left(\frac{C_p(\lambda,\beta)}{\lambda}\right)\frac{R}{V_w}(x_3 - x_{30}) + \frac{1}{2}\rho A V_w^2 \frac{d}{d\beta}\left(\frac{C_p(\lambda,\beta)}{\lambda}\right)\beta \tag{6.30}$$

where

$$\frac{d}{d\beta}\left(\frac{C_p(\lambda,\beta)}{\lambda}\right) = C_1\left(C_2 g\left(1 - \frac{C_7}{\lambda_i}\right) - C_3(1 - C_7\beta g)\right) - C_1(C_4\beta^{C_5-1}(C_5 - C_7\beta g) - C_6 C_7 g)\, e^{-\frac{C_7}{\lambda_i}} \tag{6.31}$$

In which g is formulated as

$$g = \frac{C_9}{(\lambda + C_9\beta)^2} + \frac{3\beta^2 C_{10} C_{11}}{(1 + C_{11}\beta^3)^2} \tag{6.32}$$

Thus, the derivative of the power coefficient $C_p(\lambda,\beta)$ with the tip speed ratio λ is calculated as

$$\frac{d}{d\lambda}C_p(\lambda,\beta) = C_8\left(1 + C_7\lambda\frac{dq_i}{d\lambda}\right) - C_7 C_p(\lambda,\beta)\frac{dq_i}{d\lambda} + C_1 C_2 e^{-C_7 q\frac{dq_i}{d\lambda}} \tag{6.33}$$

where

$$q_i = \frac{1}{\lambda_i} = \frac{1}{\lambda+\beta C_9} - \frac{C_{10}}{1+C_{11}\beta^3} \tag{6.34}$$

$$\frac{dq_i}{d\lambda} = \left(\frac{1}{\lambda+\beta C_9}\right)^2 \tag{6.35}$$

In which $\lambda = R\omega_m/U$.

The nominal dynamic pressure force on the wind turbine disc is denoted as $f_d = \frac{1}{2}\rho A\overline{V_w}^2$. Hence, after after linearising, T_{dr} is expressed as

$$T_{dr} = \frac{d}{d\lambda}\left(\frac{C_p(\lambda,\beta)}{\lambda}\right)\frac{f_d R}{V_w}(x_3 - x_{30}) + \frac{f_d}{\lambda}\frac{dC_p(\lambda,\beta)}{d\beta}\beta \tag{6.36}$$

The linearised driving torque is expressed as

$$T_{dr} = d_{er1}(x_3 - x_{30}) + d_{er2}\beta \tag{6.37}$$

where the stability derivatives d_{er1} are d_{er2} are defined as,

$$d_{er1} = \frac{dC_T}{d\lambda}\frac{f_d R}{V_w} = \frac{d}{d\lambda}\left(\frac{C_p(\lambda,\beta)}{\lambda}\right)\frac{f_d R}{V_w} \tag{6.38}$$

$$d_{er2} = \frac{f_d}{\lambda}\frac{dC_p(\lambda,\beta)}{d\beta} \tag{6.39}$$

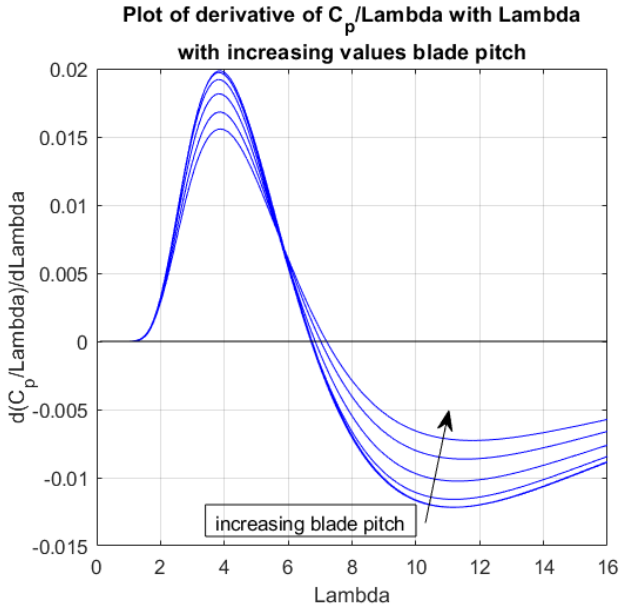

Figure 6.4: Stability derivative of the power coefficient

Plots of the derivatives of the power coefficient $C_p(\lambda, \beta)$ and the derivatives of the torque coefficient $C_T \equiv C_p(\lambda, \beta)/\lambda$ are respectively shown in Figs 6.2a and 6.2b, for increasing blade pitch angle.

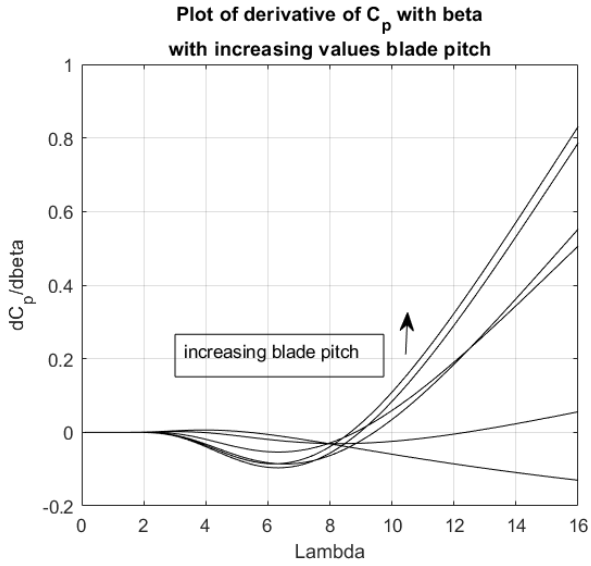

Figure 6.5: Stability derivative of the torque coefficient

It is clear from the Figs. 6.2-6.5 that wind turbine's power coefficient is effectively fully controllable only beyond λ equal to about 9. Positive $C_p(\lambda, \beta)$ values are feasible for $9 \leq \lambda \leq 13$. Thus, if one requires to reduce the value of the output power, or the value of $C_p(\lambda, \beta)$, one must necessarily increase the speed of the wind turbine. After linearising, T_{em} can be formulated as

$$T_{em} = \frac{3}{2}p\left(L_d - L_q\right)x_{10}x_2 + \emptyset_m x_2 + \frac{3}{2}p\left(L_d - L_q\right)x_1 x_{20} \quad (6.40)$$

Equation (6.40) is expressed as,

$$T_{em} = d_{er3}x_1 + d_{er4}x_2 \quad (6.41)$$

where the stability derivatives d_{er3} and d_{er4} are defined as,

$$d_{er3}\frac{3}{2}p\left(L_d - L_q\right)x_{20} \approx 0 \quad (6.42)$$

$$d_{er4} = \frac{3}{2}p\left(L_d - L_q\right)x_{10} + \emptyset \quad = \frac{3}{2}p\left(L_d - L_q\right)i_{d0} + \emptyset_m \quad (6.43)$$

Thus, the complete linear model is given as follows:

$$\mathrm{x} = [i_d \quad i_q \quad \omega_m \quad \beta]^T \quad (6.44)$$

with

$$\begin{bmatrix} L_d & 0 \\ 0 & L_q \end{bmatrix}\frac{d}{dt}\begin{bmatrix} x_1 \\ x_2 \end{bmatrix} = \begin{bmatrix} -R_a & L_q p x_{30} \\ -L_d p x_{30} & -R_a \end{bmatrix}\begin{bmatrix} x_1 \\ x_2 \end{bmatrix} + \begin{bmatrix} L_q p x_{20} \\ -L_d p x_{10} - p\emptyset_m \end{bmatrix} x_3 + \begin{bmatrix} u_d \\ u_q \end{bmatrix} \quad (6.45)$$

or in decoupled form, with the electrical feedback,

$$\begin{bmatrix} L_d & 0 \\ 0 & L_q \end{bmatrix}\frac{d}{dt}\begin{bmatrix} x_1 \\ x_2 \end{bmatrix} = \begin{bmatrix} -R_a & 0 \\ 0 & -R_a \end{bmatrix}\begin{bmatrix} x_1 \\ x_2 - x_{20} \end{bmatrix} \quad (6.46)$$

The electromagnetic torque is expressed as

$$T_{em} = \frac{3}{2}p(\left(L_d - L_q\right)x_1 x_2 + \emptyset_m x_2) \quad (6.47)$$

$$T_{dr} = \frac{P_w}{x_3} = \frac{1}{2} x_3 \rho A V_w^3 C_p(\lambda, x_4) = \frac{1}{2} \rho A V_w^2 R C_T \tag{6.48}$$

$$C_T = C_p(\lambda, x_4)/\lambda \tag{6.49}$$

Where $\lambda = x_3 R / V_w$.

$$\frac{dT_{em}}{dx_2} = \frac{3}{2} p\left(\left(L_d - L_q\right) x_1 + \emptyset_m\right), \; T_{em} = \frac{dT_{em}}{dx_2} x_2 \tag{6.50}$$

The mechanical dynamics is,

$$J x_3 + B x_3 = T_{dr} - T_{em}, T_{em} = d_{er3} x_1 + d_{er4} x_2 \tag{6.51}$$

Thus, eliminating T_{dr}, the linear mechanical dynamics is,

$$J \dot{x_3} = -d_{er3} x_1 - d_{er4} x_2 - B x_3 + d_{er1}(x_3 - x_{30}) + d_{er2} \tag{6.52}$$

and

$$\tau_b \dot{x_4} = u_c - x_4 \tag{6.53}$$

6.6 Equilibrium and Stability of the Wind Turbine

The steady state conditions for equilibrium point operation are used to define the steady state rotor mechanical speed ω_{ms} and the steady state q (quadrature) axis current, i_{qs}.

Thus, the steady state rotor mechanical speed ω_{ms} is,

$$B\omega_{ms} = T_{dr} - T_{em} \tag{6.54}$$

Hence, it follows that,

$$T_{em} = T_{dr} - B\omega_{ms} = \frac{3}{2} p\left(\left(L_d - L_q\right) i_d + \phi_m\right) i_q \tag{6.55}$$

It also follows that, the steady state $_q$ (quadrature) axis current, i_{qs} is,

$$i_{qs} = 2\left(T_{dr} - B\omega_{ms}\right)/3p\left(\left(L_d - L_q\right) i_d + \phi_m\right) = 2\left(T_{dr} - B\omega_{ms}\right)/3p\phi_m \tag{6.56}$$

To consider the stability, since the electrical system is decoupled and stable it is only essential to consider the mechanical subsystem. Thus,

$$\dot{x}_3 = -\frac{\left(d_{er3} x_1 + d_{er4} x_2\right)}{J} + \frac{\left(d_{er1} - B\right)}{J} x_3 + \frac{d_{er2}}{J} x_4 - \frac{d_{er1}}{J} x_{30} \tag{6.57}$$

$$\dot{x}_4 = -\left(x_4/\tau_b\right) + u_c/\tau_b \tag{6.58}$$

Hence the open loop stability is guaranteed when, $d_{er1} - B < 0$, or in terms of the stability derivative d_{er1} as,

$$d_{er1} = \frac{dC_T}{d\lambda}\frac{f_d R}{V_w} = \frac{d}{d\lambda}\left(\frac{C_p\left(\lambda,\beta\right)}{\lambda}\right)\frac{f_d R}{V_w} < B \tag{6.59}$$

$$\frac{dC_T}{d\lambda} = \frac{d}{d\lambda}\left(\frac{C_p\left(\lambda,\beta\right)}{\lambda}\right) < \frac{BV_w}{f_d R} \tag{6.60}$$

Since the expression on the right-hand side of the preceding equation is generally small as $B \approx 0$, the stability condition is approximately reduced to,

$$\frac{dC_T}{d\lambda} = \frac{d}{d\lambda}\left(\frac{C_p\left(\lambda,\beta\right)}{\lambda}\right) <\approx 0 \tag{6.61}$$

Referring to Fig. 6.6, the actual point of operation is determined by the equilibrium point which lies on the $C_T - \lambda$ performance curve to the right of the peak of the curve.

For an equilibrium point on the left any disturbance causing an increase in the mechanical speed, will result in an increased torque, which in turn will drive the wind turbine to run faster. Hence all equilibrium points to the left of the peak in the $C_T - \lambda$ curve are unstable while those to the right of the peak are stable. Thus, operation at the maximum power point is also seen to be feasible as it is to the right of the peak of the $C_T - \lambda$.

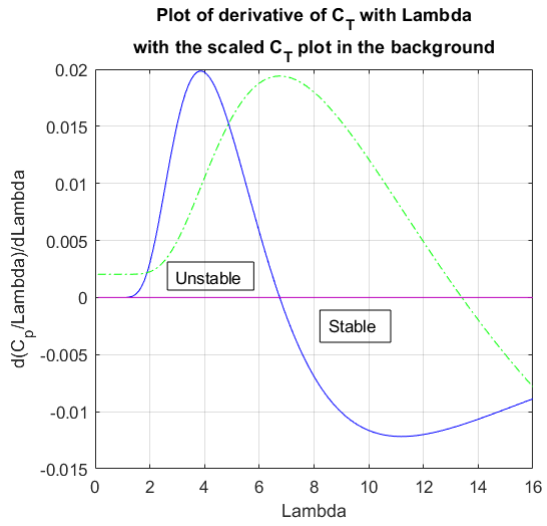

Figure 6.6: Stability diagram

To analyse the closed loop stability, assume a full state control law of the form,

$$u_c = -K_1 x_3 - K_2 x_4 \tag{6.62}$$

The last equation is,

$$\dot{x}_4 = -\left((K_2 + 1)x_4/\tau_b\right) - K_1 x_3/\tau_b \tag{6.63}$$

The characteristic polynomial is,

$$\begin{vmatrix} d_{er1} - B - s & d_{er2} \\ -K_1 & -K_2 - 1 - s \end{vmatrix} = 0 \tag{6.64}$$

It reduces to,

$$(s+K_2+1)(s+B-d_{er1})+K_1 d_{er2}=0 \tag{6.65}$$

The characteristic polynomial expands to,

$$s^2+s(K_2+1+B-d_{er1}) \ +(K_2+1)B+K_1 d_{er2}-(K_2+1)d_{er1}=0 \tag{6.66}$$

Thus, in principle, K_1 and K_2 may be chosen to guarantee stability. Ensuring that the coefficient of the second order characteristic polynomial (64), are positive,

$$K_2+1+B>d_{er1} \tag{6.67}$$

$$(K_2+1)B+K_1 d_{er2}>(K_2+1)d_{er1} \tag{6.68}$$

The second condition (66) may be expressed as,

$$\left(\frac{K_1}{K_2+1}d_{er2}+B\right)>d_{er1} \tag{6.69}$$

provided,

$$K_2>0 \tag{6.70}$$

In particular when $B\approx 0$, the second condition (6.66) is expressed entirely in terms of the stability derivatives as,

$$\frac{d_{er1}}{d_{er2}}<\frac{K_1}{K_2+1} \tag{6.71}$$

Thus, the closed loop stability is guaranteed by a proper choice of K_1 and K_2, which is feasible as long as, the stability derivative $d_{er2}\neq 0$. Clearly when $d_{er2}\approx 0$, the controller synthesis must be done while also ensuring that at the equilibrium point the stability derivative $|d_{er2}|>>0$. This may require operating with the tip speed ratio λ being sufficiently large, which is beyond the maximum power

point. This indicates that the benefits of blade pitch control can be marginal, unless the operating set point is chosen appropriately.

6.7 Control Law Synthesis: Nonlinear Model Predictive Control

In this section we shall briefly consider the synthesis of a control law for the nonlinear plant by locally linearising the plant dynamics and then applying the methodology of model predictive control at each time step. The concept of MPC is explained by Rawlings [115]. The methodology considered is based on the implementation due to Vepa [116]. To illustrate the process of synthesis of a linear control law at each time step, a typical discrete time system is defined as,

$$\mathbf{x}(k+1) = \mathbf{A}(k)\mathbf{x}(k) + \mathbf{B}(k)\mathbf{u}(k),\ \mathbf{y}(k) = \mathbf{C}(k)\mathbf{x}(k) \tag{6.72}$$

A control input sequence is defined as $\mathbf{u}(j)$, j = 0,1,2 ... N − 1, let the sequence of control inputs be expressed as a single vector defined by,

$$\mathbf{U} = \left[\mathbf{u}^T(0) \quad \mathbf{u}^T(1) \quad \cdots \quad \mathbf{u}^T(N-1)\right]^T \tag{6.73}$$

The objective is to minimize a performance index which is function of the output sequence y(k), the control input sequence $\mathbf{u}(j)$, the terminal state over the horizon, y(N) and a terminal weighting matrix $\mathbf{Q}_N$ and is assumed to be given by,

$$J(\mathbf{x}(0), \mathbf{U}) = \sum_{k=0}^{N-1} \left\{\mathbf{y}^T(k) q \mathbf{Q} \mathbf{y}(k) + \mathbf{u}^T(k) r \mathbf{R} \mathbf{u}(k)\right\} + \mathbf{y}^T(N) q \mathbf{Q}_N \mathbf{y}(N) \tag{6.74}$$

In (6.74) q and r are scalar scaling parameters. They are primarily used to re-scale the relative contributions of the states and the control inputs to the cost function. One may also define the sequence of state vectors expressed as a single vector as,

$$\mathbf{X} = \left[\mathbf{x}^T(1) \quad \mathbf{x}^T(2) \quad \cdots \quad \mathbf{x}^T(N-1) \quad \mathbf{x}^T(N)\right] \tag{6.75}$$

It may be noted that the state vector x(k) represents the state at the following instant of time. The cost function J may be written as,

$$J(x(0),U) = qx^T(0)C^T(0)QC(0)x(0) + qX^T\bar{Q}X + rU^T\bar{R}U \quad (6.76)$$

where the block diagonal matrix $\bar{\mathrm{Q}}$ is one with the matrices $\mathbf{C}^T(k)\mathbf{QC}(k)$, $\mathrm{k} = 0,1,2 \ldots \mathrm{N}-1$, along the diagonal except the last element which is $\mathbf{C}^T(N)\mathbf{Q}_N\mathbf{C}(N)$. The block diagonal matrix $\bar{\mathbf{R}}$ is one along the diagonal with the matrix R. The next step is to construct a prediction model,

$$\mathbf{X} = \mathbf{SU} + \mathbf{Tx}(0) \quad (6.77)$$

where,

$$\mathbf{S} = \begin{bmatrix} \mathbf{B} & \mathbf{0} & \mathbf{0} & \mathbf{0} \\ \mathbf{A}(1)\mathbf{B} & \mathbf{B} & \mathbf{0} & \mathbf{0} \\ \cdots & \cdots & \cdots & \cdots \\ \left(\prod_{k=N-1}^{1}\mathbf{A}(k)\right)\mathbf{B} & \left(\prod_{k=N-2}^{1}\mathbf{A}(k)\right)\mathbf{B} & \cdots & \mathbf{B} \end{bmatrix}, \ \mathbf{T} = \begin{bmatrix} \mathbf{A}(0) \\ \mathbf{A}(1)\mathbf{A}(0) \\ \cdots \\ \prod_{k=N-1}^{0}\mathbf{A}(k) \end{bmatrix} \quad (6.78)$$

It has been assumed for simplicity that B is constant but not A. The cost function could be expressed compactly in the form,

$$J(\mathbf{x}(0),\mathbf{U}) = \frac{1}{2}\mathbf{x}(0)^T\mathbf{G}\mathbf{x}(0) + \frac{1}{2}\mathbf{U}^T\mathbf{H}\mathbf{U} + \mathbf{x}^T(0)\mathbf{F}\mathbf{U} \quad (6.79)$$

with,

$$\mathbf{G} = 2q\left(\mathbf{T}^T\bar{\mathbf{Q}}\mathbf{T} + \mathbf{C}^T(0)\mathbf{QC}(0)\right), \ \mathbf{H} = 2r\bar{\mathbf{R}} + 2q\mathbf{S}^T\bar{\mathbf{Q}}\mathbf{S} \text{ and } \mathbf{F} = q\mathbf{T}^T\bar{\mathbf{Q}}\mathbf{S} \quad (6.80)$$

To obtain the optimal control sequence one may set the gradient of the cost function with respect to the sequence of control inputs, U to zero. By this process the cost function J is minimized resulting in,

$$dJ(\mathbf{x}(0),\mathbf{U})/d\mathbf{U} = \mathbf{U}^T\mathbf{H} + \mathbf{x}^T(0)\mathbf{F} = 0 \ \Rightarrow \ \mathbf{HU} + \mathbf{F}^T\mathbf{x}(0) = 0 \ \Rightarrow \ \mathbf{U} = -\mathbf{H}^{-1}\mathbf{F}^T\mathbf{x}(0) \quad (6.81)$$

Considering only the receding horizon, the optimal control input sequence is given by,

$$\mathbf{u}(k) = -\begin{bmatrix} 1 & 0 & \cdots & 0 \end{bmatrix} \mathbf{H}^{-1}\mathbf{F}^{T}\mathbf{x}(k) \tag{6.82}$$

It is recursively obtained over successive prediction windows of the control sequence. The product $\mathbf{H}^{-1}\mathbf{F}^{T}$ is expressed as

$$\mathbf{H}^{-1}\mathbf{F}^{T} = \frac{q^2}{2}\left(\frac{r}{q}\overline{\mathbf{R}} + q\mathbf{S}^{T}\overline{\mathbf{Q}}\mathbf{S}\right)^{-1}\mathbf{S}^{T}\overline{\mathbf{Q}}\mathbf{T} \tag{6.83}$$

The parameter q may be set to 1, and (6.83) reduces to,

$$\mathbf{H}^{-1}\mathbf{F}^{T} = \frac{1}{2}\left(r\overline{\mathbf{R}} + \mathbf{S}^{T}\overline{\mathbf{Q}}\mathbf{S}\right)^{-1}\mathbf{S}^{T}\overline{\mathbf{Q}}\mathbf{T} \tag{6.84}$$

where r is treated as a free parameter to be chosen.

It must be emphasized that the MPC based control ensures the closed loop stability of the wind turbine. Thus, it is important to focus on the steady state operating point.

6.8 Determining the optimum operating set point

To establish the steady state operating point, it is important to recognize the desired output power is our primary requirement. Thus, based on the demanded power and the current operating speed, the desired steady state operating point is determined. The desired power coefficient is then determined from the demanded power output and the nominal or current operating speed. Once desired power coefficient is known, for the given tip speed ratio λ, the desired maximum value of the pitch angle command is determined from the power coefficient, $C_p = C_p(\lambda, \beta)$ model defined in (8) relating the power output coefficient to blade collective pitch angle β and the tip speed ratio λ. This requires inverting the relationship $C_p = C_p(\lambda, \beta)$ given by (8) for a fixed tip speed ratio λ to determine the blade collective pitch angle $\beta =$

$\beta_{d,max}$. This inversion is done by minimising the norm of the error between the desired power output coefficient and the mathematical model relating it to the tip speed ratio λ and blade collective pitch angle β. Thus this is done by employing the *Grey Wolf* optimisation of Long and Xu [117] as well as by the MATLAB function provided for unconstrained optimisation, '*fminunc.m*' for obtaining the solution for desired blade collective pitch angle $\beta = \beta_{d,max}$.

Table 6.2: Typical parameter values for simulation

Parameter	**Value**
C_{p_nom}	0.38
R	5m
R_{root}	9.3564m
J	$5 \times 10^{-5} kgm^2$
L_q	5mH
L_d	5mH
ϕ_m	$4.4\, Nm/(rad/s)^2$
P	10
B	0.2J
V_w	10m/s
τ_b	0.01
P_{nom}	60 kW
λ_{nom}	8
N	3

It must be recognized that although the commanded pitch angle is $\beta_{d,max}$, the actual steady state pitch angle is $0 \leq \beta_{ss} \leq \beta_{d,\max}$. The control law only tracks the desired power and maintains stability but does not track $\beta_{d,max}$. This is because the mechanical speed and hence the tip speed ratio λ is not forced to track a demanded value but is a free variable.

It must be said that the MPPT algorithm may also be implemented. It is exactly same algorithm implemented by Vepa [118]. Briefly the current drawn from the generator is increased slowly till the maximum power point is reached, so the wind turbine is operating just beyond the maximum of the $C_p - \lambda$ curve. The details can be found in Vepa [118] and will not be repeated here.

Finally, the case of active stall control is not considered as in this case the relation for the power coefficient given by (6.8) is no longer valid. This case will be considered independent using a set of complementary controller synthesis tools and reported separately.

6.9 Typical Simulations and Results

A typical three bladed wind turbine is simulated and controlled as application of the above theory. The system parameter is listed in Table II. The nominal time step for integrating the equations of motion is $\Delta t = 0.0001s$. The prediction window to obtain the control input at each time instant is 10 time-steps. The actual nominal power output of the wind turbine is about $60kW$. The desired power output is nominally set at $50kW$ but could be chosen as desired.

Initially the wind turbine is operating in steady state with i_d equal to 40 amps, i_q equal to 0, the power output being 62.58 kW, and the mechanical speed being 23.7 rads/s. It is sought to reduce the power output to 0.7 of the initial power outputs. The change is initiated after 0.04 secs and the results are shown in Fig. 6.6.

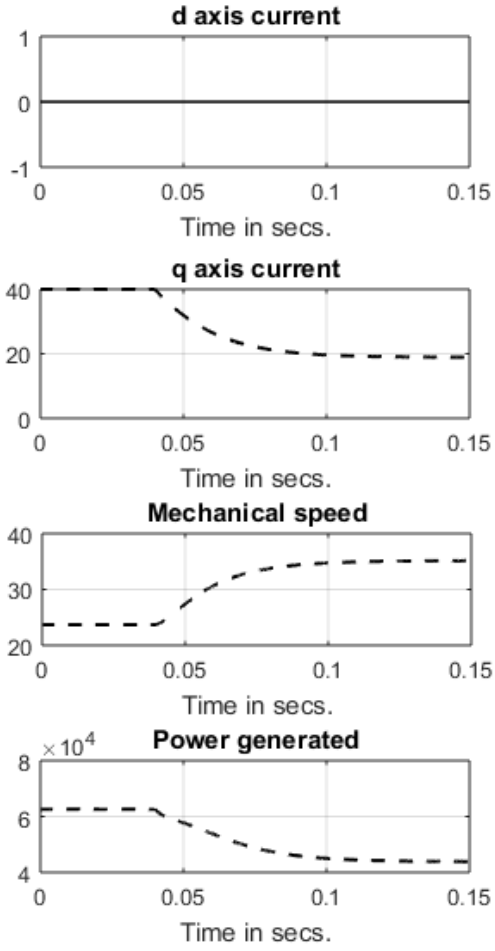

Figure 6.7: Current, mechanical speed and power output response of the wind turbine in response to power reduction command

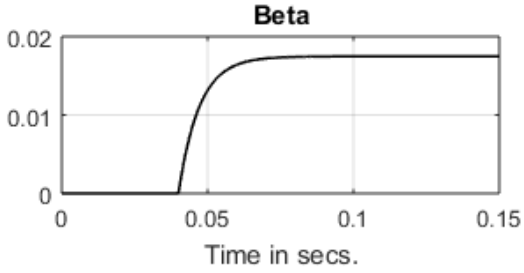

Figure 6.8: Response of the blade collective pitch angle during the reduction in power

From Fig 6.7 it is clear that the power responds to the desired power output that has been set. This implies a reduction in the q axis currenti_q. The current in the d axis continues to remain at zero. However, it is observed that the mechanical speed has gone up implying an increase in the tip speed ratio, as well, which is up by almost 50%. In Fig. 6.8 the change in the collective blade pitch angle is plotted.

The steady state pitch angle is observed to be just over 1° while the commanded pitch angle (not shown on the Fig.) was about 3.4°. Thus, although the control system does not track the commanded pitch angle it does respond to the power demanded set point and delivers the demanded power in the steady state.

6.10 Summary

In this paper, de-coupled dynamic and equilibrium models of a PMSG driven by a variable speed wind turbine were presented and used in the analysis of the stability and the synthesis of a power output controller. The generator is modelled in the synchronous rotating *d-q* reference frame and de-coupled from the turbine by feedback. Based on de-coupled dynamic model, parameter bounds for the stability of the wind turbine are derived. The stabilisation and the active blade pitch control of the wind turbine with the PMSG for power output regulation has been validated and successfully demonstrated. The issue of the instability of the wind turbine has been addressed by a linear feedback control law that stabilizes the system and also delivers the desired power output. The control law, which is designed by applying the MPC procedure, and which has the structure of a proportional-derivative stabilizing control law that ensures the demanded power output is delivered, has been validated. Moreover, the power delivered is tracked by consideration of the equilibrium conditions, using a generic non-dimensional mathematical model for the power-speed characteristics. For this reason, the controller can be applied to any wind turbine driving a PMSG, even when a turbine-specific matched mathematical model is not available.

Chapter 7 Conclusions and Future Work

7.1 Conclusion

In the thesis, control techniques and optimisation methods for three different renewable energy systems are evaluated with the purpose of improving their energy efficiency and system performance. First the scaled-up and full-scale PRO model, nonlinear PV model and WT model are mathematically derived and simulated. Following these three models, the performances of these three systems are analysed and optimised using various state-of-the art effective approaches including machine learning, optimisation techniques. The main contributions of this investigation are listed as follows:

- A novel maximum power point tracking (MPPT) scheme for efficient extraction of maximum power from a scaled-up pressure retarded osmosis process subject to rapid salinity variation is proposed. The scheme is designed using the Whale Optimisation with Differential Evolution (WODE) algorithm, which has facilitated the development of a maximum power point tracking controller with features that have helped overcome limitations such as lower tracking efficiency and steady state oscillations as encountered in the conventional methods. It is observed from results that the proposed method not only outperforms other widely used methods but is also more robust.
- Pressure Retarded Osmosis (PRO) process is optimised using Grey Wolf Optimisation (GWO) algorithms, which has suggested the optimal values of key operating parameters for a maximum energy extraction. The findings of this study reveal the significance of incorporating nature inspired machine-learning algorithms such as the GWO in the optimisation of a PRO process and identifying the preferable operating conditions in a non-ideal system.
- A new performance index is proposed for the development of a variable step-size based adaptive model predictive control (MPC) algorithm for maximum power point tracking and regulating the power output from a PV panel. A novel feature of this methodology is that the parameters of the converter have been chosen to always guarantee stability. It is shown not only that the algorithm is more efficient than traditional techniques, but it also maintains the bus voltage in the presence of both ambient temperature and wind speed variations under disturbance attenuation.

- A linearised parameter varying dynamic model of the nonlinear wind turbine system including wind disturbances is developed. The stability of the wind turbine system is analysed, and a blade pitch controller is designed, based on the linearised, parameter-varying, model-predictive control and is validated. The wind turbine is regulated in a way that the generator delivers the demanded power output to the load. Moreover, the blade pitch control system also performs the key function of augmenting the stability of the wind turbine, for the right choice of the gains.

7.2 Deliveries

Publication and submitted articles extracted from this research and above contributions are listed below.

Journal Articles

Y. Chen, R. Vepa, and M. H. Shaheed, "Enhanced and Speedy Energy Extraction from a scaled-up Pressure Retarded Osmosis process with a Whale Optimisation based Maximum Power Point Tracking," *Energy*, Apr. 2018, 10.1016/j.energy.2018.04.052.

Y. Chen, A. Ali and M. H. Shaheed, "Optimization of a Pressure Retarded Osmosis process using Machine Learning for Maximum Energy Extraction," Energy, under review.

Y. Chen, R. Vepa, and M. H. Shaheed, "Stabilization and Active Blade Pitch Control of a Wind Turbine driven PMSG for Power Output Regulation," *Wind Energy*, under review.

A. Altaee, **Y. Chen**, A. Braytee, and M. H. Shaheed, " Optimization of Dual Stage Pressure Retarded Osmosis for Maximum Power Generation," *Applied Energy*, under review.

A.Monjezi, **Y. Chen**, R. Vepa, and M. H. Shaheed, "Development of a Solar Energy powered off-grid Desalination System for Continuous Production of Freshwater with Integrated PVT Cooling," in preparation.

-

7.3 Suggestions for Future Work

Due to the high demand of the sustainable power production, the renewable energy resources such as solar, wind and water have attracted considerable interest from the energy industry over the last decade. In this research, the renewable energies including PRO, PV and WT systems have been modelled analytically and optimised using several proposed methods for a better performance. The control methodologies for these systems are evaluated to improve their efficiency. There are a few suggestions for future work below:

1. PRO is a recently investigated energy source. It needs further study and evaluation from various perspectives. Firstly, there are several researches on the chemical properties exist in the literature, however, only a few control algorithms are included in PRO systems for a better performance. The published work including MPPT method for a PRO system is all model- and simulation- based. Thus, collaboration is required between materials scientists and engineering scientists, with the purpose of driving a better PRO model in preparation for practical implementation. Moreover, dual-stage PRO systems can be studied and optimised using control methods, which can give a better performance than using a single-stage PRO system.

2. From a mechanical engineering point of view, other optimisation and control methods can be utilised in a PRO system to maximize the generated power. For instance, the MPC method can be used in a more complex PRO model. Furthermore, considering the cost of PRO membrane, optimisation methods can also be used to determine optimal costs in the PRO system.

3. Three main renewable energy systems are investigated in the work. Hybrid systems can be utilised from this research. However, wind energy and photovoltaic energy have a few limitations owing to the wind speed and the variability of solar irradiance, resulting in restricted operational time frames. Thus, scientists can investigate alternative renewable energy generation methods, such as a hybrid system combining all three modules. Moreover, a

PRO system combined with FO or RO modules for desalination can be a popular topic or interest.

Appendix Source Code of the simulation programmes

The source codes of all the programmes developed in this research are presented in this part.

The codes related to the PRO model are written in two separate files; the first file is used to describe full-scale PRO process, which forms and prepares the data for the full-scale PRO power plant and the second file deals with the scaled-up PRO model (chapter 3).

```
format long

n=2;R=8.314e-2;T=293;Wid=1;area=24;P=105.7144;x=0.1;

Aw=1.23e-3; B=0.0026;K=30.71581197;k=0.180;

Qdi=2000;Qfi=2000;

cdo=5;cfo=0.6;Qp=0;

%%%%%%%%%%%%%%%%% changing parameters %%%%%%%%

% parameters;

i=1;w2=1;

% i=1;

for i=1:40

%     Cdi=cdi(i);Cfi=cfi(i);

    Cdi=cdo;Cfi=cfo;

    iii=1;

%     %%%%%%%%%%%%%%%%train Jw%%%%%%%%%%%%%%%%%%%%%

     for j=1:0.001:24
```

```
        C63=j;
% %          C63=Jw_initial(i);
        %%%%%%%%%%%%%%%%%%%%Jw%%%%%%%%%%%%%%%%%%%%%%



pdb=((n*0.082*T*Cdi)*(1+(1/(1+(C63*Wid*x/(Qdi/area+sum(Qp))))
)))/2;
        pfb=((n*0.082*T*Cfi)*(1+(1/(1-
(C63*Wid*x/(Qfi/area+sum(Qp)))))))/2;
        B61=(pdb*exp(-C63/(1000*k))-
pfb*exp((C63*K/(1000))+(C63/(1000*k))));


B62=(1+(B*1000/C63)*(exp((C63*K/(1000)+(C63/(1000*k))))-exp(-
C63/(1000*k))));
        Jw_trial(iii)=Aw*(B61/B62-P)*1000;
        pdi(iii)=pdb;
        pfi(iii)=pfb;
        diff(iii)=(abs(Jw_trial(iii)-C63));
        Jw_c(iii)=C63;
        iii=iii+1;
     end
     [w1 w2]=min(diff);
    Jw_1(i,1)=Jw_c(w2);
    Pdb=pdi(w2);
    Pfb=pfi(w2);
```

```
    Jw(i,1)=Jw_trial(w2);
    %%%%%%%%%%%%%%%%%%%%%Qp%%%%%%%%%%%%%%%%%%%%%
    Qp(i,1)=Jw(i,1)*x*Wid;
    %%%%%%%%%%%%%%%%%%%%%Cdo,Cdi%%%%%%%%%%%%%%%%%%%%%
    Cdo(i,1)=(Pdb/n/0.082/T)*2-Cdi;
    cdo=Cdo(i,1);
    Cfo(i,1)=(Pfb/n/0.082/T)*2-Cfi;
    cfo=Cfo(i,1);
    %%%%%%%%%%%%%%%%%%%%%deltaG,eff%%%%%%%%%%%%%%%%%%%%%
    deltaGi(i,1)=((n*R*T)*(Cdi-Cfi)^2)/(4*36*(Cdi+Cfi));
    deltaGo(i,1)=((n*R*T).*(Cdo(i,1)-
Cfo(i,1))^2)/(4*36.*(Cdo(i,1)+Cfo(i,1)));
    eff(i,1)=deltaGo(i,1)/deltaGi(i,1);
 end
```

In a scaled-up PRO process, the osmotic power model is simulated in MATLAB as follows (chapter 4):

```
clear all
format long
Cos=0.7307;
delta_p=0:25;
mem=0.1;
A=1.74;
```

```
B=0.16;

S=307e-6;

D=3600*1.490*10^-6;

k=138.6;

c_d0=35;

c_f0=0.1;

q_f0=1;

%%%%%%%%%%%%%%%%%%%%%%%%Change fai %%%%%%%%%%%%%%%%%%%%%%%%

fai=0.2;

q_d0=q_f0*(1-fai)/fai;

l=length(delta_p);

for i=[1:l]

con=PRO_co_mem([c_d0,q_d0,c_f0,q_f0,delta_p(i),mem],[A,B,S,D,
k]);

c_d=con(2);

c_f=con(3);

V_ad(i)=con(1);

E_ad(i)=con(6);

%%%%%%%%%%%%%%%%%%%%%%%%Update Jw %%%%%%%%%%%%%%%%%%%%%%%%

%%AD-PRO

C1=1+(S.*B)./D+B./k;

Jw_AD=A*(Cos*(c_d-c_f)/C1-
delta_p(i))/(1+A*Cos*(c_d/k+c_f*S/D)/C1);

%%Ideal-PRO
```

```
Jw_id=A*(Cos*(c_d-c_f)-delta_p(i));

V_id(i)=Jw_id;

E_id(i)=V_id(i).*delta_p(i)*10^5/(3600*10^3);

end

%%%%%%%%%%%%%%%%%%%%%%%%
plot %%%%%%%%%%%%%%%%%%%%%%%%%%%%%%%%%%%%%

Figure(1)

hold on

plot(delta_p,E_ad,'hexagram');

ylim([0 0.5])

xlabel('applied hydraulic pressure');

ylabel('Extractable energy');

Figure(2)

% plot(delta_p,V_id);

hold on

plot(delta_p,V_ad,'hexagram');

ylim([0 1])

xlabel('applied hydraulic pressure');

ylabel('Mass rate of permeated water');
```

The following codes, **PV_model.m**, includes all calculation of a PV cell. The parameters included in the code is the same as which in the manufacturer's sheet (chapter 5).

```
function I_ou=pv_sim_G(Vin,G)

%Imp=7.61;Vmp=26.3;Pme=200.143;Isc=8.21;Voc=32.9;Kv=-
0.123;KI=0.0032;

Rp=415.405;Rs=0.221; a=1.3; I0=9.825e-08;Ipvn=8.2;I02=9.825e-
08;a2=1;Ns=54;

T=300;q=1.60217646e-19;k=1.3806503e-23;

Vt=Ns*k*T/q;

Ipv=Ipvn*G/1000;

nv=size(Vin,2);

I_ou=[];

    for j=1:nv

        V=Vin(j);

        I_inn=8.1;

        for iter=1:100

            I_in=I_inn;

            I_out=Ipvf(Ipv, V, I0, I_in,Rs, Rp, Vt, a);

            if abs(I_out-I_in)<1.0e-03

                break

            else

            I_in=I_out;

            end

        end

        I_ou=[I_ou I_out];

    end
```

```
function I_out=Ipvf(Ipv, V, I0, I_in,Rs, Rp, Vt, a)

i=I_in;

v=V+Rs*i;

e=exp(v/(Vt*a))-1;

I_out=Ipv-I0*e-v/Rp;
```

The codes related to the WT model are shown below, which is used to develop decoupled dynamic and equilibrium models of a permanent magnet synchronous generator (PMSG) driven by a variable speed wind turbine system (chapter 6).

```
close all

clear all

clc

global Lambda thetaref thetaref0 Cpref rpr

format long g

pi=4*atan(1.);% pi=3.14159265358979323846264 3;

rads=pi/180;

N=1500;

dt=0.0001;

ns=4;



% wms=280;

iqs=40;% was 40

R=1/sqrt(3);
```

```
R=5;

Lq=0.005;Ld=Lq; %9*0.405*1.0e-03

Rs=0.425; %0.9067

Kt=4.4;%Nm/(rads/s)^2;was 4.4

P=10;

vw0=14; % Mean wind speed

wms=8*vw0/R;

vwsig=0;

vw=vw0+vwsig*randn(1, 1);

Lambda=wms*R/vw;

Jeq=0.5e-04;%0.00062

Beq=0.2*Jeq;% 0.5*Jeq

%wn=2*pi*10;

%zetan=0.1;

toub=0.01;

Pe_nom=60000;

H=60;

thetaref=0.0;

thetaref0=0.0;

Kfbk=0;

x0=[0 iqs wms 0]';

xin=x0;
```

```
Xf=[];time=[];V3ph=[];I3ph=[];Pw=[];Qw=[];Vdc=[];V_vsc=[];vsa
=[];vsb=[];vsc=[];

kubl=400;

t0=0;

t=t0;

Np=10;Nc=10;Rc=0.1;Qc=2*eye(4);ro=1;Kfbt=zeros(1,5);Amat=zero
s(4,4,Np);

blc=0;% blade control

Pms=0;

for k=1:N


  kstar=k-100*floor(k/100) ;

  if kstar==0

      k

  end

  tspan=[t t+dt];

  options = odeset('RelTol',1e-4,'AbsTol',1e-5);

  if k>300

      options = odeset('RelTol',1e-01,'AbsTol',1e-3);

  end

  if k==kubl

      wms=x0(3);

      beta=x0(4);

      Pms=Pow;
```

```
        losses=0.0;
        rpr=0.7-losses; % reduced power ratio
        model=0;
          if model==0
          coefs=[0.5176;116;0.4;0;0;5;21;0.006795;0.08;0.035;
1];
          end
        Lambda=wms*R/vw;
        rho=1.225-H*1.194e-04; %kg/m3 density of air
              kw=3.06; % For Egypt
              kwi=1/kw;
              cb=gamma(1+kwi);
              fac=gamma(1+3*kwi)/(cb^3);
          fac=1;
          Pdemand=Pms*rpr;

Cpref=0.381513129441701; %thetaref=0.0601067970493237.
%         Cpref=Pdemand/(0.5*fac*rho*pi*R*R*vw^3);
          %Cpref=rpr*Cp;
          thetaref1=thetaref+1*(thetaref-thetaref0);
          jgw=1;
          if jgw==0
          % Using fminunc instead of Grey_wolf
```

```
        options =
optimoptions(@fminunc,'Display','off','Algorithm','quasi-
newton');

        Best_pos = (pi/180)*fminunc(@(x) power_fun(x,Lambda,
Cpref, coefs),thetaref1*180/pi, options);

        else

%         [Best_pos,Best_score]=Grey_Wolf_Main(thetaref1);

        Best_pos=0.0600995076471497;

        end

        thetaref0=thetaref;

        thetaref=Best_pos;



  end

  if k<kubl

  if k==601

      wms=x0(3);

  end

  if k==1001

      wms=x0(3);

  end

  end

  if k>kubl

      blc=1;
```

```
  end

    if blc==1

        [a, b]=vs_hawt_PMSG_linear_eqns_2018(x0,H, R,
Lq,Ld,Rs,Kt, P, Jeq, Beq, toub, vw);

        a=eye(ns)+a*dt; b=b*dt;

        %size(a); size(b)

        for ii=1:ns

        for jj=1:ns

            Amat(ii,jj,1)=a(ii,jj);

        end

        end

        Kfbtm=mpclint(Amat,b,eye(ns),ro,Qc, Rc, Nc,Np);

        Kfbt=Kfbtm(1,:);

    end

  [tf, xf]=ode45(@(t,y)vs_hawt_PMSG_eqns_2018(t,y,H, R,
Lq,Ld,Rs,Kt, P, Jeq, Beq, wms, Pms, toub, vw,
blc,iqs,Kfbt),tspan,x0);

  [nt nj]=size(xf);

  x0n=xf(nt,:);

  x0n=x0n';

  x0=x0n;

  time=[time tf(nt)];

  Xf=[Xf x0];

  t=t+dt;
```

```
  iq=x0(2);wm=x0(3);id=x0(1);
  Pow=wm*(3/2)*(P*(Ld-Lq)*id*iq+P*Kt*iq);
  Pw=[Pw Pow];
end

figure(1)
subplot(4,1,1)
plot(time,Xf(1,:),'k-', 'LineWidth',1,'MarkerSize',2)
grid on
title('d axis current')
subplot(4,1,2)
plot(time,Xf(2,:),'k--', 'LineWidth',1.5,'MarkerSize',2)
grid on
title('q axis current')
subplot(4,1,3)
plot(time, Xf(3,:),'k--', 'LineWidth',1.5,'MarkerSize',2)
grid on
title('mechanical speed')
subplot(4,1,4)
plot(time,Pw,'k--', 'LineWidth',1.5,'MarkerSize',2)
grid on
title('Power generated')
```

```
figure(2)

plot(time,Xf(4,:),'k-', 'LineWidth',1,'MarkerSize',2)

grid on

title('Theta')
```

References

[1] S. Loeb and R. S. Norman, "Osmotic power plants.," *Science*, vol. 189, no. 4203, pp. 654–655, 1975.

[2] S. Loeb, "Production of energy from concentrated brines by pressure-retarded osmosis," *J. Memb. Sci.*, vol. 1, pp. 49–63, 1976.

[3] A. Dai and K. E. Trenberth, "Estimates of Freshwater Discharge from Continents: Latitudinal and Seasonal Variations," *J. Hydrometeorol.*, vol. 3, no. 6, pp. 660–687, 2002.

[4] A. Altaee, J. Zhou, A. Alhathal Alanezi, and G. Zaragoza, "Pressure retarded osmosis process for power generation: Feasibility, energy balance and controlling parameters," *Appl. Energy*, vol. 206, pp. 303–311, 2017.

[5] J. Maisonneuve, C. B. Laflamme, and P. Pillay, "Experimental investigation of pressure retarded osmosis for renewable energy conversion: Towards increased net power," *Appl. Energy*, vol. 164, pp. 425–435, 2016.

[6] W. He, Y. Wang, and M. H. Shaheed, "Maximum power point tracking (MPPT) of a scale-up pressure retarded osmosis (PRO) osmotic power plant," *Appl. Energy*, vol. 158, pp. 584–596, 2015.

[7] G. Han, Q. Ge, and T. S. Chung, "Conceptual demonstration of novel closed-loop pressure retarded osmosis process for sustainable osmotic energy generation," *Appl. Energy*, vol. 132, pp. 383–393, 2014.

[8] S. Lin, A. P. Straub, and M. Elimelech, “Thermodynamic limits of extractable energy by pressure retarded osmosis,” *Energy Environ. Sci.*, vol. 7, no. 8, pp. 2706–2714, 2014.

[9] E. Nagy, “A general, resistance-in-series, salt- and water flux models for forward osmosis and pressure-retarded osmosis for energy generation,” *J. Memb. Sci.*, vol. 460, pp. 71–81, 2014.

[10] M. Kurihara and M. Hanakawa, “Mega-ton Water System: Japanese national research and development project on seawater desalination and wastewater reclamation,” *Desalination*, vol. 308, pp. 131–137, 2013.

[11] S. E. Skilhagen, J. E. Dugstad, and R. J. Aaberg, “Osmotic power - power production based on the osmotic pressure difference between waters with varying salt gradients,” *Desalination*, vol. 220, no. 1–3, pp. 476–482, 2008.

[12] A. Achilli, T. Y. Cath, and A. E. Childress, “Power generation with pressure retarded osmosis: An experimental and theoretical investigation,” *J. Memb. Sci.*, vol. 343, no. 1–2, pp. 42–52, 2009.

[13] M. Villalva, J. Gazoli, and E. Filho, “Comprehensive Approach to Modeling and Simulation of Photovoltaic Arrays,” *IEEE Trans. Power Electron.*, vol. 24, no. 5, pp. 1198–1208, 2009.

[14] A. M. Davis, “Microelectronic circuits,” *Proc. IEEE*, vol. 71, no. 4, pp. 543–543, 1983.

[15] S. H. Hur and B. Leithead, “Model predictive control of a variable-speed pitch-regulated wind turbine,” in *2016 UKACC International Conference on Control, UKACC Control 2016*, 2016.

[16] D. Q. Dang, Y. Wang, and W. Cai, “Offset-free predictive control for variable speed wind turbines,” *IEEE Trans. Sustain. Energy*, 2013.

[17] S. H. Hosseini, A. Farakhor, and S. K. Haghighian, “Novel algorithm of maximum power point tracking (MPPT) for variable speed PMSG wind generation systems through model predictive control,” *2013 8th Int. Conf. Electr. Electron. Eng.*, 2013.

[18] V. Yaramasu and B. Wu, “Predictive control of a three-level boost converter and an NPC inverter for high-power PMSG-based medium voltage wind energy conversion systems,” *IEEE Trans. Power Electron.*, 2014.

[19] V. Yaramasu, B. Wu, S. Alepuz, and S. Kouro, “Predictive control for low-voltage ride-through enhancement of three-level-boost and NPC-converter-based PMSG wind turbine,” *IEEE Trans. Ind. Electron.*, 2014.

[20] A. M. Dizqah, A. Maheri, K. Busawon, and A. Kamjoo, “A Multivariable Optimal Energy Management Strategy for Standalone DC Microgrids,” *IEEE Trans. Power Syst.*, 2015.

[21] M. H. Sharqawy, L. D. Banchik, and J. H. L. V, “Effectiveness – mass transfer units (ε – MTU) model of an ideal pressure retarded osmosis membrane mass exchanger,” *J. Memb. Sci.*, vol. 445, pp. 211–219, 2013.

[22] N. Y. Yip and M. Elimelech, “Thermodynamic and energy efficiency analysis of power generation from natural salinity gradients by pressure retarded osmosis,” *Environ. Sci. Technol.*, vol. 46, no. 9, pp. 5230–5239, 2012.

[23] G. L. Wick and W. R. Schmitt, “Prospects for Renewable Energy from the Sea,” *Mar. Technol. Soc. J.*, vol. 11, pp. 16–21, 1977.

[24] G. Z. Ramon, B. J. Feinberg, and E. M. V. Hoek, “Membrane-based production of salinity-gradient power,” *Energy Environ. Sci.*, vol. 4, no. 11, p. 4423, 2011.

[25] W. He, X. Luo, O. Kiselychnyk, J. Wang, and M. H. Shaheed, “Maximum power point tracking (MPPT) control of pressure retarded osmosis (PRO) salinity power plant: Development and comparison of different techniques,” *Desalination*, vol. 389, pp. 187–196, 2016.

[26] S. Mirjalili and A. Lewis, “The Whale Optimization Algorithm,” *Adv. Eng. Softw.*, vol. 95, pp. 51–67, 2016.

[27] S. K. Cherukuri and S. R. Rayapudi, “A Novel Global MPP Tracking of Photovoltaic System based on Whale Optimization Algorithm,” *Int. J. Renew. Energy Dev.*, vol. 5, no. 3, p. 225, 2016.

[28] N. Kumar, I. Hussain, B. Singh, and B. K. Panigrahi, “MPPT in Dynamic Condition of Partially Shaded PV System by Using WODE Technique,” *IEEE Trans. Sustain. Energy*, vol. 8, no. 3, pp. 1204–1214, 2017.

[29] A. Altaee, G. Zaragoza, E. Drioli, and J. Zhou, “Evaluation the potential and energy efficiency of dual stage pressure retarded osmosis process,” *Appl. Energy*, vol. 199, pp. 359–369, 2017.

[30] A. Altaee, G. Zaragoza, and A. Sharif, “Pressure retarded osmosis for power generation and seawater desalination: Performance analysis,” *Desalination*, vol. 344, pp. 108–115, Jul. 2014.

[31] W. Yang, L. Song, J. Zhao, Y. Chen, and B. Hu, “Numerical analysis of performance of ideal counter-current flow pressure retarded osmosis,” *Desalination*, vol. 433, pp. 41–47, 2018.

[32] D. Sera, R. Teodorescu, and P. Rodriguez, “PV panel model based on datasheet values,” in *IEEE International Symposium on Industrial Electronics*, 2007, pp. 2392–2396.

[33] M. A. Alghoul *et al.*, “Design and experimental performance of brackish water reverse osmosis desalination unit powered by 2 kW photovoltaic system,” *Renew. Energy*, vol. 93, pp. 101–114, 2016.

[34] W. De Soto, S. A. Klein, and W. A. Beckman, “Improvement and validation of a model for photovoltaic array performance,” *Sol. Energy*, vol. 80, no. 1, pp. 78–88, 2006.

[35] B. Andrade da Costa and J. M. Lemos, “An adaptive temperature control law for a solar furnace,” *Control Eng. Pract.*, vol. 17, no. 10, pp. 1157–1173, 2009.

[36] S. Armstrong and W. G. Hurley, “A new methodology to optimise solar energy extraction under cloudy conditions,” *Renew. Energy*, vol. 35, no. 4, pp. 780–787, 2010.

[37] H. Patel and V. Agarwal, “MATLAB-based modeling to study the effects of partial shading on PV array characteristics,” *IEEE Trans. Energy Convers.*, 2008.

[38] A. Dolara, S. Leva, and G. Manzolini, “Comparison of different physical models for PV power output prediction,” *Sol. Energy*, vol. 119, pp. 83–99, 2015.

[39] T. Esram and P. L. Chapman, “Comparison of Photovoltaic Array Maximum Power Point Tracking Techniques,” *IEEE Trans. Energy Convers.*, vol. 22, no. 2, pp. 439–449, 2007.

[40] M. B. Shadmand, R. S. Balog, and H. Abu-Rub, “Model predictive control of PV sources in a smart DC distribution system: Maximum power point tracking and droop control,” *IEEE Trans. Energy Convers.*, vol. 29, no. 4, pp. 913–921, 2014.

[41] V. Salas, E. Olías, A. Barrado, and A. Lázaro, “Review of the maximum power point tracking algorithms for stand-alone photovoltaic systems,” *Solar Energy Materials and Solar Cells*, vol. 90, no. 11. pp. 1555–1578, 2006.

[42] N. Femia, G. Petrone, G. Spagnuolo, and M. Vitelli, “Optimization of perturb and observe maximum power point tracking method,” *IEEE Trans. Power*

Electron., vol. 20, no. 4, pp. 963–973, 2005.

[43] G. C. Hsieh, H. I. Hsieh, C. Y. Tsai, and C. H. Wang, "Photovoltaic power-increment-aided incremental-conductance MPPT with two-phased tracking," *IEEE Trans. Power Electron.*, vol. 28, no. 6, pp. 2895–2911, 2013.

[44] B. N. Alajmi, K. H. Ahmed, S. J. Finney, and B. W. Williams, "Fuzzy-logic-control approach of a modified hill-climbing method for maximum power point in microgrid standalone photovoltaic system," *IEEE Trans. Power Electron.*, 2011.

[45] K. Punitha, D. Devaraj, and S. Sakthivel, "Artificial neural network based modified incremental conductance algorithm for maximum power point tracking in photovoltaic system under partial shading conditions," *Energy*, vol. 62, pp. 330–340, 2013.

[46] F. Zhang, L. Du, F. Z. Peng, and Z. Qian, "A new design method for high-power high-efficiency switched-capacitor DC-DC converters," *IEEE Trans. Power Electron.*, vol. 23, no. 2, pp. 832–840, 2008.

[47] F. Amato, C. Cosentino, A. S. Fiorillo, and A. Merola, "Stabilization of bilinear systems via linear state-feedback control," *IEEE Trans. Circuits Syst. II Express Briefs*, vol. 56, no. 1, pp. 76–80, 2009.

[48] a. S. Kislovski and R. Redl, "Maximum-power-tracking using positive feedback," *Proc. 1994 Power Electron. Spec. Conf. - PESC'94*, pp. 1065–1068, 1994.

[49] S. E. Babaa, M. Armstrong, and V. Pickert, “Overview of Maximum Power Point Tracking Control Methods for PV Systems,” *J. Power Energy Eng.*, vol. 02, no. 08, pp. 59–72, 2014.

[50] P. E. Kakosimos and A. G. Kladas, “Implementation of photovoltaic array MPPT through fixed step predictive control technique,” *Renew. Energy*, vol. 36, no. 9, pp. 2508–2514, 2011.

[51] D. Gonzalez, C. A. Ramos-Paja, and C. Carrejo, “Predictive control of a photovoltaic dc/dc converter,” in *Power Electronics, Machines and Drives (PEMD 2012), 6th IET International Conference on*, 2012, pp. 1–6.

[52] S. Sajadian and R. Ahmadi, “Model Predictive-Based Maximum Power Point Tracking for Grid-Tied Photovoltaic Applications Using a Z-Source Inverter,” *IEEE Transactions on Power Electronics*, vol. 31, no. 11. pp. 7611–7620, 2016.

[53] P. Petit, M. Aillerie, J. P. Sawicki, and J. P. Charles, “High efficiency DC-DC converters including a performed recovering leakage energy switch,” in *Energy Procedia*, 2013, vol. 36, pp. 642–649.

[54] M. D. Seeman and S. R. Sanders, “Analysis and optimization of switched-capacitor DC-DC converters,” in *Proceedings of the IEEE Workshop on Computers in Power Electronics, COMPEL*, 2006, pp. 216–224.

[55] M. . Shadmand, R. S. . Balog, and H. . Abu Rub, “Maximum Power Point Tracking using Model Predictive Control of a flyback converter for

photovoltaic applications," *IEEE Power Energy Conf. Illinois, PECI 2014*, 2014.

[56] J. Hu, J. Zhu, and D. G. Dorrell, "Model-predictive control of grid-connected inverters for PV systems with flexible power regulation and switching frequency reduction," in *2013 IEEE Energy Conversion Congress and Exposition, ECCE 2013*, 2013, pp. 540–546.

[57] T. Geyer, G. Papafotiou, and M. Morari, "Hybrid Model Predictive Control of the Step-Down DC-DC Converter," *Control Syst. Technol. IEEE Trans.*, vol. 16, no. 6, pp. 1112–1124, 2008.

[58] S. Adhikari and F. Li, "Coordinated V-f and P-Q control of solar photovoltaic generators with MPPT and battery storage in microgrids," *IEEE Trans. Smart Grid*, vol. 5, no. 3, pp. 1270–1281, 2014.

[59] Y. Jiang, J. A. Abu Qahouq, and T. A. Haskew, "Adaptive step size with adaptive-perturbation-frequency digital MPPT controller for a single-sensor photovoltaic solar system," *IEEE Trans. Power Electron.*, vol. 28, no. 7, pp. 3195–3205, 2013.

[60] C. Li, S. K. Chaudhary, T. Dragicevic, J. C. Vasquez, and J. M. Guerrero, "Power flow analysis for DC voltage droop controlled DC microgrids," in *11th International Multi-Conference on Systems, Signals Devices (SSD)*, 2014, pp. 1–5.

[61] D. Velasco De La Fuente, C. L. Trujillo Rodríguez, G. Garcerá, E. Figueres,

and R. Ortega Gonzalez, “Photovoltaic power system with battery backup with grid-connection and islanded operation capabilities,” *IEEE Trans. Ind. Electron.*, vol. 60, no. 4, pp. 1571–1581, 2013.

[62] O. Elbeji, M. Ben Hamed, and L. Sbita, “PMSG Wind Energy Conversion System: Modeling and Control,” *Int. J. Mod. Nonlinear Theory Appl.*, vol. 03, no. 03, pp. 88–97, 2014.

[63] M. Hussein, T. Senjyu, M. Orabi, M. Wahab, and M. Hamada, “Control of a Stand-Alone Variable Speed Wind Energy Supply System †,” *Appl. Sci.*, vol. 3, no. 2, pp. 437–456, 2013.

[64] A. Rolan, A. Luna, G. Vazquez, D. Aguilar, and G. Azevedo, “Modeling of a variable speed wind turbine with a Permanent Magnet Synchronous Generator,” in *2009 IEEE International Symposium on Industrial Electronics*, 2009, pp. 734–739.

[65] D. C. Aliprantis, S. A. Papathanassiou, M. P. Papadopoulos, and A. G. Kladas, “Modeling and control of a variable-speed wind turbine equipped with permanent magnet synchronous generator,” *Proc. ICEM*, vol. 3, pp. 558–562, 2000.

[66] M. S. Camara, M. B. Camara, B. Dakyo, and H. Gualous, “Permanent magnet synchronous generator for offshore wind energy system connected to grid and battery-modeling and control strategies,” *Int. J. Renew. Energy Res.*, vol. 5, no. 2, pp. 386–393, 2015.

[67] T. Tafticht, K. Agbossou, A. Cheriti, and M. L. Doumbia, “Output power maximization of a permanent magnet synchronous generator based stand-alone wind turbine,” *2006 Ieee Int. Symp. Ind. Electron. Vols 1-7*, pp. 2412–2416, 2006.

[68] E. Hamatwi, I. E. Davidson, and M. N. Gitau, “Rotor Speed Control of a Direct-Driven Permanent Magnet Synchronous Generator-Based Wind Turbine Using Phase-Lag Compensators to Optimize Wind Power Extraction,” *J. Control Sci. Eng.*, vol. 2017, 2017.

[69] M. Cheah-Mane, J. Liang, and N. Jenkins, “Permanent magnet synchronous generator for wind turbines: Modelling, control and Inertial Frequency Response,” *2014 49th Int. Univ. Power Eng. Conf.*, no. 1, pp. 1–6, 2014.

[70] C. M. Hackl, M. Pfeifer, K. Schechner, P. Jané-Soneira, and S. Hohmann, “Full-& Reduced-Order State-Space Modeling of Wind Turbine Systems with Permanent-Magnet Synchronous Generator,” *arXiv Prepr. arXiv1802.00799*, Feb. 2018.

[71] M. A. A. El Hamied and N. H. E. Amary, “Permanent Magnet Synchronous Generator Stability Analysis and Control,” *Procedia Comput. Sci.*, vol. 95, pp. 507–515, 2016.

[72] J. L. Prante, J. A. Ruskowitz, A. E. Childress, and A. Achilli, “RO-PRO desalination: An integrated low-energy approach to seawater desalination,” *Appl. Energy*, vol. 120, pp. 104–114, May 2014.

[73] N.-N. Bui, J. T. Arena, and J. R. McCutcheon, “Proper accounting of mass transfer resistances in forward osmosis: Improving the accuracy of model predictions of structural parameter,” *J. Memb. Sci.*, vol. 492, pp. 289–302, Oct. 2015.

[74] N. Y. Yip and M. Elimelech, “Performance limiting effects in power generation from salinity gradients by pressure retarded osmosis,” *Environ. Sci. Technol.*, vol. 45, no. 23, pp. 10273–10282, 2011.

[75] W. He, Y. Wang, and M. H. Shaheed, “Modelling of osmotic energy from natural salt gradients due to pressure retarded osmosis: Effects of detrimental factors and flow schemes,” *J. Memb. Sci.*, vol. 471, pp. 247–257, 2014.

[76] J. W. Post *et al.*, “Salinity-gradient power: Evaluation of pressure-retarded osmosis and reverse electrodialysis,” *J. Memb. Sci.*, vol. 288, no. 1–2, pp. 218–230, 2007.

[77] N. Y. Yip *et al.*, “Thin-film composite pressure retarded osmosis membranes for sustainable power generation from salinity gradients,” *Environ. Sci. Technol.*, vol. 45, no. 10, pp. 4360–4369, 2011.

[78] E. Nagy, J. Dudás, and I. Hegedüs, “Improvement of the energy generation by pressure retarded osmosis,” *Energy*, vol. 116, pp. 1323–1333, 2016.

[79] A. P. Straub, S. Lin, and M. Elimelech, “Module-scale analysis of pressure retarded osmosis: Performance limitations and implications for full-scale operation,” *Environ. Sci. Technol.*, vol. 48, no. 20, pp. 12435–12444, 2014.

[80] B. Zhang, Q. Li, L. Wang, and W. Feng, “Robust optimization for energy transactions in multi-microgrids under uncertainty,” *Appl. Energy*, vol. 217, pp. 346–360, 2018.

[81] H. Islam *et al.*, “Performance Evaluation of Maximum Power Point Tracking Approaches and Photovoltaic Systems,” *Energies*, vol. 11, no. 2, p. 365, Feb. 2018.

[82] S. M. Mirjalili, S. M. Mirjalili, and A. Lewis, “Grey Wolf Optimizer,” *Adv. Eng. Softw.*, vol. 69, pp. 46–61, 2014.

[83] S. Mohanty, B. Subudhi, and P. K. Ray, “A Grey Wolf-Assisted Perturb & Observe MPPT Algorithm for a PV System,” *IEEE Trans. Energy Convers.*, vol. 32, no. 1, pp. 340–347, 2017.

[84] A. Azizivahed, H. Narimani, M. Fathi, E. Naderi, H. R. Safarpour, and M. R. Narimani, “Multi-objective dynamic distribution feeder reconfiguration in automated distribution systems,” *Energy*, vol. 147, pp. 896–914, Mar. 2018.

[85] Q. She, L. Zhang, R. Wang, W. B. Krantz, and A. G. Fane, “Pressure-retarded osmosis with wastewater concentrate feed: Fouling process considerations,” *J. Memb. Sci.*, vol. 542, pp. 233–244, Nov. 2017.

[86] J. Kim, M. Park, S. A. Snyder, and J. H. Kim, “Reverse osmosis (RO) and pressure retarded osmosis (PRO) hybrid processes: Model-based scenario study,” *Desalination*, vol. 322, pp. 121–130, Aug. 2013.

[87] E. Abbasi-Garravand, C. N. Mulligan, C. B. Laflamme, and G. Clairet, “Investigation of the fouling effect on a commercial semi-permeable membrane in the pressure retarded osmosis (PRO) process,” *Sep. Purif. Technol.*, vol. 193, pp. 81–90, Mar. 2018.

[88] A. P. Straub, A. Deshmukh, and M. Elimelech, “Pressure-retarded osmosis for power generation from salinity gradients: is it viable?,” *Energy Environ. Sci.*, vol. 9, no. 1, pp. 31–48, 2016.

[89] C. Fritzmann, J. Löwenberg, T. Wintgens, and T. Melin, “State-of-the-art of reverse osmosis desalination,” *Desalination*, vol. 216, no. 1–3, pp. 1–76, Oct. 2007.

[90] G. K. Pearce, “UF/MF pre-treatment to RO in seawater and wastewater reuse applications: a comparison of energy costs,” *Desalination*, vol. 222, no. 1–3, pp. 66–73, Mar. 2008.

[91] A. K. Plappally and J. H. Lienhard V, “Energy requirements for water production, treatment, end use, reclamation, and disposal,” *Renew. Sustain. Energy Rev.*, vol. 16, no. 7, pp. 4818–4848, Sep. 2012.

[92] W. He, Y. Wang, I. M. Mujtaba, and M. H. Shaheed, “An evaluation of membrane properties and process characteristics of a scaled-up pressure retarded osmosis (PRO) process,” *Desalination*, vol. 378, pp. 1–13, 2016.

[93] A. Altaee, G. J. Millar, and G. Zaragoza, “Integration and optimization of pressure retarded osmosis with reverse osmosis for power generation and

high efficiency desalination," *Energy*, vol. 103, pp. 110–118, 2016.

[94] W. He, Y. Wang, and M. H. Shaheed, "Enhanced energy generation and membrane performance by two-stage pressure retarded osmosis (PRO)," *Desalination*, vol. 359, pp. 186–199, 2015.

[95] K. Touati, F. Tadeo, and H. Elfil, "Osmotic energy recovery from Reverse Osmosis using two-stage Pressure Retarded Osmosis," *Energy*, vol. 132, pp. 213–224, 2017.

[96] H. S. Rauschenbach, "SOLAR CELL ARRAY DESIGN HANDBOOK," *JPL SP*, 1976.

[97] Kyocera, "High Efficiency Multicrystal Photovoltaic Module," *Technology*, 2009.

[98] R. Vepa, *Dynamic Modeling, Simulation and Control of Energy Generation*, vol. 20. London: Springer London, 2013.

[99] J. McCool, *Using the Weibull distribution : reliability, modeling, and inference*. John Wiley & Sons, 2012.

[100] M. A. Elgendy, B. Zahawi, and D. J. Atkinson, "Evaluation of perturb and observe MPPT algorithm implementation techniques," in *6th IET International Conference on Power Electronics, Machines and Drives (PEMD 2012)*, 2012, pp. P110–P110.

[101] A. K. Abdelsalam, A. M. Massoud, S. Ahmed, and P. N. Enjeti, “High-performance adaptive Perturb and observe MPPT technique for photovoltaic-based microgrids,” *IEEE Trans. Power Electron.*, vol. 26, no. 4, pp. 1010–1021, 2011.

[102] N. Khaehintung, T. Wiangtong, and P. Sirisuk, “FPGA Implementation of MPPT Using Variable Step-Size P&O Algorithm for PV Applications,” *2006 Int. Symp. Commun. Inf. Technol.*, no. 1, pp. 212–215, 2006.

[103] D. Sera, L. Mathe, T. Kerekes, S. V. Spataru, and R. Teodorescu, “On the perturb-and-observe and incremental conductance mppt methods for PV systems,” *IEEE J. Photovoltaics*, vol. 3, no. 3, pp. 1070–1078, 2013.

[104] K. S. Tey and S. Mekhilef, “Modified incremental conductance algorithm for photovoltaic system under partial shading conditions and load variation,” *IEEE Trans. Ind. Electron.*, vol. 61, no. 10, pp. 5384–5392, 2014.

[105] M. A. Abdourraziq, M. Maaroufi, and M. Ouassaid, “A new variable step size INC MPPT method for PV systems,” in *International Conference on Multimedia Computing and Systems -Proceedings*, 2014, vol. 0, pp. 1563–1568.

[106] J. Rodriguez *et al.*, “State of the Art of Finite Control Set Model Predictive Control in Power Electronics,” *IEEE Trans. Ind. Informatics*, vol. 9, no. 2, pp. 1003–1016, 2013.

[107] M. A. Abdourraziq, M. Ouassaid, and M. Maaroufi, “Comparative study of

MPPT using variable step size for photovoltaic systems," in *2014 Second World Conference on Complex Systems (WCCS)*, 2014, pp. 374–379.

[108] M. H. Moradi, "Predictive control with constraints," *Int. J. Adapt. Control Signal Process.*, vol. 17, no. 3, pp. 261–262, Apr. 2003.

[109] A. Loukriz, M. Haddadi, and S. Messalti, "Simulation and experimental design of a new advanced variable step size Incremental Conductance MPPT algorithm for PV systems," *ISA Trans.*, vol. 62, pp. 30–38, 2016.

[110] S. Augustine, M. K. Mishra, and N. Lakshminarasamma, "Adaptive droop control strategy for load sharing and circulating current minimization in low-voltage standalone DC microgrid," *IEEE Trans. Sustain. Energy*, vol. 6, no. 1, pp. 132–141, 2015.

[111] W. Parton, J. L.-A. Meteorology, and undefined 1981, "A model for diurnal variation in soil and air temperature," *Elsevier*.

[112] H. Voltolini, M. H. Granza, J. Ivanqui, and R. Carlson, "Modeling and simulation of the Wind Turbine Emulator using induction motor driven by torque control inverter," *2012 10th IEEE/IAS Int. Conf. Ind. Appl. INDUSCON 2012*, 2012.

[113] S. Heier, *Grid Integration of Wind Energy Conversion Systems*, vol. 21. 2006.

[114] S. Wijewardana, M. H. Shaheed, and R. Vepa, "Optimum Power Output Control of a Wind Turbine Rotor," *Int. J. Rotating Mach.*, vol. 2016, 2016.

[115] J. B. Rawlings, “Tutorial Overview of Model Predictive Control,” *IEEE Control Syst.*, vol. 20, no. 3, pp. 38–52, 2000.

[116] R. Vepa, “Application of the Nonlinear Tschauner-Hempel Equations to Satellite Relative Position Estimation and Control,” *J. Navig.*, vol. 71, no. 01, pp. 44–64, Jan. 2018.

[117] W. Long and S. Xu, “A novel grey wolf optimizer for global optimization problems,” in *Proceedings of 2016 IEEE Advanced Information Management, Communicates, Electronic and Automation Control Conference, IMCEC 2016*, 2017, pp. 1266–1270.

[118] R. Vepa, “Nonlinear, optimal control of a wind turbine generator,” *IEEE Trans. Energy Convers.*, vol. 26, no. 2, pp. 468–478, 2011.